REGULATION OF HEPATIC CHOLESTEROL HOMEOSTASIS THROUGH ACCELERATED DEGRADATION OF HMG COA REDUCTASE

APPROVED BY SUPERVISORY COMMITTEE

Russell DeBose-Boyd, Ph.D.

Guosheng Liang, Ph.D.

Richard Bruick, Ph.D.

Philipp Scherer, Ph.D.

DEDICATION

This work is dedicated to my parents,

Wooncheon Hwang and Myungsook Jang.

ACKNOWLEDGMENTS

I would like to first express my gratitude to my advisor, Dr. Russell DeBose-Boyd, for his mentorship and support during my dissertation research. I have been fortunate to have such an understanding person as an advisor under whose guidance I have had wonderful opportunities to learn and grow as a researcher.

I also would like to thank the members of my dissertation committee: Drs. Guosheng Liang, Richard Bruick, and Philipp Scherer. I appreciate the insightful advice and feedback that they provided over the course of my dissertation research.

I am particularly grateful for the assistance given by the members of the DeBose-Boyd laboratory and Department of Molecular Genetics. Drs. Youngah Jo, Isamu Hartman, Dong-Jae Jun, and Marc Schumacher have been always willing to share their knowledge, experience, and resources. I would like to thank Kristi Garland and Gennipher Young for excellent technical assistance. I am thankful for generous support from Lisa Beatty and tissue culture technicians. Also, it has been a great pleasure spending time with the people in Room L5.218: Drs. Rania Elsabrouty and Lindsey Morris, Brittany Johnson, and Tammy Dinh.

I am also thankful to our collaborators, Drs. James Brugarolas, Luke Engelking, Helen Hobbs, Jonathan Cohen, and the members of their laboratories for constructive comments, providing resources, and conducting experiments.

I would like to present my appreciation to my previous advisor, Dr. Sang Geon Kim at Seoul National University, and my former colleagues from the laboratory of Dr. Kim, especially Dr. Sung Hwan Ki.

Last, but not least, I owe my deepest gratitude to my parents. Without their love and encouragement, this dissertation would not have been possible.

REGULATION OF HEPATIC CHOLESTEROL HOMEOSTASIS THROUGH ACCELERATED DEGRADATION OF HMG COA REDUCTASE

by

SEONGHWAN HWANG

DISSERTATION

Presented to the Faculty of the Graduate School of Biomedical Sciences

The University of Texas Southwestern Medical Center at Dallas

In Partial Fulfillment of the Requirements

For the Degree of

DOCTOR OF PHILOSOPHY

The University of Texas Southwestern Medical Center at Dallas

Dallas, Texas

May, 2017

REGULATION OF HEPATIC CHOLESTEROL HOMEOSTASIS THROUGH ACCELERATED DEGRADATION OF HMG COA REDUCTASE

Seonghwan Hwang, Ph.D.

The University of Texas Southwestern Medical Center at Dallas, 2017

Supervising Professor: Russell A. DeBose-Boyd, Ph.D.

Cholesterol biosynthesis is rigorously controlled by negative feedback regulation. This reaction occurs, in part, through sterol-accelerated degradation of HMG CoA reductase (HMGCR), which catalyzes the rate-limiting step in cholesterol biosynthesis. The molecular mechanisms for the degradation of HMGCR have been actively investigated; however, the physiological relevance of the degradative regulation in animals is unclear.

The current study investigates the role of sterol-accelerated degradation of HMGCR in overall regulation of HMGCR protein and cholesterol homeostasis in the liver. This was achieved by utilizing two mouse models: (1) liver-specific transgenic mice expressing the membrane domain of HMGCR, which is necessary and sufficient for sterol-regulated

degradation of HMGCR in cultured cells and (2) knock-in mice expressing mutant HMGCR that is resistant to sterol-induced ubiquitination. These models were subjected to various feeding regimens known to modulate Insig and Scap, key players in feedback regulation of HMGCR. Cholesterol replenishment accelerates degradation of HMGCR in the liver of transgenic animals, whereas deprivation of sterols by lovastatin administration suppresses degradation of HMGCR. Ubiquitination-resistant HMGCR accumulated in the liver and resulted in the elevation of hepatic cholesterol, indicating degradation plays a significant role in the *in vivo* regulation of the enzyme and cholesterol homeostasis.

This study further explored the physiological settings other than changing cholesterol status that may modulate the degradation of HMGCR in the two mouse models. As cholesterol synthesis is an oxygen-consumptive process, I determined the link between oxygen sensing and feedback control of cholesterol synthesis. In cultured human fibroblasts, stabilization of oxygen-sensitive transcription factor, hypoxia-inducible factor-1α (HIF-1α) directly activates transcription of *INSIG-2* gene. Insig-2 inhibits cholesterol synthesis by mediating sterol-induced ubiquitination and subsequent degradation of HMGCR. Hepatic levels of Insig-2 mRNA are enhanced in mouse models of hypoxia. Moreover, pharmacologic stabilization of HIF-1α in liver stimulates HMGCR degradation through a reaction that requires the protein's prior ubiquitination and the presence of Insig-2. These results indicate that HIF-mediated induction of Insig-2 and degradation of HMGCR are physiologically relevant events in the cellular adaptation to hypoxic stress.

Overall, the current study provides evidence supporting the physiological significance of the accelerated degradation of HMGCR in cholesterol homeostasis.

TABLE OF CONTENTS

Chapter One and Chapter Four were written by Seonghwan Hwang. Chapter Two was modified by Seonghwan Hwang for the purpose of this dissertation from a published article "*J Biol Chem* **291**:13479-13494 (2016)" written by co-authors Seonghwan Hwang, Isamu Hartman, and Russell DeBose-Boyd. Chapter Three was modified by Seonghwan Hwang for the purpose of this dissertation from a manuscript submitted for publication written by co-authors Seonghwan Hwang, Andrew Nguyen, and Russell DeBose-Boyd. All figures were generated by experiments conducted by Seonghwan Hwang except for a subset of experiments included in Fig. 6, 9-13, 16, 21, and 22 that were conducted by other authors of the manuscripts.

PRIOR PUBLICATIONS

Hwang S, Nguyen AD, Jo Y, Engelking LJ, Brugarolas J, DeBose-Boyd RA. (2017) Requirement of Insig-2 for hypoxia-inducible factor-mediated regulation of of 3-hydroxy-3-methylglutaryl coenzyme A reductase degradation in the liver (manuscript submitted for publication).

Hwang S, Hartman IZ, Calhoun LN, Garland K, Young GA, Mitsche MA, McDonald J, Xu F, Engelking L, DeBose-Boyd RA. (2016) Contribution of accelerated degradation to feedback regulation of 3-hydroxy-3-methylglutaryl coenzyme A reductase and cholesterol metabolism in the liver. *J Biol Chem* **291**:13479-13494.

Hwahng SH*, Ki SH*, Bae EJ, Kim HE, Kim SG. (2009) Role of adenosine monophosphate-activated protein kinase–p70 ribosomal S6 kinase-1 pathway in repression of liver X receptor-alpha-dependent lipogenic gene induction and hepatic steatosis by a novel class of dithiolethiones. *Hepatology* **49**:1913-1925 (*equal contribution).

LIST OF FIGURES

LIST OF TABLES

LIST OF ABBREVIATIONS

24,25-DHL – 24,25-dihydrolanosterol

AAA – ATPases associated with diverse cellular activities

ABCG5 – ATP-binding cassette sub-family G member 5

ABCG8 – ATP-binding cassette sub-family G member 8

AMPK – adenosine monophosphate-activated protein kinase

ccRCC – clear-cell renal cell carcinoma

ChIP – chromatin immunoprecipitation

CMV – cytomegalovirus

DMOG – dimethyloxalylglycine

ER – endoplasmic reticulum

ERAD – ER-associated degradation

FCS – fetal calf serum

FRT – flippase recognition target

GLUT1 – glucose transporter-1

HIF – hypoxia-inducible factor

HMG CoA – 3-hydroxy-3-methylglutaryl coenzyme A

HMGCR – HMG CoA reductase

HMGCR (TM1-8) – transmembrane domains 1-8 of hamster HMGCR

HRE – hypoxia-response element

LDL – low-density lipoprotein

LKB1 – liver kinase B1

LXR – liver X receptor

pVHL – von Hippel-Lindau tumor suppressor protein

RT-PCR – real time PCR

siRNA – small interfering RNA

SRE – sterol regulatory element

SREBP – sterol regulatory element-binding protein

TK – thymidine kinase

UBIAD1 – ubiA prenyltransferase domain containing 1

VCP – valosin-containing protein

VEGF – vascular endothelial growth factor

WT – wild type

CHAPTER ONE

Introduction

Cholesterol is a 27-carbon tetracyclic lipid molecule that constitutes the mammalian cell membranes. It also serves as the precursor of steroid hormones, bile acids, vitamin D, and lipoproteins (1, 2). Despite the vital functions of cholesterol, cells must finely adjust the levels of cholesterol to prevent its over-accumulation which can be deleterious to cells by forming toxic crystal structure and stimulating atheroma formation in arterial walls (1, 3). Homeostatic regulation of the levels of cellular cholesterol is coordinated by *de novo* synthesis and low-density lipoprotein (LDL) receptor-mediated endocytosis (4). When cholesterol levels fail to satisfy the cellular demand, *de novo* synthesis is activated and the expression of LDL receptor is increased to promote the uptake of cholesterol from the bloodstream, whereas an excess of cellular cholesterol inhibits *de novo* synthesis and LDL receptor expression (5).

Fig. 1 describes the mevalonate pathway which mediates the *de novo* synthesis of cholesterol. The rate-limiting process in this pathway is the conversion of 3-hydroxy-3-methylglutaryl coenzyme A (HMG CoA) into mevalonate that is catalyzed by an endoplasmic reticulum (ER) membrane-localized enzyme called HMG CoA reductase (HMGCR) (6, 7). Mevalonate is an important intermediate in the synthesis of sterols and nonsterol isoprenoids that are necessary for normal cellular function (8, 9). Among these molecules are ubiquinone and heme A, which are involved in aerobic cellular respiration,

dolichol, which participate in glycosylation of proteins, and farnesyl pyrophosphate and geranylgeranyl pyrophosphate that are required for post-translational modification of proteins (10). Mevalonate-derived sterols and nonsterol isoprenoids inhibit the levels and activity of HMGCR through a feedback regulatory system that operates at multiple levels involving transcriptional and post-translational control (10). These two regulatory mechanisms are mediated by a pair of ER membrane proteins called Insig-1 and Insig-2 (11).

1.1. Insig-Mediated Feedback Inhibition of Cholesterol Synthesis

Insig-1 and Insig-2 are polytopic ER membrane proteins with hydrophilic NH_2-terminal and COOH-terminal domains projecting into the cytosol (12, 13). Human Insig-1 is comprised of 277 amino acids, while human Insig-2 contains 225 amino acids. Two Insig genes in human genome encode highly similar proteins (59% identity) (14). The differences are mostly limited to the hydrophilic regions. Insig-1 possesses NH_2-terminal 50 amino acids that are absent in Insig-2. These structural differences between Insig-1 and Insig-2 are highly conserved across mammalian species. Two Insigs similarly contribute to the feedback regulation of HMGCR; both mediate the suppression of the transcription of HMGCR and activation of the ER-associated degradation (ERAD) of HMGCR in sterol-replete cells, thereby inhibiting the expression of the enzyme. RNA interference-mediated gene silencing in cultured cells and germ-line or tissue-specific deletion of Insig in mice provided evidence supporting the physiological relevance of Insig in the feedback regulation of HMGCR; loss-of-function of both Insigs accumulated HMGCR in cultured

cells and animal tissues and elevated hepatic cholesterol contents in mice (15-17). However, deletion of single Insig failed to significantly increase the expression of HMGCR and cholesterol contents, indicating that the two Insigs are functionally redundant.

1.2. Insig-Mediated Transcriptional Regulation of HMGCR

Synthesis of cholesterol and fatty acids in mammalian cells is regulated by the basic helix-loop-helix leucine zipper family of transcription factors designated sterol regulatory element-binding proteins (SREBPs) (5). Mammalian cells express three closely related isoforms of SREBPs: SREBP-1a, SREBP-1c, and SREBP-2. SREBP-1a and -1c are encoded from the same gene by alternative promoters and alternative splicing. SREBPs are translated as inactive precursor forms and inserted into the ER membranes where they bind the escort protein called Scap (Fig. 2) (18, 19). Scap also serves as a sensor of sterols along with Insigs; in sterol-deprived cells, Scap escorts the SREBPs from the ER to the Golgi apparatus, where the two proteases, site 1 protease and site 2 protease, sequentially cleave the SREBPs to release the transcriptionally active NH_2-terminal domain (Fig. 2) (7, 11). This domain translocates to the nucleus, where it binds to sterol regulatory elements (SREs) in the promoter/enhancer regions of their target genes to activate the transcription of genes required for cholesterol synthesis (SREBP-2) and fatty acid synthesis (SREBP-1a and -1c) (5). However, when cellular cholesterol contents are high, binding of cholesterol to the sterol-sensing domain in the membrane-embedded region of Scap and subsequent conformational change of Scap causes Insig to associate with Scap (18). As a result, Scap-SREBP complex is sequestered in the ER membrane, thereby inhibiting the transcriptional

activation of SREBP target genes. HMGCR and LDL receptor are among the SREBP-2-activated genes essential for the cholesterol uptake and cholesterol biosynthesis (20, 21). Therefore, Insig-mediated regulation of SREBP-2 activation is the critical mechanism for maintaining proper levels of cholesterol in cells through the modulation of cholesterol synthesis and its uptake from the bloodstream.

1.3. Insig-Mediated Degradative Regulation of HMGCR

Another important aspect of the negative feedback regulation of cholesterol synthesis is Insig-mediated ERAD of HMGCR. HMGCR is anchored to the ER membranes through an NH_2-terminal membrane domain with eight membrane-spanning helices, followed by a cytosolic COOH-terminal domain that exerts enzymatic activity (22, 23). Accumulation of sterols in the ER membranes promotes the binding of Insig to the membrane domain of HMGCR (16, 24). Insig is associated with ubiquitin ligases gp78 and Trc8 that facilitate ubiquitination of cytosolically exposed lysine residues in the membrane domain of HMGCR (16, 25-27); Insig-1 bridges both gp78 and Trc8 to HMGCR, whereas Insig-2 recruits only Trc8 to HMGCR (26). Notably, cholesterol does not enhance the ubiquitination of HMGCR but directly binds to Scap (28), facilitates its conformational change, and allows for Insig binding to its membrane domain that inhibits proteolytic activation of SREBP-2. Instead, 25-hydroxycholesterol and 24,25-dihydrolanosterol (24,25-DHL) which are an oxysterol and a cholesterol biosynthetic intermediate, respectively, are two major players that induce the ubiquitination of HMGCR (29, 30).

The post-ubiquitination steps crucial for the proteasomal degradation of the ubiquitinated HMGCR occur in a nonsterol-regulated manner (Fig. 3). Sterols cause another membrane protein called ubiA prenyltransferase domain containing 1 (UBIAD1) to bind HMGCR and sequester it in the ER membranes (31). UBIAD1 constantly shuttles between ER and Golgi; however, in the presence of a 20-carbon isoprenoid geranylgeranyl pyrophosphate, UBIAD1 dissociates from HMGCR and translocates to the Golgi (31, 32). The ubiquitinated HMGCR is then extracted across the ER membranes by AAA (ATPases associated with diverse cellular activities)-ATPase valosin-containing protein (VCP)/p97, released into the cytosol, and delivered into the proteolytic chamber of the 20S proteasome through reactions mediated by the proteasome 19S regulatory particle, which contains six AAA-ATPases, and eventually degraded by 26S proteasome (33, 34).

1.4. Contribution of the Degradative Regulation to Cholesterol Homeostasis

As the rate-limiting enzyme in the cholesterol biosynthetic pathway, feedback regulatory mechanisms of HMGCR have been extensively investigated as a therapeutic target for the prevention and treatment of cardiovascular diseases. The transcriptional component of the HMGCR regulatory system governed by SREBPs has been rigorously examined in livers of mice through analyses of transgenic and knock-out animals (20). In contrast, degradation of HMGCR in animal livers has not been studied in detail, partly due to the inability to directly measure the reaction *in vivo*. Livers of Insig-deficient mice accumulate 20-fold higher levels of HMGCR protein as compared to that of wild type (WT) mice (17). Considering that Insigs play a major role in sterol-mediated inhibition of

SREBP activation, this accumulation presumably results from the combination of defects in transcriptional and degradative regulation of the enzyme. However, the extent to which transcription and degradation individually contributed to regulation of HMGCR in livers of these mice remains obscure.

To corroborate the value of the degradative regulation as a therapeutic target, it needs to be determined whether HMGCR is properly degraded in a sterol-regulated manner *in vivo*, and the extent to which the degradative process contributes to the overall regulation of HMGCR and cholesterol homeostasis *in vivo*. Thus, in the current study, it was investigated whether replenishment and depletion of sterols can modulate the degradation of HMGCR in the liver of mice, and whether other conditions that modulate Insig can affect the degradation of HMGCR *in vivo*. These questions were addressed in two mouse models: 1) transgenic mice expressing the membrane domain of HMGCR, which is necessary and sufficient for accelerated degradation (35, 36), under the control of a promoter that confers constitutive, liver-specific expression, and 2) knock-in mice expressing ubiquitination-resistant HMGCR under the control of the gene's endogenous promoter.

There is a gap of knowledge on the physiological settings other than depletion and replenishment of sterol that can modulate the degradation of HMGCR and whether this is mediated through a mechanism involving Insig-1 and Insig-2. In this regard, as will be discussed below, the current study investigated whether lack of oxygen can disrupt the biosynthetic pathway of cholesterol due to the high demand of oxygen by enzymes involved in cholesterol synthesis (37).

1.5. Oxygen-Dependent Regulation of Cholesterol Synthesis

The synthesis of one molecule of cholesterol from the precursor acetyl-CoA requires 4 oxidation steps that consume 11 molecules of dioxygen (37, 38) (Fig. 1). One molecule of dioxygen is required for the epoxidation of squalene, which is catalyzed by the enzyme squalene monooxygenase. Nine molecules of dioxygen are utilized by lanosterol 14-α demethylase and C4-methyl sterol oxidase in the successive removal of the 4α, 4β, and 14α methyl groups in lanosterol and 24,25-DHL. Finally, sterol 5-desaturase consumes one molecule of dioxygen in the reduction of lathosterol to 7-dehydrocholesterol. It was previously reported that oxygen-deprivation (hypoxia) triggers accumulation of the cholesterol synthesis intermediate 24,25-DHL in Chinese hamster ovary cells (39). 24,25-DHL reduces flux through the mevalonate pathway via Insig-mediated degradation of HMGCR. Notably, hypoxia does not cause chronic accumulation of 24,25-DHL, because 24,25-DHL specifically acts on Insig-mediated degradation of HMGCR but does not stimulate Insig binding to Scap-SREBP complex and subsequent inhibition of SREBP-dependent cholesterol biosynthetic enzymes. Thus, 24,25-DHL feeds into the downstream steps in the mevalonate pathway for cholesterol biosynthesis and subsequently cholesterol begins to accumulate. Accumulation of cholesterol eventually suppresses the entire mevalonate pathway.

Nguyen et al., also demonstrated that hypoxia enhances expression of Insig which mediates ERAD of HMGCR (39). However, hypoxia failed to induce Insig in cells deficient in hypoxia-inducible factor (HIF)-1α. HIF is a heterodimeric transcription factor composed of a labile α subunit and a stable β subunit (40, 41) and functions as a molecular

sensor of oxygen (Fig. 4) (42, 43). Under normal oxygen conditions, the α subunit is hydroxylated on two proline residues by prolyl hydroxylases (Fig. 4), allowing the protein to become recognized by the von Hippel-Lindau tumor suppressor protein (pVHL) for subsequent ubiquitination and proteasomal degradation. Under low oxygen conditions (hypoxia), the α subunit is not hydroxylated owing to the strict requirement for molecular oxygen by prolyl hydroxylases that modify the protein. Stabilized α subunits bind to β subunits and activate transcription by binding to hypoxia-response elements (HREs) present in more than 70 HIF target genes (44). Enhanced expression of HIF target genes, which mediate several cellular processes such as growth and apoptosis, angiogenesis, and energy metabolism, allows for adaptation to hypoxia at the cellular, tissue, and organismal levels (43).

The accumulation of 24,25-DHL together with the HIF-mediated increase in Insig accelerates HMGCR degradation, which ultimately slows the rate of cholesterol synthesis. There are many questions remaining about the oxygen regulation of cholesterol biosynthetic pathway. Firstly, because the studies conducted by Nguyen et al., utilized Chinese hamster ovary cells cultured in medium deficient in sterols (39), it needs to be verified whether this reaction is conserved *in vivo* and cultured cells derived from other mammalian species such as human. Another important question is the molecular mechanisms responsible for the up-regulation of Insig under hypoxic condition; does HIF directly up-regulate Insig through transactivation? If so, does mammalian Insig genes have consensus HREs where HIF binds and activates transcription of its target genes? Does hypoxia enhance the promoter activity of Insig genes? Lastly, to what extent does the

degradation of HMGCR contribute to the overall repression of HMGCR under hypoxic condition? These questions will be further discussed in Chapter Three.

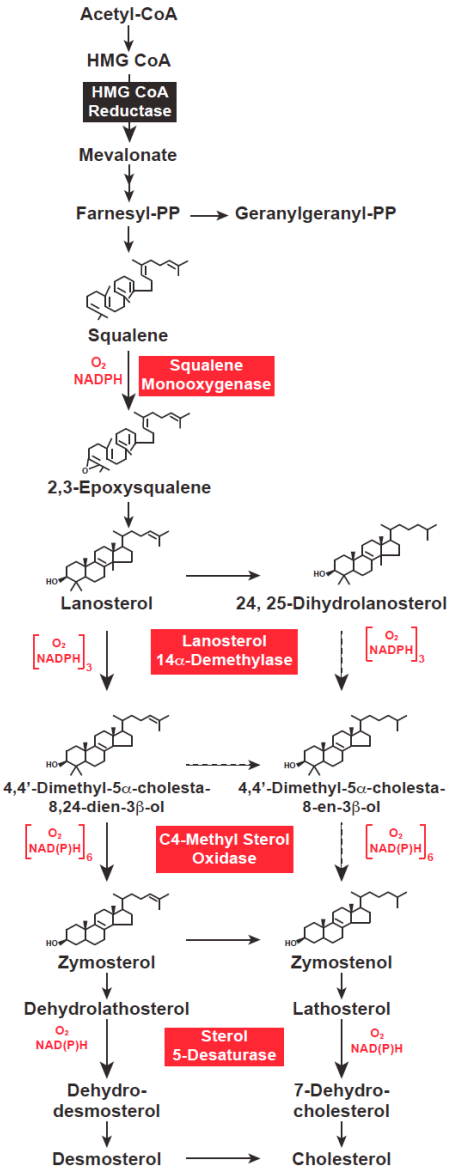

Figure 1. Cholesterol biosynthesis via the mevalonate pathway in mammalian cells. The end products of the mevalonate metabolism, sterols and isoprenoids, participate in homeostatic control of cholesterol through feedback regulation of HMGCR, the rate-limiting enzyme in the pathway. The four enzymes highlighted in red catalyze oxidation reactions; 11 molecules of dioxygen are consumed by the four enzymes for the synthesis of one molecule of cholesterol from acetyl CoA, implying that cholesterol synthesis is an oxygen-intensive process.

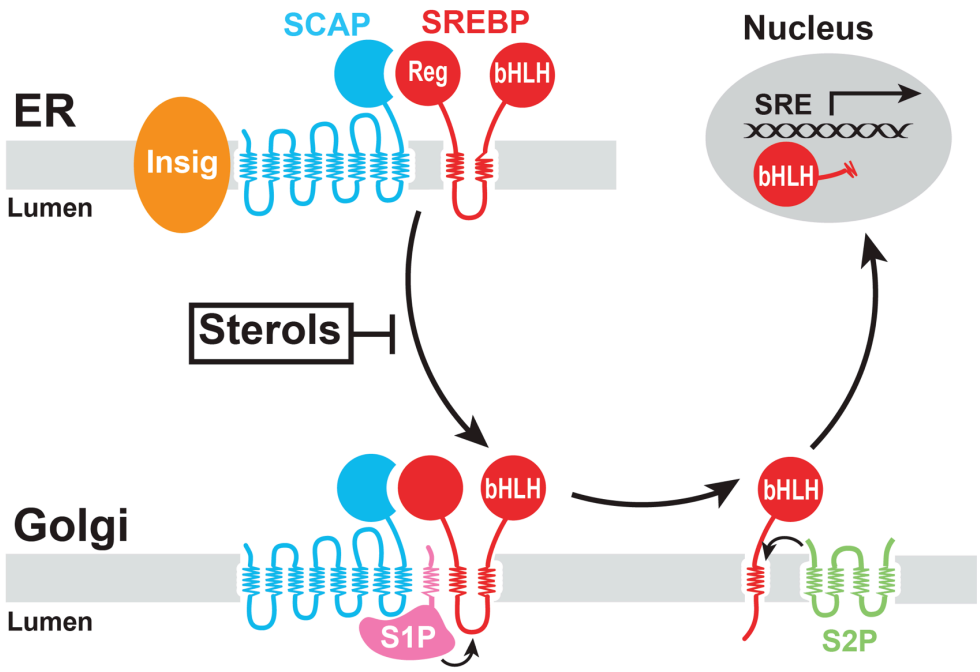

Figure 2. Insig-mediated transcriptional regulation of HMGCR.

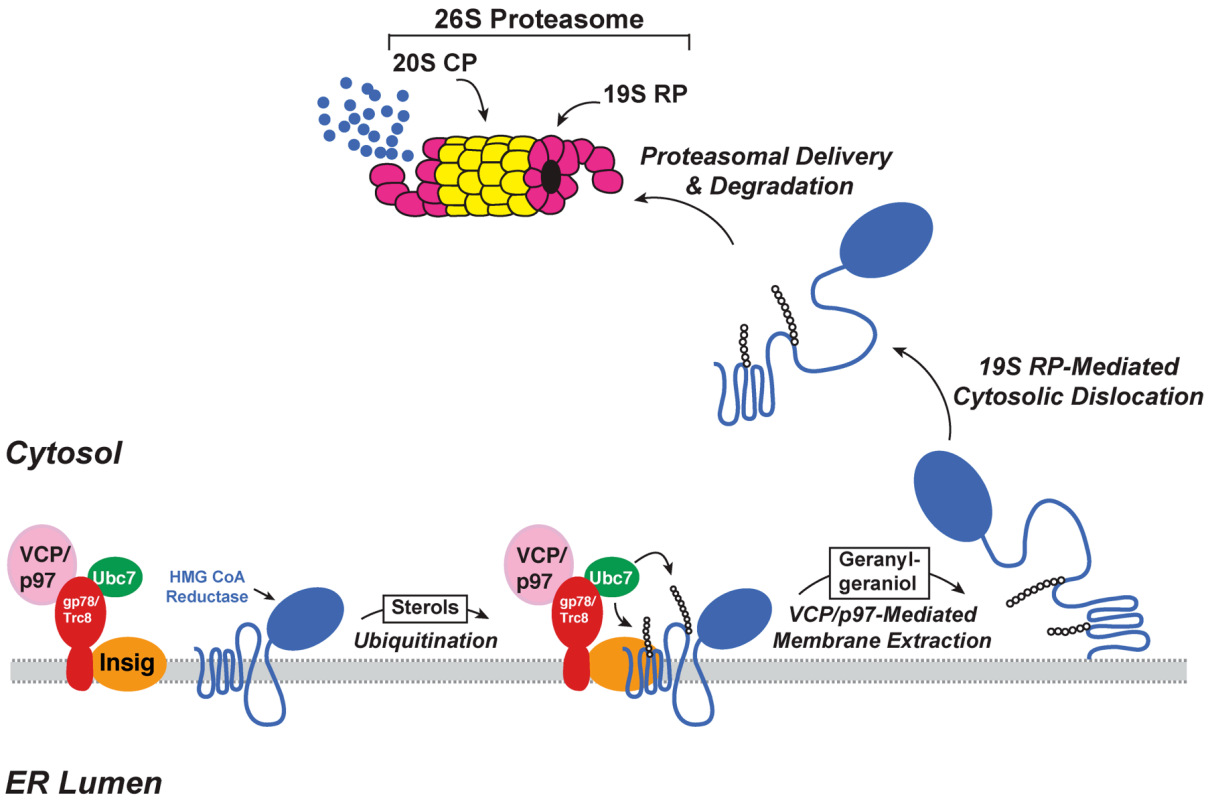

Figure 3. Insig-mediated degradative regulation (ERAD) of HMGCR.

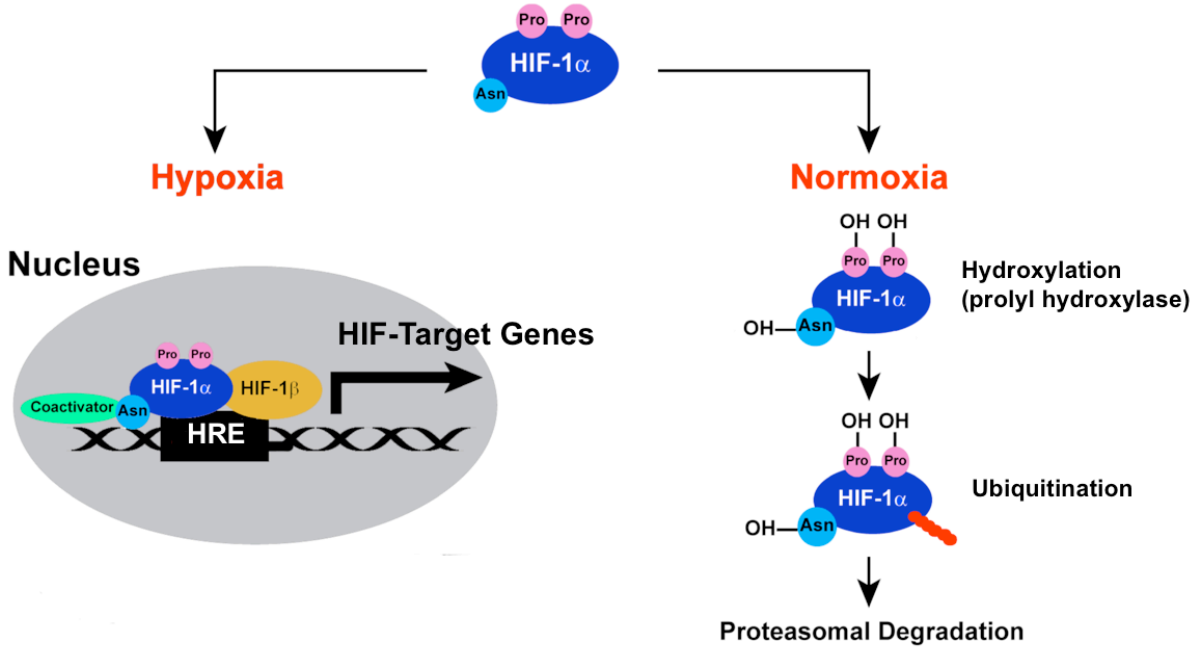

Figure 4. Oxygen-dependent transcriptional regulation of HIF target genes.

CHAPTER TWO

Contribution of Accelerated Degradation to Feedback Regulation of HMG CoA Reductase and Cholesterol Metabolism in the Liver

2.1. Introduction

HMGCR is a polytopic protein of ER membranes that catalyzes conversion of HMG CoA to mevalonate, a rate-limiting reaction in synthesis of cholesterol as well as nonsterol isoprenoids such as dolichol, ubiquinone, farnesyl pyrophosphate, and geranylgeranyl pyrophosphate (10). Multiple feedback mechanisms converge on HMGCR to ensure that essential nonsterol isoprenoids are continuously synthesized, while avoiding overaccumulation of cholesterol and other sterols (9). Recent work indicates additional control points in the cholesterol biosynthetic pathway beyond HMGCR (45). One mechanism for feedback control of HMGCR involves its accelerated degradation from ER membranes (6, 11). This degradation is initiated by intracellular accumulation of sterols, which causes HMGCR to bind to ER membrane proteins called Insig-1 and Insig-2 (24). Insig binding is mediated entirely by the membrane domain of HMGCR, which contains eight transmembrane helices and precedes a cytosolic catalytic domain (22, 23). Insig-associated ubiquitin ligases facilitate ubiquitination of cytosolically exposed lysine residues in the membrane domain of HMGCR (25-27), marking the enzyme for extraction across ER membranes and dislocation into the cytosol for proteasomal degradation (33, 34).

A second mechanism for feedback regulation of HMGCR involves sterol-induced binding of Insigs to Scap, another polytopic protein of ER membranes (46). Scap

associates with membrane-bound SREBPs that modulate transcription of genes encoding HMGCR and other cholesterol biosynthetic enzymes (47). In sterol-depleted cells, Scap facilitates transport of SREBPs from ER to Golgi, where transcriptionally active SREBP fragments are proteolytically released from membranes. These fragments migrate to the nucleus and activate target gene transcription. Excess sterols cause Insigs to bind to Scap, which inhibits transport of Scap-SREBP complexes from ER to Golgi. In the absence of transport, proteolytic activation of SREBPs does not occur and as a result, expression of mRNAs encoding SREBP target genes and cholesterol synthesis decline.

Transcriptional control of HMGCR governed by Scap-SREBP has been extensively studied in livers of transgenic and knock-out mice (5). In contrast, little is known about degradative control of hepatic HMGCR, due in part to the inability to directly measure the parameter *in vivo* (48-50). In Insig-deficient mouse livers, HMGCR protein accumulates disproportionately to its mRNA (17), which is likely due to the combination of defects in transcriptional and degradative control of HMGCR. However, the extent to which these mechanisms individually contributed to HMGCR regulation in Insig-deficient livers remains to be determined.

To clarify the role of accelerated degradation in feedback regulation of HMGCR, two lines of mice were generated: 1) liver-specific transgenic mice expressing the membrane domain of HMGCR, which is necessary and sufficient for Insig-mediated, sterol-accelerated degradation (24); and 2) knock-in mice harboring mutations in the endogenous HMGCR gene that change lysine residues 89 and 248 to arginine. These mutations abolish sterol-induced ubiquitination and subsequent degradation of HMGCR in

cultured cells (16). Characterization of these mice reveal that sterols directly modulate degradation of HMGCR in the liver through mechanisms similar to those previously established in cultured cells. Moreover, our results indicate that sterol-accelerated degradation contributes to regulation of HMGCR and cholesterol metabolism *in vivo*.

2.2. Materials and Methods

Determination of Metabolic Parameters – Blood was drawn from the vena cava after WT, knock-in, and transgenic mice were anesthetized in a bell-jar atmosphere containing isoflurane. Plasma was immediately separated and stored at -80 °C until use. Commercial kits from Wako Chemicals USA, Inc. (Richmond, VA) were used to measure non-esterified fatty acids (HR Series NEFA-HR (2)). Levels of plasma and liver cholesterol and triglycerides were measured using the Infinity Total Cholesterol and the Infinity Triglyceride kits (ThermoFisher Scientific, Waltham, MA). The level of plasma insulin in WT, knock-in, and transgenic mice was measured using an ELISA kit from Crystal Chem (catalog #90080, Downers Grove, IL). Plasma glucose was measured with a Contour Glucometer (Bayer) from the tail nick of conscious mice.

Generation of Hmgcr Knock-in and Tg-HMGCR (TM1-8) Mice – HMGCR knock-in mice, which harbor mutations of lysines-89 (AAG) and -248 (AAA) to arginine (AGG and AGA, respectively), were generated by the Gene Targeting and Transgenic Facility at the Howard Hughes Medical Institute Janelia Research Campus (Ashburn, VA). Genotyping was carried out as described below.

To generate Tg-HMGCR (TM1-8) mice, the pLiv-11 vector containing the constitutive human apoE gene promoter and its hepatic control region was used (51). Transgenic plasmid pLiv-11-HMGCR (TM1-8) was generated by cloning a cDNA fragment encoding the membrane domain (amino acids 1-346) of hamster HMGCR followed by three T7 epitopes (24) into MluI-ClaI sites of pLiv-11. The SalI-SpeI fragment of pLiv-11-HMGCR (TM1-8) was isolated and injected into fertilized eggs to generate transgenic mice by the Transgenic Core Facility at the University of Texas Southwestern Medical Center. Founder mice were identified and positive founders were bred to C57BL/6J mice and three lines of Tg-HMGCR (TM1-8) mice were established. One line expressing a moderate level of HMGCR (TM1-8) in the liver was chosen for further study.

WT and *Hmgcr* knock-in mice ($Hmgcr^{WT/Ki}$ and $Hmgcr^{Ki/Ki}$) littermates were obtained for experiments from intercrosses of $Hmgcr^{WT/Ki}$ heterozygous male and female mice, all of which were hybrids of C57BL/6J and 129Sv/Ev strains. Tg-HMGCR (TM1-8) mice were maintained as hemizygotes by breeding with WT C57BL/6J mice. Mice were housed in colony cages with a 12-h light/12-h dark cycle and fed Teklad Mouse/Rat Diet 2016 from Harlan Teklad (Madison, WI). For experiments, non-transgenic WT littermates were used as controls for the transgenic mice. All animal experiments were performed with the approval of the Institutional Animal Care and Use Committee at University of Texas Southwestern Medical Center at Dallas.

Genotyping of Tg-HMGCR (TM1-8) and Hmgcr Knock-in Mice – Genomic DNA was extracted from tails of Tg-HMGCR (TM1-8) mice using DNeasy Blood and Tissue kit (Qiagen, Venlo, Netherlands) according to the manufacturer's protocol. To genotype the transgenic animals, genomic DNA was amplified with the following primers: forward, 5'-GCCCTAAGTTCAAACTCTCAGGATGAAG-3'; reverse, 5'-GGGCCCTCTAGATCACATATTAATTAAACCC-3'. A primer set targeting mouse Hbb-b1 gene (forward, 5'-CCAATCTGCTCACACAGGATAGAGAGGGCAGG-3'; reverse, 5'-CCTTGAGGCTGTCCAAGTGATTCAGGCCATCG-3') was used as a positive control. To genotype the *Hmgcr* knock-in animals, genomic DNA from tails was used for PCR with the following primers: set A forward, 5'-GTCCATGAACATGTTCACCG-3'; set A reverse, 5'-CAGCACGTCCTATTGGCAGA-3'; set B forward, 5'-TCGGTGATGTTCCAGTCTTC-3'; set B reverse, 5'-GGTGGCAAACACCTTGTATC-3'. Genotypes of the knock-in animals were further verified by DNA Sanger Sequencing Core Facility at University of Texas Southwestern Medical Center using the sequencing primers (K89R, 5'-GTATCACTGAGGCCTCTCAT-3'; K248R, 5'-AGTGCCCACTTCCTTCGTAG-3') after amplification of the genomic DNA with the following primers: K89R forward, 5'-TTCTCTGCCAATAGGACGTG-3'; K89R reverse, 5'- TAGAAGAGCACTGCCACGTT-3'; K248R forward, 5'-AGTAGTACTTCCCATGCTGC-3'; K248R reverse, 5'-GAAGACTGGAACATCACCGA-3'.

Diet Studies – For the cholesterol feeding studies, mice were fed a chow diet (Teklad Mouse/Rat 2016, 0% cholesterol) or chow diet supplemented with 0.05, 0.2, or 2% cholesterol for 5 days prior to study. For lovastatin feeding studies, mice were fed Teklad Mouse/Rat diet 7002 (Harlan Teklad Premier Laboratory Diets, Madison, WI) or the identical diet supplemented with 0.02, 0.06, or 0.2% lovastatin (Abblis Chemicals LLC, Houston, TX). For fasting and refeeding experiments, mice were divided into three groups: nonfasted (NF), fasted (F), and refed (R). The nonfasted group was fed ad libitum, the fasted group was fasted 12 h, and the refed group was fasted for 12 h and then refed a high carbohydrate/low fat diet (MP Biomedicals, Santa Ana, CA) for 12 h prior to study. The starting times for the experiments were staggered such that all mice were sacrificed at the same time, which was at the end of the dark cycle. Liver cholesterol content of WT and Tg-HMGCR (TM1-8) mice fed cholesterol in Fig. 6 were as follows. WT: chow (2.3 mg/g ± 0.2), 0.05% cholesterol (2.3 mg/g ± 0.2), 0.2% cholesterol (4.5 mg/g ± 0.2), and 2% cholesterol (3.6 mg/g ± 0.4); Tg-HMGCR (TM1-8): Chow (2.1 mg/g ± 0.3), 0.05% cholesterol (2.5 mg/g ± 0.3), 0.2% cholesterol (3.6 mg/g ± 0.3), and 2% cholesterol (4.3 mg/g ± 0.2). Liver cholesterol content of WT and Tg-HMGCR (TM1-8) mice fed lovastatin in Fig. 7 were as follows. WT: Chow (2.0 mg/g ± 0.1), 0.2% lovastatin (2.0 mg/g ± 0.2); Tg-HMGCR (TM1-8): Chow (1.4 mg/g ± 0.3), 0.2% lovastatin (2.1 mg/g ± 0.2). Values represent mean ± S.E. of data from 4 mice.

Quantitative Real-Time PCR (RT-PCR) – Total RNA was prepared from mouse tissues using the RNA STAT-60 kit (TEL-TEST "B", Friendswood, TX). Equal amounts of RNA

from individual mice were treated with DNase I (DNA-free™, Ambion/Life Technologies, Grand Island, NY). First strand cDNA was synthesized from 2 μg of DNase I-treated total RNA with random hexamer primers using TaqMan Reverse Transcription Reagents (Applied Biosystems/Roche, Branchburg, NJ). Specific primers for each gene were designed using Primer Express software (Life Technologies). RT-PCR reaction was set up in a final volume of 20 μl containing 20 ng of reverse-transcribed total RNA, 167 nM of the forward and reverse primers, and 10 μl of 2X SYBR Green PCR Master Mix (Life Technologies). PCR reactions were done in triplicate. The relative amount of all mRNAs was calculated using the comparative threshold cycle (C_T) method. Mouse apoB mRNA was used as the invariant controls. The primers for RT-PCR were described previously (17).

Subcellular Fractionation and Immunoblot Analysis – Approximately 50 mg of frozen liver was homogenized in 350 μl buffer (10 mM HEPES-KOH, pH 7.6, 1.5 mM $MgCl_2$, 10 mM KCl, 5 mM EDTA, 5 mM EGTA, and 250 mM sucrose) supplemented with a protease inhibitor cocktail consisting of 0.1 mM leupeptin, 5 mM dithiothreitol, 1 mM PMSF, 0.5 mM Pefabloc, 5 μg/ml pepstatin A, 25 μg/ml N-acetyl-leu-leu-norleucinal, and 10 μg/ml aprotinin. The homogenates were then passed through a 22-gauge needle 10-15 times and subjected to centrifugation at 1000 X g for 5 min at 4 °C. The 1000 X g pellet was resuspended in 500 μl of buffer (20 mM HEPES-KOH, pH 7.6, 2.5% (v/v) glycerol, 0.42 M NaCl, 1.5 mM $MgCl_2$, 1 mM EDTA, 1 mM EGTA) supplemented with the protease inhibitor cocktail, rotated for 30 min at 4 °C, and centrifuged at 100,000 X g for 30 min at

4 °C. The supernatant from this spin was precipitated with 1.5 ml cold acetone at -20 °C for at least 30 min; the precipitated material was collected by centrifugation, resuspended in SDS-lysis buffer (10 mM Tris-HCl, pH 6.8, 1% (w/v) SDS, 100 mM NaCl, 1 mM EDTA, and 1 mM EGTA), and designated the nuclear extract fraction. The post-nuclear supernatant from the original spin was used to prepare the membrane fraction by centrifugation at 100,000 X g for 30 min at 4 °C. Each membrane fraction was resuspended in 100 µl SDS-lysis buffer.

Protein concentration of nuclear extract and membrane fractions were measured using the BCA Kit (ThermoFisher Scientific). Prior to SDS-PAGE, aliquots of the nuclear extract fractions were mixed with 4X SDS-PAGE loading buffer to achieve a final concentration of 1X. Aliquots of the membrane fractions were mixed with an equal volume of buffer containing 62.5 mM Tris-HCl, pH 6.8, 15% (w/v) SDS, 8 M urea, 10% (v/v) glycerol, and 100 mM DTT, after which 4X SDS loading buffer was added to a final concentration of 1X. Nuclear extract fractions were boiled for 5 min, and membrane fractions were incubated for 20 min at 37 °C prior to SDS-PAGE. After SDS-PAGE, proteins were transferred to Hybond C-Extra nitrocellulose filters (GE Healthcare, Piscataway, NJ). The filters were incubated with the antibodies described below and in the figure legends. Bound antibodies were visualized with peroxidase-conjugated, affinity-purified donkey anti-mouse or anti-rabbit IgG (Jackson ImmunoResearch Laboratories, Inc., West Grove, PA) using the SuperSignal CL-HRP substrate system (ThermoFisher Scientific) according to the manufacturer's instructions. Gels were calibrated with prestained molecular mass markers (Bio-Rad, Hercules, CA). Filters were exposed to film

at room temperature. Antibodies used for immunoblotting to detect mouse SREBP-1 (rabbit polyclonal IgG-211C), SREBP-2 (rabbit monoclonal IgG-22D5), Insig-1 (rabbit polyclonal anti-Insig-1 antiserum), Insig-2 (rabbit polyclonal IgG-940), HMGCR (IgG-839c), gp78 (rabbit polyclonal IgG-740F), and Scap (IgG-R139) were previously described (17, 26, 52). Mouse monoclonal anti-T7 Tag IgG was obtained from EMD Biosciences (San Diego, CA). Rabbit polyclonal anti-calnexin IgG was purchased from Novus Biologicals (Littleton, CO). Rabbit polyclonal anti-LSD1 IgG was obtained from Cell Signaling (Beverly, MA). All antibodies were used at a final concentration of 1-5 μg/ml; the anti-Insig-1 antiserum was used at a dilution of 1:1000.

Ubiquitination of Hepatic HMGCR – Approximately 35 mg of frozen liver was homogenized in 1 mL PBS containing 1% Nonidet P-40, 1% deoxycholic acid, 5 mM EDTA, 5 mM EGTA, 0.1 mM leupeptin, 10 mM N-ethylmaleimide, and the protease inhibitor mixture, and subjected to centrifugation at 16,000 × g for 15 min at 4 °C. Immunoprecipitation of the clarified lysates was carried out with polyclonal antibodies against the catalytic domain of human HMGCR as previously described (16). Aliquots of the immunoprecipitates were subjected to SDS-PAGE followed by immunoblot analysis with mouse monoclonal antibodies IgG-A9 (against HMGCR), IgG-P4D1 (against ubiquitin), and IgG-819 against UBXD8 (53).

Lipid Analysis **–** Sterol biosynthetic intermediates were measured using LC-MS/MS according to the method of McDonald et al. (54, 55). Briefly, sterols were isolated on an

LC gradient (Shimadzu LC-20) and detected using the MRM pair on a triple quadrapole MS (ABSciex 4000 q-TRAP) and quantified against authentic sterol standards (Avanti Polar Lipids, Alabaster, AL).

Cholesteryl esters were measured by directly infusing a Bligh-Dyer extract into a triple-TOF MS (ABSciex 5600+), commonly known as "shotgun lipidomics." Cholesteryl esters were identified based on their characteristic 369 Da fragment ion and the fatty acid by the neutral loss. The intensity of each sterol was normalized to the total lipid signal, which was reported as percentage of all lipids.

The absolute levels of free cholesterol and cholesteryl esters in the liver were determined by first homogenizing 20 mg frozen liver in 400 µl chloroform:isopropanol: Nonidet P-40 (7:11:0.1). The homogenates were then centrifuged at 15,000 X g for 10 min at 4 °C. The supernatant from this spin was subjected to quantification of free cholesterol and cholesterol ester using Cholesterol/Cholesteryl Ester Quantitation Kit (Abcam, Cambridge, UK) according to manufacturer's procedure.

Cholesterol and Fatty Acid Synthesis In Vivo – Rates of cholesterol and fatty acid synthesis were measured in control WT and *Hmgcr* knock-in mice fed ad libitum with chow diet using ^{3}H-labeled water as previously described (56). The rates of cholesterol and fatty acid synthesis were calculated as nmol of ^{3}H-labeled water incorporated into fatty acids or digitonin-precipitable sterols per hour per gram of tissue.

2.3. Results

Fig. 5A shows a schematic of a transgene encoding transmembrane domains 1-8 of hamster HMGCR (HMGCR (TM1-8)) fused to three T7 epitopes that was used to generate transgenic mice hereafter designated Tg-HMGCR (TM1-8). Liver-directed expression of HMGCR (TM1-8) was driven by the apoE promoter and its hepatic control region (51). Tg-HMGCR (TM1-8) mice were maintained as hemizygotes by breeding with WT C57BL/6 mice. As expected, expression of HMGCR (TM1-8) mRNA and protein was highest in livers of transgenic mice (Fig. 5B and 5C). Tg-HMGCR (TM1-8) mice were grossly indistinguishable from WT littermates normal and had similar body and liver weights as their WT counterparts. No significant differences were observed in plasma and hepatic levels of cholesterol, triglycerides, and free fatty acids between WT and transgenic mice (data not shown).

Fig. 5D shows the strategy utilized to generate *Hmgcr* knock-in mice ($Hmgcr^{Ki/Ki}$) in which lysine residues 89 and 248 were replaced with arginines. For all experiments described here, $Hmgcr^{WT/Ki}$ heterozygous male and female mice were crossed to obtain WT and $Hmgcr^{Ki/Ki}$ littermates (Fig. 5E). Mice homozygous for both knock-in mutations were born at expected Mendelian ratios. WT and *Hmgcr* knock-in littermates were externally indistinguishable and had similar body and liver weights; there was also no significant differences between WT and *Hmgcr* knock-in mice in plasma cholesterol, triglycerides, and free fatty acids or hepatic triglycerides (data not shown). However, levels of free cholesterol were slightly, but significantly increased in *Hmgcr* knock-in mouse livers,

which was accompanied by a 2- to 3-fold increase in hepatic cholesteryl esters (Fig. 6A and 6B and Table 1).

Immunoblot analysis revealed that livers of *Hmgcr*$^{WT/Ki}$ and *Hmgcr*$^{Ki/Ki}$ mice fed chow diet ad libitum exhibited a marked increase in HMGCR protein as compared to that in WT littermates, despite a reduction in HMGCR mRNA (Fig. 7A). When normalized to the amount of hepatic HMGCR mRNA, HMGCR protein accumulated approximately 6- and 14-fold, respectively, in livers of *Hmgcr*$^{WT/Ki}$ and *Hmgcr*$^{Ki/Ki}$ mice relative to WT animals. The relative amount of HMGCR protein (normalized to tissue HMGCR mRNA) was increased between 3- and 18-fold in other tissues of *Hmgcr*$^{Ki/Ki}$ mice including the kidney, spleen, brain, and testes (Fig. 8A). These results indicate that mutation of lysine residues 89 and 248 to arginine blocks ubiquitination and subsequent degradation of hepatic HMGCR, causing the enzyme to accumulate. Indeed, Fig. 8B reveals that ubiquitination of HMGCR protein was reduced despite its accumulation in livers of *Hmgcr*$^{WT/Ki}$ and *Hmgcr*$^{Ki/Ki}$ mice (compare *lanes 1*, *2*, and *5*). Similar results were observed in an independent repeat experiment (data not shown). Notably, ubiquitination of HMGCR in knock-in mice was not completely eliminated, which could result from ubiquitination at the protein's NH_2-terminus (57).

Comparison of various components of the Scap-SREBP pathway in WT and *Hmgcr* knock-in mice shows that precursor and nuclear forms of SREBP-2 were reduced in livers of *Hmgcr*$^{WT/Ki}$ and *Hmgcr*$^{Ki/Ki}$ mice (Fig. 7B). This reduction was associated with elevated sterol levels in livers of *Hmgcr* knock-in mice (Fig. 6A – 6C and Table 1) and reduced levels (20-70%) of mRNAs encoding HMGCR and the other SREBP-2 target genes

encoding cholesterol biosynthetic enzymes (Fig. 8C and data not shown). Hepatic sterol synthesis was similar between WT and *Hmgcr* knock-in mice (Fig. 6D); however, the reaction was significantly enhanced in testes and brains of *Hmgcr* knock-in mice despite a reduction in SREBP-2 target genes in the tissues (data not shown). In addition, levels of cholesteryl esters were increased in testes and brains of knock-in mice but, the difference observed in brains was not statistically significant (Fig. 6E).

In contrast to SREBP-2, nuclear SREBP-1 was increased in livers of *Hmgcr* knock-in mice (Fig. 7B). This increase likely results from sterol-mediated activation of liver X receptors (LXRs) that modulate expression of SREBP-1c, the major SREBP-1 isoform expressed in mouse livers (58). Indeed, mRNAs encoding SREBP-1c and its target genes including fatty acid synthase, stearoyl coenzyme A desaturase-1, and glycerol-3-phosphate acyltransferase, were elevated in livers of *Hmgcr* knock-in mice (Fig. 8C).

Fig. 9A compares expression of HMGCR (TM1-8) protein in livers of Tg-HMGCR (TM1-8) mice fed diets containing varying amounts of cholesterol. When transgenic mice were fed as little as 0.05% cholesterol, the level of HMGCR (TM1-8) protein was substantially reduced in hepatic membranes (Fig. 9A, compare *lanes e* and *f*); higher amounts of cholesterol led to complete disappearance of HMGCR (TM1-8) (*lanes g* and *h*). Cholesterol feeding failed to inhibit expression of HMGCR (TM1-8) mRNA (Fig. 9B).

Dietary cholesterol caused a reduction of endogenous HMGCR protein in membranes from livers of WT (Fig. 9A, *lanes a-d*) and Tg-HMGCR (TM1-8) mice (*lanes e-h*). Membrane-bound precursor and nuclear forms of SREBP-2 were also reduced in livers of cholesterol-fed animals (Fig. 9C). Levels of SREBP-1 precursor (Fig. 9C) and

mRNA (Fig. 10A) were increased in livers of WT and transgenic mice fed cholesterol, whereas nuclear SREBP-1 levels remained largely unchanged. This is likely due to combined effects of cholesterol on ER to Golgi transport of Scap-SREBP and activation of LXRs (59). As expected, expression of mRNAs encoding SREBP-2 target genes were reduced to similar levels in cholesterol-fed WT and Tg-HMGCR (TM1-8) mice (Fig. 10A).

Fig. 9D shows that elevated levels of HMGCR protein in *Hmgcr*$^{WT/Ki}$ and *Hmgcr*$^{Ki/Ki}$ mice were reduced by cholesterol feeding to an extent similar to that observed in WT mice (compare *lanes 1-3* with *4-6*). Dietary cholesterol also reduced the mRNA for HMGCR, Insig-1, and other SREBP target genes in WT and *Hmgcr* knock-in mice (Fig. 9D and Fig. 10B), which resulted from inhibition of SREBP-2 processing (Fig. 9E, compare *lanes 1-3* with *4-6*). Notably, Insig-1 protein levels were also reduced upon cholesterol feeding (Fig. 9E, *lanes 7-12*). Levels of the SREBP-1 precursor were elevated by cholesterol feeding in WT and knock-in mice (Fig. 9E, compare *lanes 1-3* with *4-6*), which correlated with an increase in mRNAs for SREBP-1c and two other LXR target genes, ATP-binding cassette sub-family G member 5 (ABCG5) and ATP-binding cassette sub-family G member 8 (ABCG8) (Fig. 10B). Processing of SREBP-1 was mostly resistant to dietary cholesterol in WT and *Hmgcr* knock-in animals (Fig. 9E, *lanes 4-6*).

The response of HMGCR (TM1-8) degradation to cholesterol deprivation was examined by feeding Tg-HMGCR (TM1-8) mice a chow diet containing the HMGCR inhibitor lovastatin. Consumption of chow diet containing 0.2% lovastatin caused an increase in the amount of HMGCR (TM1-8) protein in membranes of transgenic mouse livers (Fig. 11A, compare *lanes 3* and *4*). However, the treatment did not alter expression

of HMGCR (TM1-8) mRNA (Fig. 1B). Endogenous HMGCR protein and mRNA were increased in livers of WT and Tg-HMGCR (TM1-8) mice fed lovastatin (Fig. 11A, compare *lanes 1* and *3* with *2* and *4*; Fig. 12A). This was associated with an increase in the nuclear content of SREBP-2 in livers of lovastatin-fed WT and transgenic mice (Fig. 11A, *lanes 2* and *4*) and enhanced expression of mRNAs encoding its target genes (Fig. 12A). In contrast, lovastatin lowered the amount of both precursor and nuclear forms of SREBP-1 (Fig. 11A, compare *lanes 1* and *3* with *2* and *4*), which can be attributed to loss of an endogenous sterol ligand for LXR (60). In the second cholesterol deprivation experiment, Tg-HMGCR (TM1-8) mice were treated with various amounts of lovastatin. As little as 0.02% lovastatin noticeably stabilized HMGCR (TM1-8) (Fig. 11C, compare *lanes a* and *b*); the protein was further stabilized by higher concentrations of the inhibitor (lanes c and d). Precursor and nuclear forms of SREBP-2 and SREBP-1 were induced and suppressed, respectively, by lovastatin in a dose-dependent fashion (Fig. 11C, *lanes a-d*).

Fig. 11D shows that lovastatin triggered an increase in HMGCR protein in livers of *Hmgcr* knock-in mice (*lanes 3* and *4*); however, the increase was blunted compared to that observed in WT mice (*lanes 1* and *2*; see quantification). This is likely due to accumulation of HMGCR protein combined with increased sterol levels and inhibition of SREBP-2 processing in livers of knock-in mice. Lovastatin inhibited levels of precursor and nuclear forms of SREBP-1 (Fig. 11E, *lanes 1-4*) and enhanced levels of precursor and nuclear SREBP-2 (*lanes 1-4*). Furthermore, mRNAs for SREBP-2 and its target genes were elevated upon lovastatin feeding, whereas SREBP-1c mRNA was reduced (Fig. 12B).

Studies were next carried out to determine whether modulation of Insig levels affect degradation of HMGCR (TM1-8). The hormone insulin reciprocally regulates levels of Insig-1 and Insig-2 in livers of mice (61). To modulate insulin levels in WT and Tg-HMGCR (TM1-8) mice, the animals were subjected to a 12 hr fast, which lowered plasma insulin by 80-90%, followed by a 12 hr period of refeeding, which increased insulin greater than 10-fold over the fasted level (Table 4). Compared to nonfasted animals, fasting reduced the amount of precursor and nuclear forms of SREBP-1 in WT and transgenic mice (Fig. 13A, *lanes 1*, *2*, *4*, and *5*); refeeding restored levels of SREBP-1 precursor and caused an overshoot in the nuclear form of the protein (*lanes 3* and *6*). Fasting also reduced nuclear SREBP-2 and refeeding restored these levels (Fig. 13A, *lanes 2*, *3*, *5*, and *6*). As previously reported, fasting caused the disappearance of Insig-1 (owing to the down-regulation of nuclear SREBP) and the appearance of Insig-2 (Fig. 13B, compare *lanes 1* and *4* with *2* and *5*). These changes in Insig-1 and Insig-2 protein levels were completely reversed by refeeding (*lanes 3* and *6*). Endogenous HMGCR protein was reduced upon fasting of WT and transgenic mice (Fig. 13B, *lanes 2* and *5*); its expression was restored by refeeding (*lanes 3* and *6*). The mRNAs for HMGCR, Insig-1, and Insig-2a mRNAs varied with fasting/refeeding in a manner mirroring that of their respective proteins (Fig. 14A). In contrast to endogenous HMGCR, levels of HMGCR (TM1-8) protein (Fig. 13B, *lanes 4-6*) and mRNA (Fig. 13C) were not reduced in livers of fasted transgenic mice.

The experiment shown in Fig. 13D was conducted to confirm that fasting reduced levels of endogenous HMGCR through inhibition of SREBP-mediated transcription rather

than sterol-accelerated degradation. The results show that fasting reduced levels of HMGCR protein and mRNA in both WT and *Hmgcr* knock-in mice (Fig. 13D, *lanes 2* and *5*). However, when normalized to the amount of HMGCR mRNA, the relative amount of HMGCR protein was unchanged in livers of fasted mice. Precursor and nuclear forms of SREBP-1 and SREBP-2 were reduced by fasting (Fig. 13E, *lanes 2* and *5*) and restored by refeeding (*lanes 3* and *6*). Insig-1 and -2 were reciprocally regulated at the protein (Fig. 13E, *lanes 2*, *3*, *5*, and *6*) and mRNA levels (Fig. 14B) by fasting and refeeding.

2.4. Discussion

Two lines of genetically manipulated mice were used to determine whether sterols modulate degradation of HMGCR in the liver and how sterol-accelerated ERAD contributes to multivalent feedback regulation of cholesterol homeostasis. Characterization of Tg-HMGCR (TM1-8) mice, which express HMGCR (TM1-8) in liver, revealed that cholesterol feeding caused the protein to disappear from hepatic membranes (Fig. 9A). Conversely, HMGCR (TM1-8) accumulated in hepatic membranes when diets were supplemented with the HMGCR inhibitor lovastatin to deplete cholesterol (Fig. 11A and 11C). Importantly, mRNA encoding HMGCR (TM1-8) remained unchanged, regardless of feeding regimen (Fig. 9B and 11B). Together, these results indicate that changes in expression of HMGCR (TM1-8) protein upon cholesterol and lovastatin feeding resulted from sterol-mediated modulation of its degradation.

Knock-in mice expressing ubiquitination-resistant HMGCR accumulated significant amounts of the protein in liver and other tissues, even though levels of HMGCR mRNA were reduced (Fig. 7A and 8A). The decline in HMGCR mRNA can be attributed to

reduced levels of nuclear SREBP-2 (Fig. 7B), owing to accumulation of cholesterol (Fig. 6). In contrast, levels of nuclear SREBP-1 were elevated in livers of *Hmgcr* knock-in mice, which likely results from activation of LXRs in response to cholesterol accumulation. HMGCR protein also accumulates disproportionately to its mRNA in livers of mice deficient in gp78 (27), a ubiquitin ligase that facilitates HMGCR ubiquitination. However, it should be noted that levels of Insig-2 and, to a lesser extent, Insig-1 protein are increased in gp78-deficient livers. As a result, processing of both SREBP-1 and SREBP-2 is inhibited. Thus, changes in cholesterol metabolism observed in gp78-deficient livers cannot be solely attributed to defects in degradation of HMGCR.

Fig. 6 shows that while levels of free and unesterified cholesterol were elevated in livers of *Hmgcr* knock-in mice, incorporation of ^{3}H-labeled water into sterols was unchanged. This discrepancy could be explained in part, by increases in some of the sterol intermediates, which could contribute to the increase observed in ^{3}H-labeled water studies that measure synthesis of all digitonin-precipitable sterols. It should be noted that accumulation of sterol intermediates has also been observed in Insig-deficient mice and interferes with normal fusion of midline facial structures, producing cleft palate (62). The exact mechanism whereby these sterol intermediates accumulate is unknown and merits further investigation.

Experiments in which cholesterol levels were modulated by diet were conducted to examine the role of sterol-regulated ubiquitination and degradation of HMGCR in regulation of cholesterol homeostasis. When normalized to its cognate mRNA, the relative amount of HMGCR protein was reduced by ≈70% in livers of WT mice subjected to

cholesterol feeding (Fig. 9D). However, mRNA-normalized HMGCR protein was reduced by less than 30% in livers of cholesterol-fed *Hmgcr* knock-in mice, indicating resistance to sterol-accelerated degradation. Despite this resistance, the absolute amount of HMGCR protein in knock-in mouse livers was markedly diminished by cholesterol feeding, which was accompanied by a similar reduction in HMGCR mRNA. Thus, it can be concluded that feeding mice high levels of cholesterol reduces HMGCR levels primarily through reduced transcription of the HMGCR gene resulting from sterol-mediated inhibition of SREBP-2 activation. Cholesterol depletion studies show that lovastatin-induced accumulation of HMGCR protein was blunted in *Hmgcr* knock-in mice compared to their WT littermates (Fig. 11D). This indicates that inhibition of degradation significantly contributes to the increase in HMGCR protein that occurs upon lovastatin treatment, which not only depletes sterols, but also nonsterol isoprenoids that modulate HMGCR degradation (16). Taken together, results of Fig. 9D and 11D reveal that sterol-induced ubiquitination and degradation plays a direct and significant role in feedback regulation of HMGCR and cholesterol homeostasis *in vivo*.

An unexpected result was obtained when Tg-HMGCR (TM1-8) and *Hmgcr* knock-in mice were subjected to a fasting and refeeding regimen. Fasting, which lowers plasma insulin, inhibited activation of SREBPs as indicated by the fall in nuclear SREBP-1 and SREBP-2 as well as mRNA and protein for SREBP targets Insig-1 and HMGCR (Fig. 13 and 14). In contrast to results with endogenous HMGCR, fasting failed to accelerate degradation of HMGCR (TM1-8) (Fig. 13B). This observation is substantiated by results with *Hmgcr* knock-in mice, which show that fasting reduced mRNA encoding endogenous

HMGCR, but did not accelerate degradation of HMGCR protein (Fig. 13D). Thus, fasting appears to represent a condition under which transcription of the HMGCR gene and degradation of HMGCR protein are uncoupled. This uncoupling could, in part, result from a fasting-induced post-translational modification that prevents incorporation of Scap and its bound SREBP into COPII vesicles destined for the Golgi. Alternatively, the uncoupling of ER to Golgi transport of Scap and accelerated degradation of reductase may result from differential affinity of the two proteins for Insigs whose levels are reciprocally regulated during fasting. It will be important in future studies to appraise these notions and determine the underlying basis for uncoupling of transcriptional and post-transcriptional regulation of HMGCR during fasting.

The importance of the regulatory system that governs feedback regulation of reductase is highlighted by the widespread use of statins to lower plasma levels of LDL-cholesterol and reduce the incidence of atherosclerosis and associated cardiovascular disease (47). However, statins inhibit production of sterol and nonsterol isoprenoids that mediate feedback regulation of reductase. Animals and humans respond to this inhibition by developing high levels of reductase in the liver (63, 64), prompting the need for high levels of the drugs to maintain reductase inhibition and cholesterol-lowering. The current analysis of Tg-HMGCR (TM1-8) and *Hmgcr* knock-in mice provides direct evidence that sterol-accelerated degradation significantly contributes to feedback regulation of HMGCR. These novel animal models may prove useful in development of new drugs that accelerate HMGCR degradation, thereby preventing the accumulation of the enzyme associated with

statin therapy. These new drugs may improve the effectiveness of statins or provide alternative therapies.

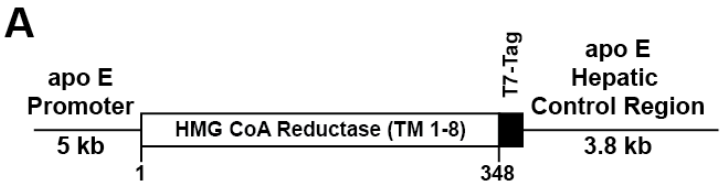
A
apo E
Promoter
5 kb
HMG CoA Reductase (TM 1-8)
T7-Tag
apo E
Hepatic
Control Region
3.8 kb
1
348

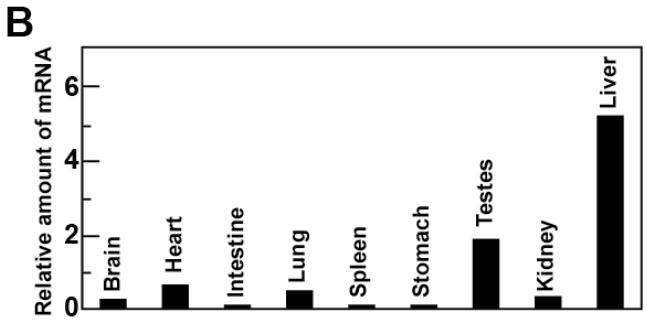
B
Relative amount of mRNA
0
2
4
6
Brain
Heart
Intestine
Lung
Spleen
Stomach
Testes
Kidney
Liver

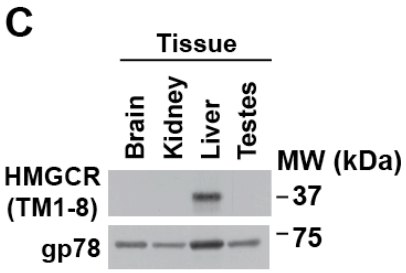
C
Tissue
Brain
Kidney
Liver
Testes
HMGCR
(TM1-8)
gp78
MW (kDa)
37
75

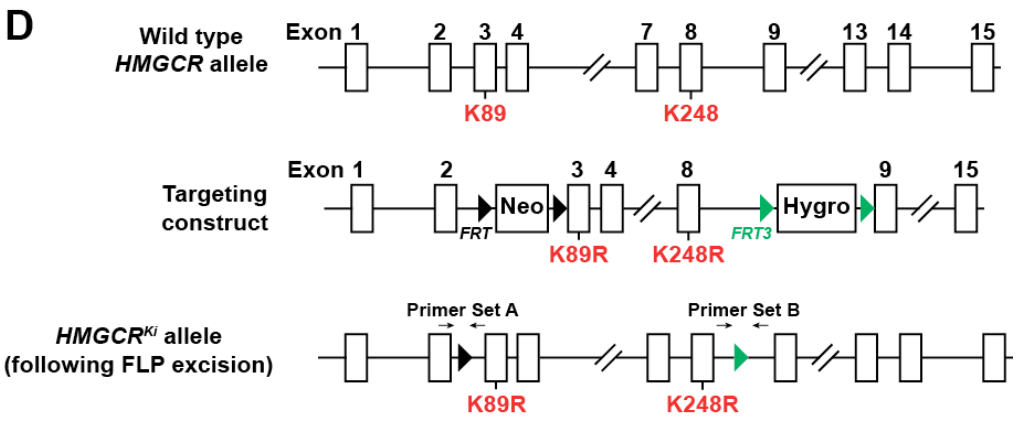
D
Wild type
HMGCR allele
Exon 1
2
3
4
7
8
9
13
14
15
K89
K248
Targeting
construct
Neo
FRT
Hygro
FRT3
K89R
K248R
HMGCR^Ki allele
(following FLP excision)
Primer Set A
Primer Set B

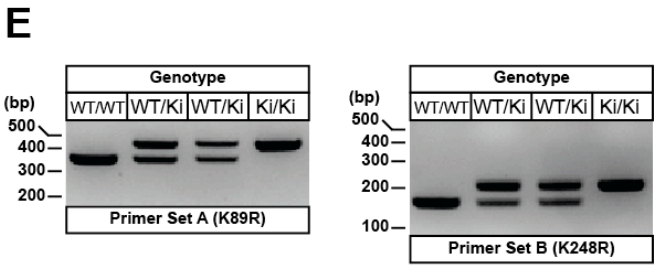
E
Genotype
WT/WT
WT/Ki
WT/Ki
Ki/Ki
(bp)
500
400
300
200
Primer Set A (K89R)
100
Primer Set B (K248R)

Figure 5. Generation of Tg-HMGCR (TM1-8) mice expressing HMGCR (TM1-8) in the liver and *Hmgcr* knock-in mice expressing ubiquitination-resistant HMGCR. (A) Schematic of transgenic construct used to generate Tg-HMGCR (TM1-8) mice. The transgenic construct contains a cDNA fragment encoding transmembrane domains 1-8 (corresponding to amino acids 1-348) of hamster HMG CoA reductase followed by three copies of the T7 epitope under control of the human apoE promoter and its hepatic control region. (B) Total RNA extracted from the indicated tissues of four male Tg-HMGCR (TM1-8) mice (12-14 weeks of age) fed ad libitum a chow diet was pooled and subjected to quantitative RT-PCR using transgene-specific primers as described in "Materials and Methods." The relative amount of transgene mRNA was calculated using the comparative threshold cycle (C_T) method and the mouse glyceraldehyde 3-phosphate dehydrogenase mRNA as an invariant control. (C) Detergent lysates of the indicated tissue from the same animals used in (B) were prepared and pooled as described in "Materials and Methods." Aliquots of pooled lysates (45 μg protein/lane) were subjected to SDS-PAGE and immunoblot analysis was carried out with anti-T7 IgG (against HMGCR (TM1-8)) and anti-gp78 IgG. (D) Targeting strategy for constructing the *Hmgcr* knock-in allele harboring mutations of lysines-89 (K89R) and -248 (K248R) to arginine. Flippase recognition target (FRT) sites and FRT3 sites are indicated by small black and green triangles, respectively. Neo, neomycin resistance gene; Hygro, hygromycin resistance gene. The location of two primer sets used for genotyping is denoted by arrows. (E) Genomic DNA isolated from the tails of mice of the indicated genotype were amplified by PCR using primer set A and primer set B and fractionated on 2 % agarose gels. Bands corresponding to the K89R and K248R alleles were visualized by staining of gels with ethidium bromide.

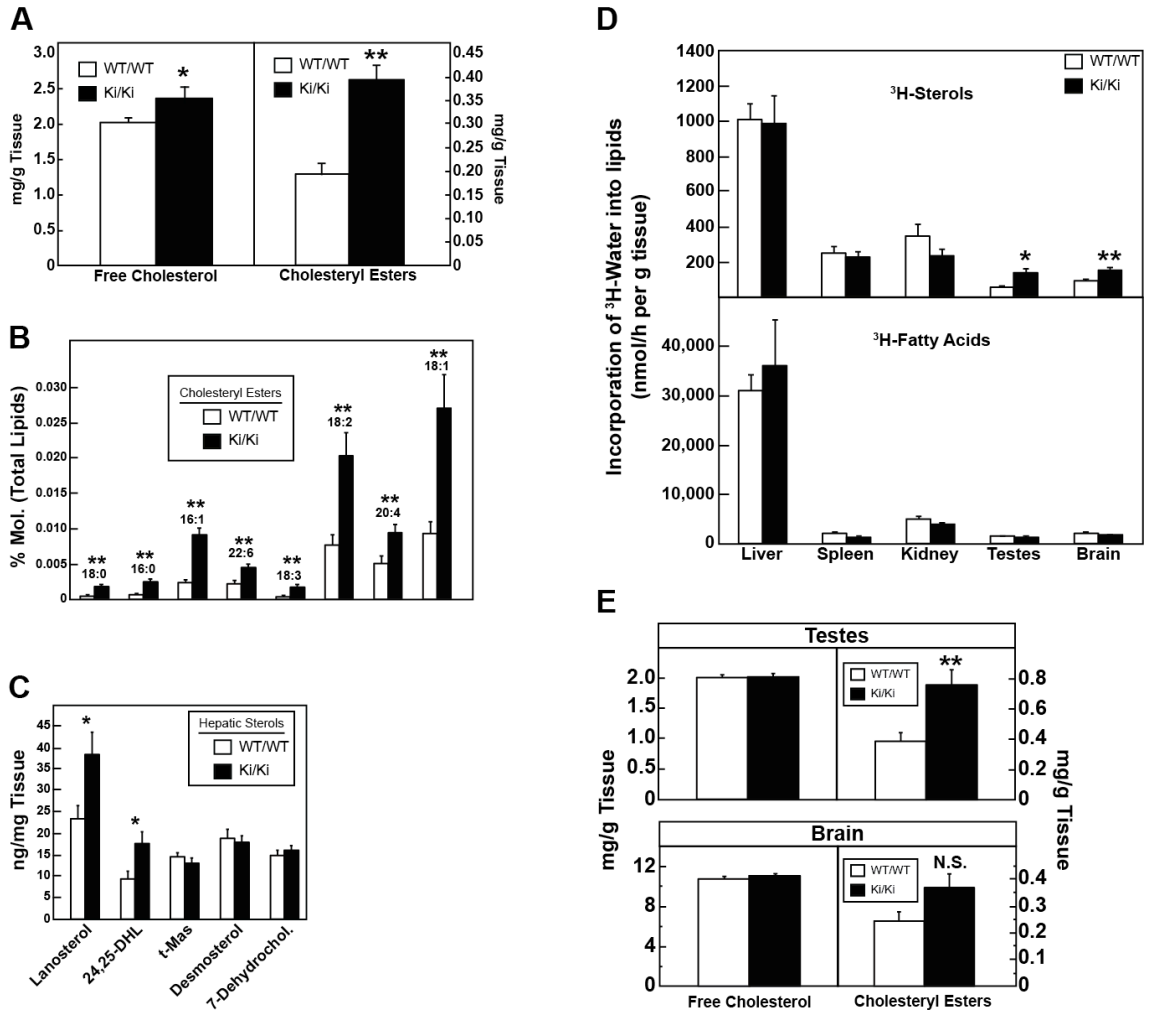

Figure 6. Analysis of cholesteryl esters, cholesterol biosynthetic intermediates, and sterol synthesis in WT and *Hmgcr* knock-in mice. Male mice (6-8 weeks of age, 5 or 6 per group) were fed ad libitum a chow diet prior to study. Livers (A-C) or brains and testes (E) were collected and the amounts of free cholesterol, cholesteryl esters, and cholesterol biosynthetic intermediates were determined by colorimetric assay (A and E) or by LC-MS/MS (C) as described in "Materials and Methods." Error bars indicate ± S.E.. (D) Male mice (6-8 weeks of age, 5 or 6 per group) were fed chow diet ad libitum and injected intraperitoneally with ^{3}H-labeled water (50 mCi in 0.2 ml of isotonic saline). One hour later, tissues were removed for measurement of ^{3}H-labeled fatty acids and digitonin-precipitable sterols. Each bar represents the mean ± S.E. of the values from 5 or 6 mice. 24,25-DHL, 24,25-dihydrolanosterol; t-MAS, testis-specific meiosis-activating sterol; 7-Dehydrochol., 7-dehydrocholesterol. *, $p<0.05$; **, $p<0.01$.

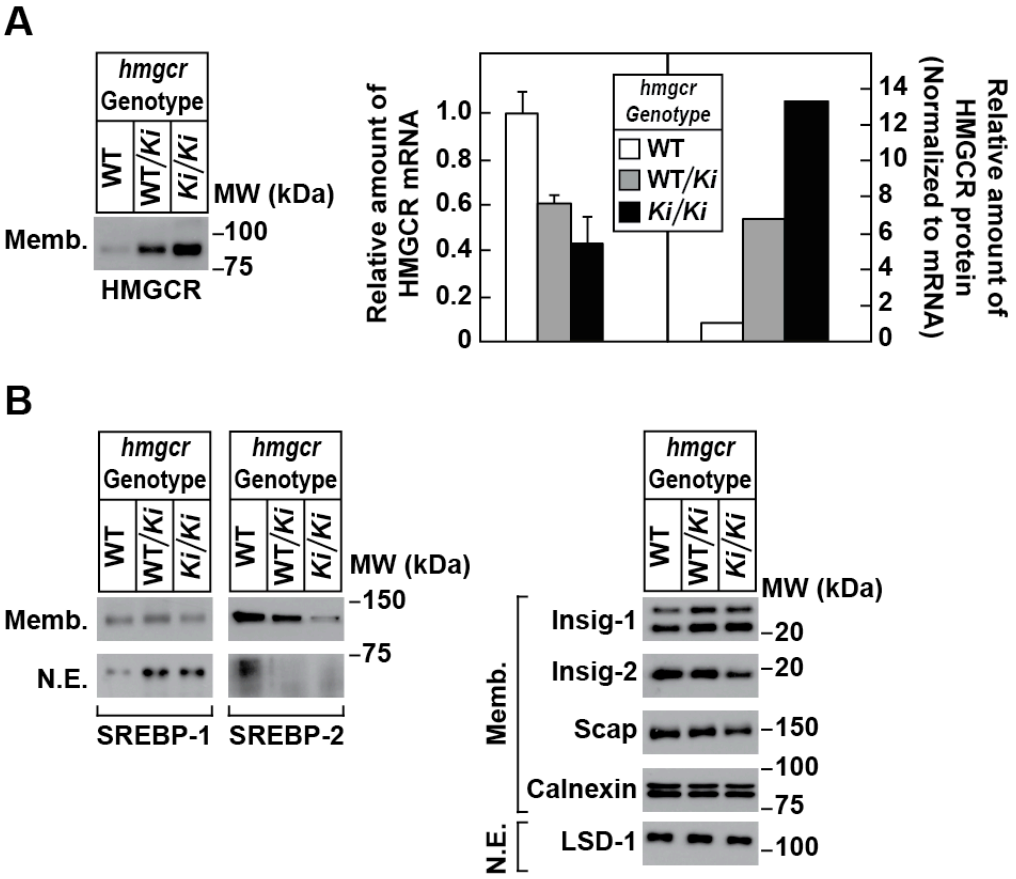

Figure 7. Levels of endogenous HMGCR in livers of WT and *Hmgcr* knock-in mice. Male WT, *Hmgcr*$^{WT/Ki}$, and *Hmgcr*$^{Ki/Ki}$ littermates (13 weeks of age, 4 per group) were fed an ad libitum chow diet prior to study. Livers of mice were subjected to subcellular fractionation as described in "Materials and Methods." Aliquots of resulting membrane (Memb., 30 μg protein/lane) and nuclear extract (N.E., 20-50 μg protein/lane) fractions for each group were pooled and subjected to immunoblot analysis using antibodies against endogenous HMGCR, SREBP-1, SREBP-2, Insig-1, Insig-2, Scap, calnexin, and LSD-1. Although shown in separate panels, Scap and calnexin serve as loading controls for the HMGCR immunoblot. For mRNA analysis (A), equal amounts of RNA from individual mice were subjected to quantitative RT-PCR using primers against the HMGCR mRNA and apoB mRNA as an invariant control. The relative amount of HMGCR protein in *Hmgcr* knock-in mice was determined by quantifying the band corresponding to HMGCR using Image J software and normalizing it to the amount of HMGCR mRNA.

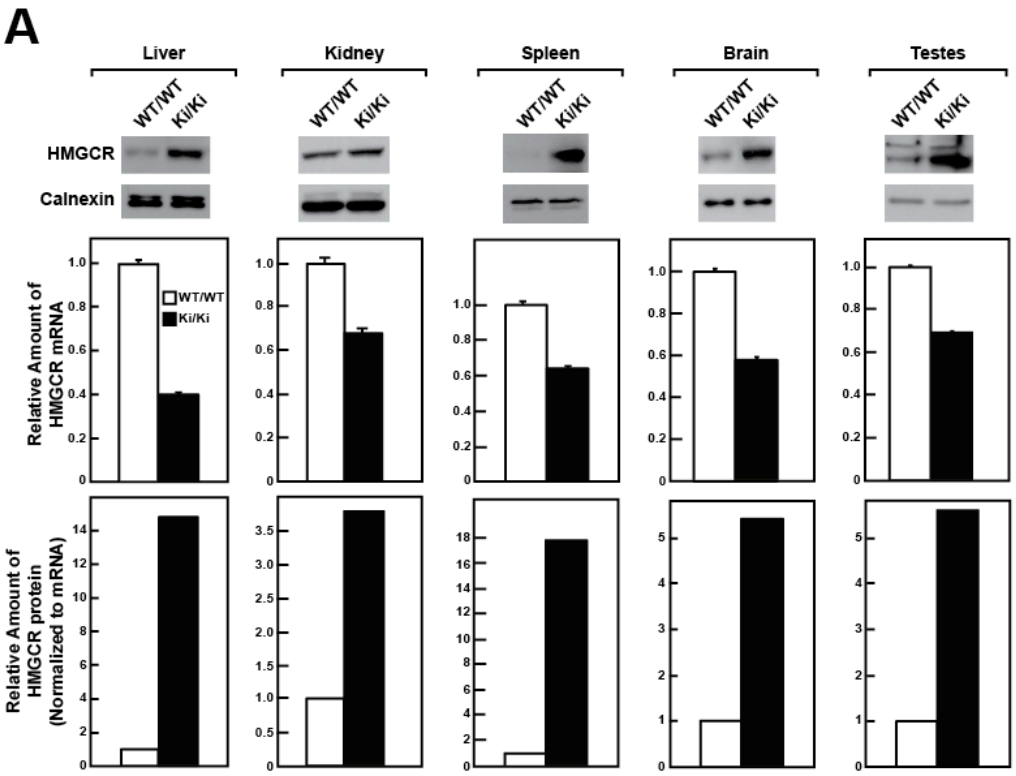
A
Liver
Kidney
Spleen
Brain
Testes
WT/WT
Ki/Ki
HMGCR
Calnexin
Relative Amount of HMGCR mRNA
Relative Amount of HMGCR protein (Normalized to mRNA)

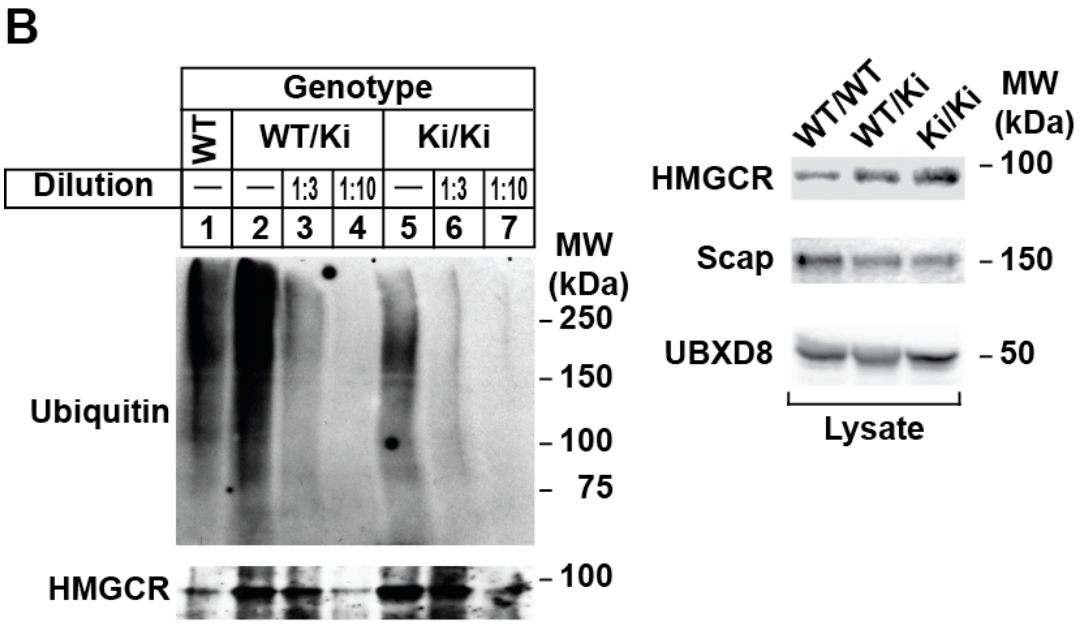
B
Genotype
WT
WT/Ki
Ki/Ki
Dilution
—
1:3
1:10
1
2
3
4
5
6
7
MW (kDa)
250
150
100
75
Ubiquitin
HMGCR
WT/WT
WT/Ki
Ki/Ki
Scap
UBXD8
50
Lysate

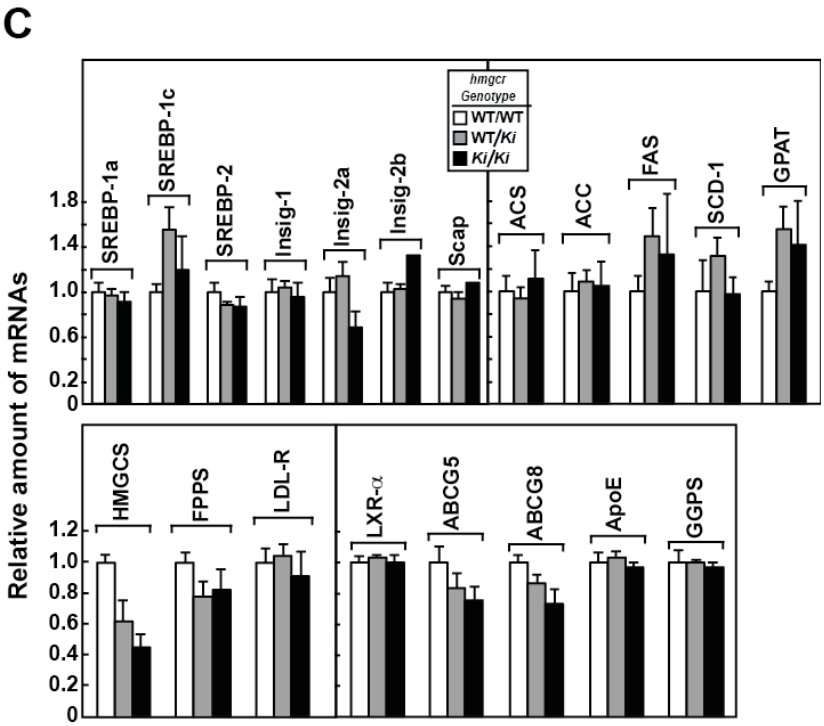

Figure 8. Hepatic HMGCR accumulates in tissues of *Hmgcr* knock-in mice, owing to resistance to ubiquitination. (A) Membrane extract fractions were obtained from liver, kidney, spleen, brain, and testis of six- to seven-week-old male WT and $Hmgcr^{Ki/Ki}$ mice fed an ad libitum chow diet (5 mice per group). Aliquots of membrane extract fractions for each group were pooled and subjected to immunoblotting (30 μg/lane) for HMGCR and calnexin (top). Total RNA from each tissue was reverse-transcribed and aliquots of cDNA were pooled for each group. cDNA was subjected to quantitative RT-PCR as indicated in "Materials and Methods" (middle). The relative amount of HMGCR protein was obtained as described in the legend to Fig. 7 (bottom). Each bar represents the mean ± S.E. of triplicate samples. (B) Eight- to ten-week-old male WT, $Hmgcr^{WT/Ki}$, and $Hmgcr^{Ki/Ki}$ littermates (four per group) were fed an ad libitum chow diet prior to study. Aliquots of liver lysates for each group were pooled and immunoprecipitated with anti-HMGCR polyclonal antibodies and immunoblotted for ubiquitin or HMGCR (left). To adjust the amount of HMGCR protein subjected to immunoprecipitation, liver lysates were diluted as indicated. Ten percent of the lysates were subjected to immunoblotting for HMGCR, Scap, and UBXD8 (right). (C) Total RNA from livers of mice used in Fig. 7 was separately isolated. Equal amounts of RNA from individual mice were subjected to quantitative RT-PCR using apoB mRNA as an invariant control. Each value represents the amount of mRNA relative to that in WT mice, which was arbitrarily set as 1. Each bar represents the mean ± S.E. of data from 5 mice. ApoE, apolipoprotein E; FPPS, farnesyl pyrophosphate synthase; HMGCS, HMG coenzyme A synthase; LDL-R, LDL-receptor; FAS, fatty acid synthase; SCD-1, stearoyl coenzyme A desaturase-1; GGPS, geranylgeranyl pyrophosphate synthase; GPAT, glycerol-3-phosphate acyltransferase; ACS, acetyl coenzyme A

synthetase; ACC, acetyl coenzyme A carboxylase; ABCG5 and ABCG8, ATP-binding cassette sub-family G member 5 and 8.

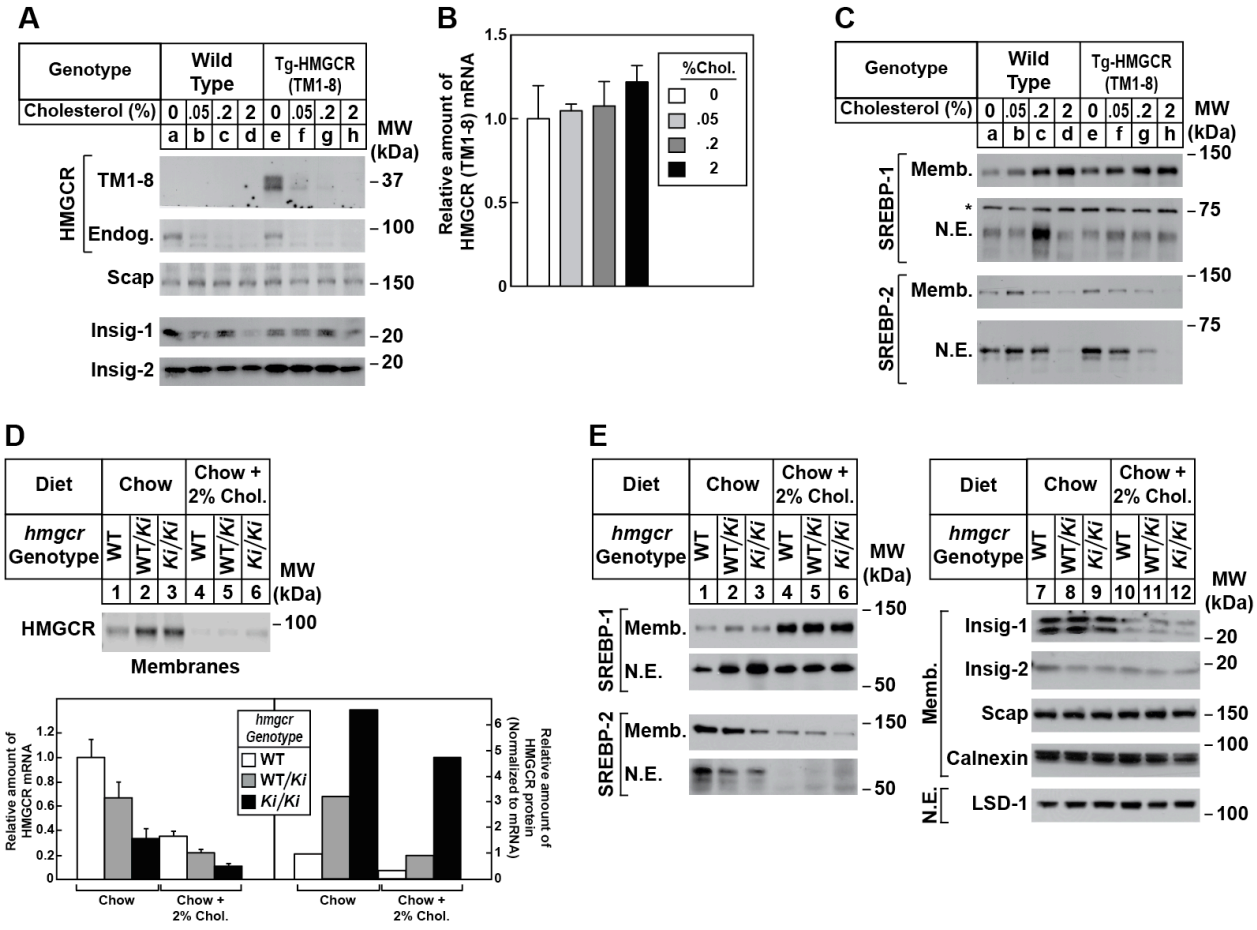

Figure 9. Dietary cholesterol suppresses expression of HMGCR (TM1-8) in Tg-HMGCR (TM1-8) mouse livers and endogenous HMGCR in *Hmgcr* knock-in mouse livers. (A-C) Male mice (6-8 weeks of age, four per group) were fed an ad libitum chow diet supplemented with the indicated amount of cholesterol for 5 days. (A and C) Aliquots of membrane (Memb.) and nuclear extract (N.E.) fractions from homogenized livers (10-30 μg total protein/lane) were analyzed by immunoblot analysis with anti-T7 IgG (against HMGCR (TM1-8)) and antibodies against the indicated proteins. (B) Equal amounts of RNA from the individual mice used in (A and C) were subjected to quantitative RT-PCR using primers against the HMGCR (TM1-8) mRNA; apoB mRNA was used as an invariant control. Values represent the amount of HMGCR (TM1-8) mRNA relative to that in transgenic mice fed a chow diet, which is arbitrarily defined as 1. Bars represent the mean ± S.E. of data from 4 mice. Asterisk denotes a non-specific cross-reactive band. (D and E) Male WT, *Hmgcr*$^{WT/Ki}$, and *Hmgcr*$^{Ki/Ki}$ littermates (6-8 weeks of age, 4 per group) were fed an ad libitum chow diet supplemented with 2% cholesterol as indicated for 5 days. Aliquots of membrane (Memb., 30 μg protein/lane) and nuclear extract (N.E., 20-50 μg protein/lane) fractions from homogenized livers were analyzed by immunoblot as described in the legend to Fig. 7. Although shown in separate panels, Scap and calnexin serve as loading controls for the HMGCR immunoblot. For mRNA analysis (*D*), equal amounts of RNA

from individual mice were subjected to quantitative RT-PCR as described in the legend to Fig. 7A. Values represent the amount of mRNA relative to that in WT mice, which was arbitrarily set as 1. Bars represent the mean ± S.E. of data from 4 mice. The relative amount of HMGCR protein in *Hmgcr* knock-in mice was determined as described in the legend to Fig. 7. Metabolic parameters for cholesterol-fed WT and *Hmgcr* knock-in mice are provided in Table 2.

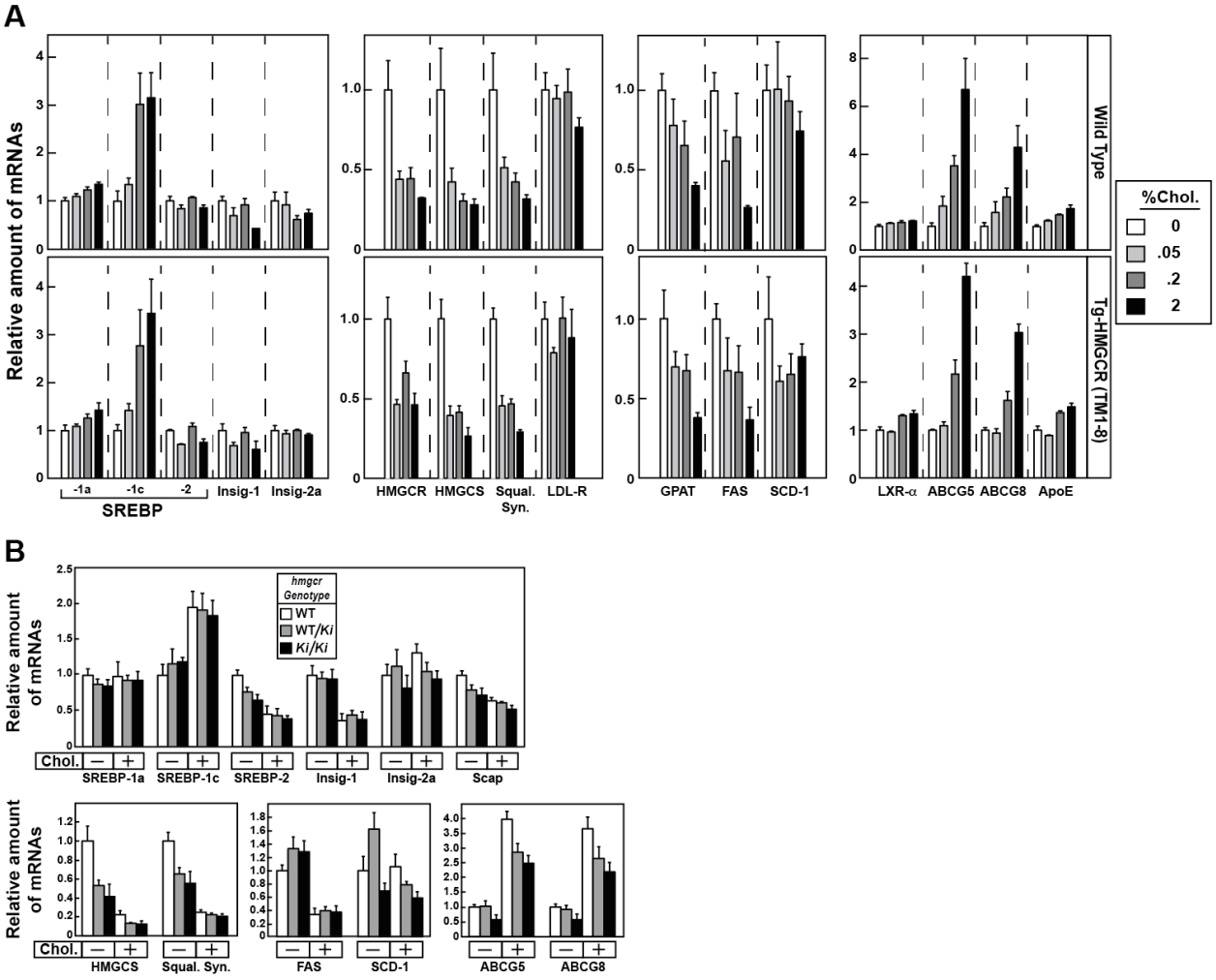

Figure 10. Effect of dietary cholesterol on expression of mRNAs encoding components of the Scap-SREBP pathway in livers of Tg-HMGCR (TM1-8) and *Hmgcr* knock-in mice. Total RNA from livers of mice used in Fig. 8A and 9D (4 mice/group) was separately isolated. Equal amounts of RNA from the individual mice were subjected to quantitative RT-PCR using primers against the indicated gene; apoB mRNA was used as an invariant control. Each value represents the amount of mRNA relative to that in WT and transgenic mice (A) or WT mice (B) fed a chow diet, which is arbitrarily defined as 1. Bars represent the mean ± S.E. of data from 4 mice. Squal. Syn., squalene synthase.

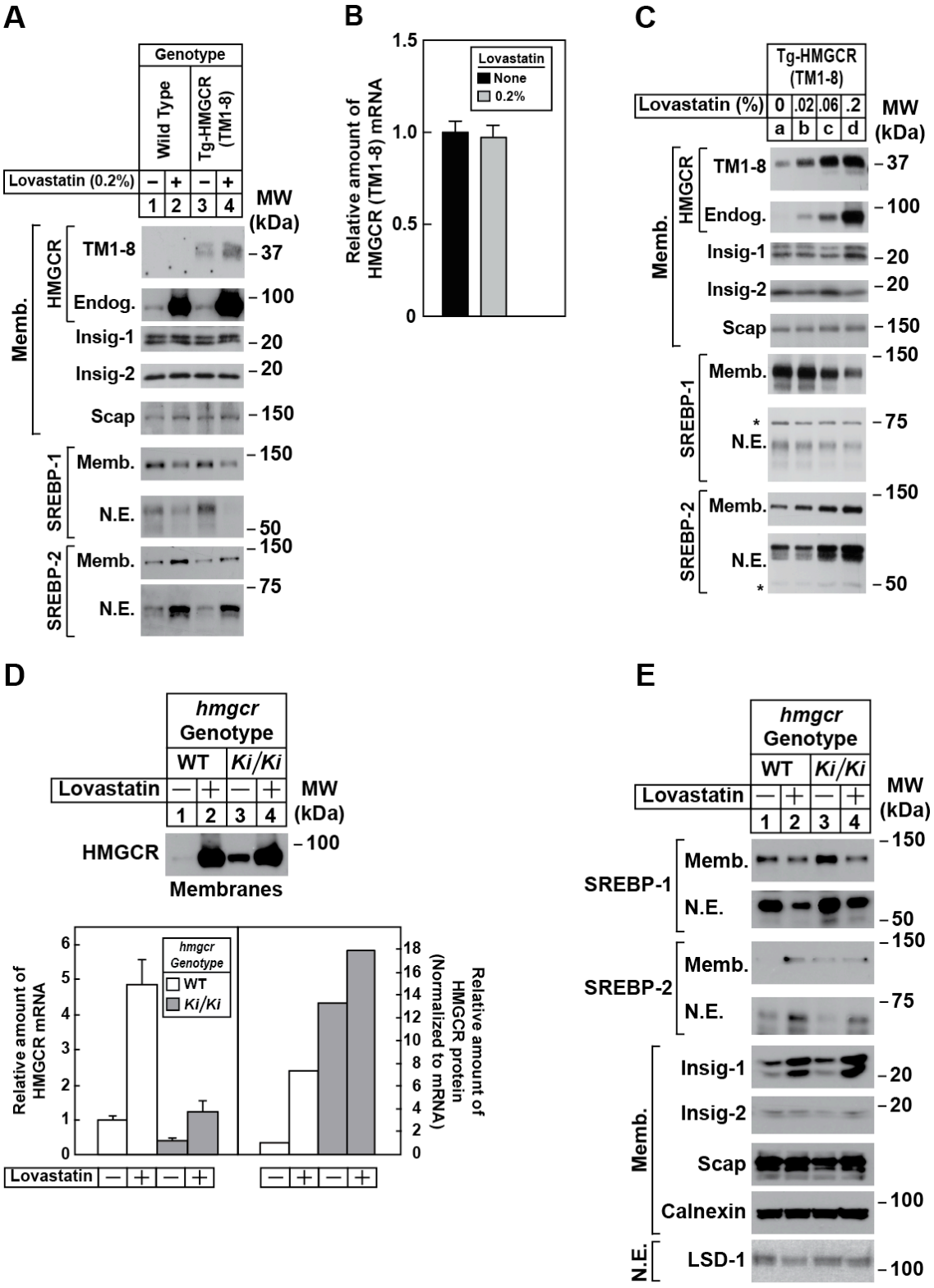
A
Genotype
Wild Type
Tg-HMGCR (TM1-8)
Lovastatin (0.2%)
MW (kDa)
Memb.
HMGCR
TM1-8
Endog.
Insig-1
Insig-2
Scap
SREBP-1
Memb.
N.E.
SREBP-2
Memb.
N.E.
B
Relative amount of HMGCR (TM1-8) mRNA
Lovastatin
None
0.2%
C
Tg-HMGCR (TM1-8)
Lovastatin (%)
MW (kDa)
D
hmgcr Genotype
WT
Ki/Ki
Lovastatin
MW (kDa)
HMGCR
Membranes
Relative amount of HMGCR mRNA
Relative amount of HMGCR protein (Normalized to mRNA)
E
hmgcr Genotype
WT
Ki/Ki
Lovastatin
MW (kDa)
SREBP-1
SREBP-2
Memb.
N.E.
Insig-1
Insig-2
Scap
Calnexin
LSD-1

Figure 11. Cholesterol deprivation enhances expression of HMGCR (TM1-8) in livers of transgenic mice and endogenous HMGCR in livers of *Hmgcr* knock-in mice. (A – C) Male mice (6-8 weeks of age, five mice per group in A and B or three mice per group in C) were fed an ad libitum chow diet in absence or presence of the indicated concentration of lovastatin for 5 days. (A and C) Aliquots of membrane and nuclear extract fractions (10-30 μg protein/lane) from homogenized livers were analyzed by immunoblot as described in the legend to Fig. 9A and 9C. Asterisks denote nonspecific cross-reactive bands. Equal amounts of RNA from individual mice used in (A) were subjected to quantitative RT-PCR as described in the legend to Fig. 9B. Values represent the amount of HMGCR (TM1-8) mRNA relative to that in chow-fed transgenic mice, which is arbitrarily defined as 1. Bars represent the mean ± S.E. of data from 5 mice. (D and E) Male WT and $Hmgcr^{Ki/Ki}$ littermates (6-8 weeks of age, 4 per group) were fed an ad libitum chow diet in absence or presence of 0.2% lovastatin for 5 days. Aliquots of membrane (Memb., 30 μg protein/lane) and nuclear extract (N.E., 20-50 μg protein/lane) fractions from homogenized livers were analyzed by immunoblot as described in the legend to Fig. 7. Although shown in separate panels, Scap and calnexin serve as loading controls for the HMGCR immunoblot. For mRNA analysis (D), equal amounts of RNA from individual mice were subjected to quantitative RT-PCR as described in the legend to Fig. 7A. Values represent the amount of mRNA relative to that in WT mice, which was arbitrarily set as 1. Bars represent the mean ± S.E. of data from 4 mice. The relative amount of HMGCR protein in *Hmgcr* knock-in mice was determined as described in the legend to Fig. 7. Metabolic parameters for lovastatin-fed WT and *Hmgcr* knock-in mice are provided in Table 3.

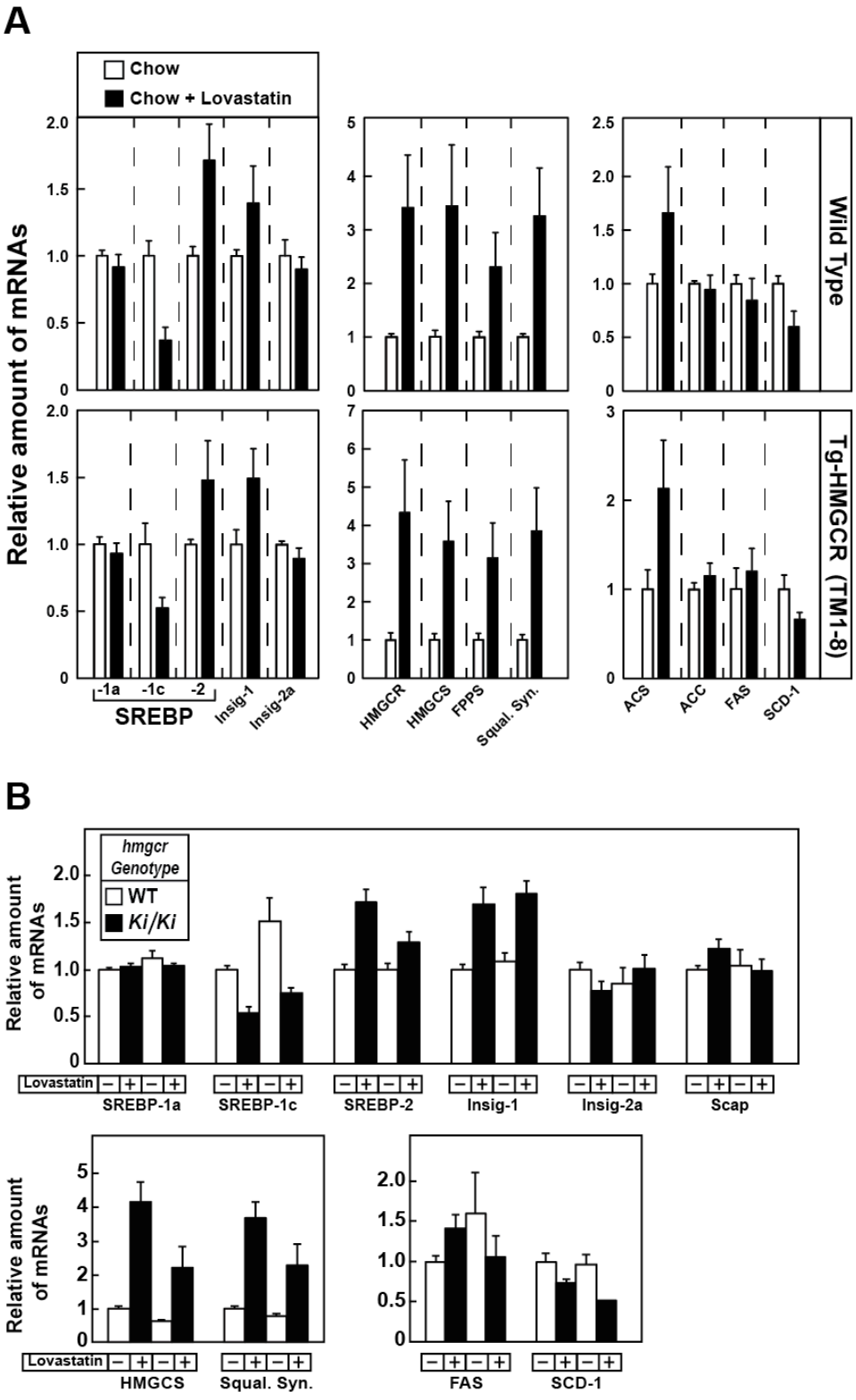
A
Chow
Chow + Lovastatin
Relative amount of mRNAs
Wild Type
Tg-HMGCR (TM1-8)
-1a
-1c
-2
SREBP
Insig-1
Insig-2a
HMGCR
HMGCS
FPPS
Squal. Syn.
ACS
ACC
FAS
SCD-1
B
hmgcr Genotype
WT
Ki/Ki
Relative amount of mRNAs
Lovastatin
SREBP-1a
SREBP-1c
SREBP-2
Insig-1
Insig-2a
Scap
HMGCS
Squal. Syn.
FAS
SCD-1

Figure 12. Effect of cholesterol deprivation on expression of mRNAs encoding components of the Scap-SREBP pathway in livers of Tg-HMGCR (TM1-8) and *Hmgcr* knock-in mice. Total RNA from livers of mice used in Fig. 11A and 11D (4 or 5 mice/group) was separately isolated. Equal amounts of RNA from the individual mice were subjected to quantitative RT-PCR using primers against the indicated gene; apoB mRNA was used as an invariant control. Each value represents the amount of mRNA relative to that in WT and transgenic mice (A) or WT mice (B) fed a chow diet, which is arbitrarily defined as 1. Bars represent the mean ± S.E. of data from 4 or 5 mice.

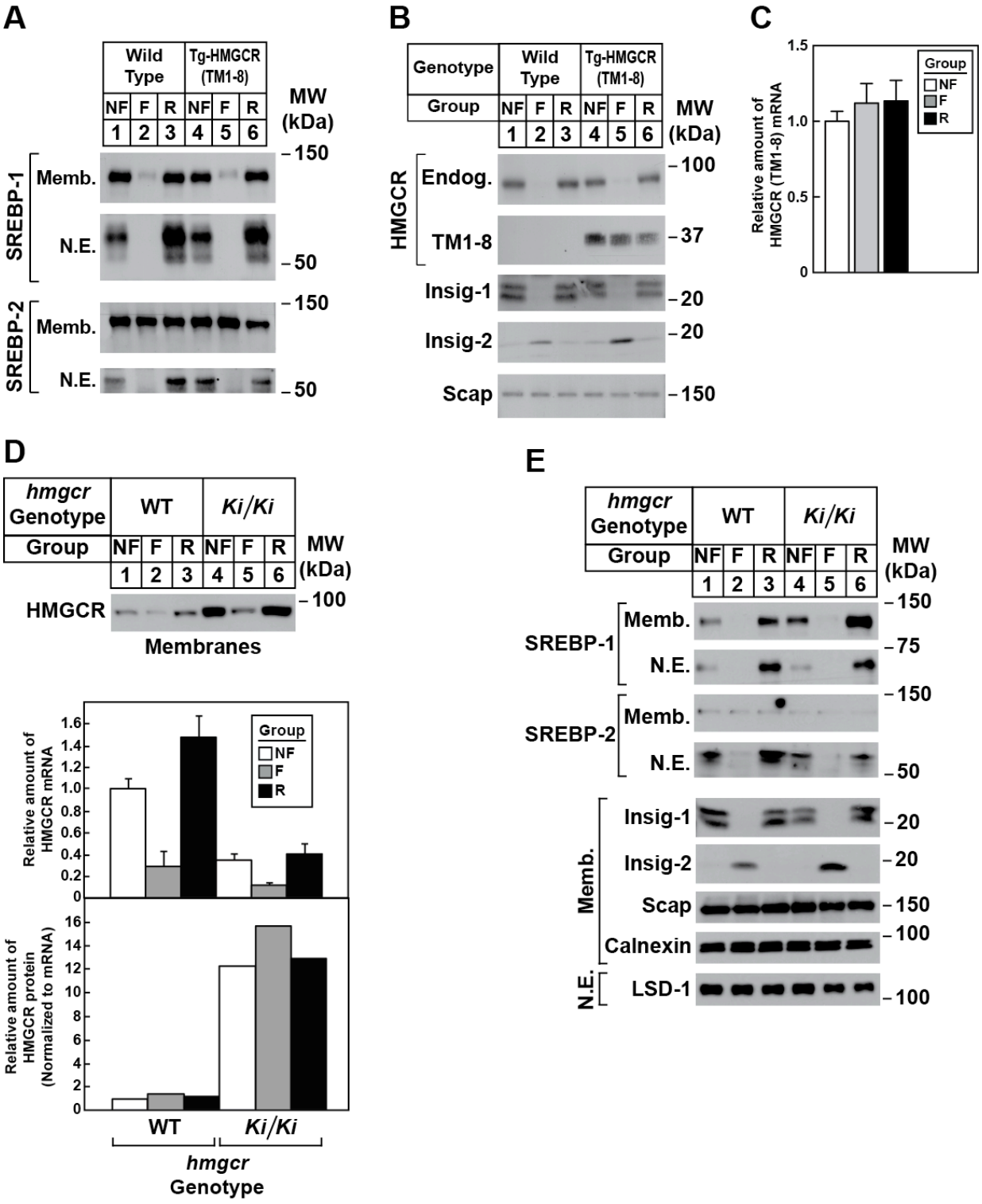
A
Wild Type
Tg-HMGCR (TM1-8)
NF F R NF F R
1 2 3 4 5 6
MW (kDa)
SREBP-1
Memb.
N.E.
SREBP-2
Memb.
N.E.
150
50
150
50
B
Genotype
Wild Type
Tg-HMGCR (TM1-8)
Group
NF F R NF F R
1 2 3 4 5 6
MW (kDa)
HMGCR
Endog.
TM1-8
Insig-1
Insig-2
Scap
100
37
20
20
150
C
Relative amount of HMGCR (TM1-8) mRNA
Group
NF
F
R
1.5
1.0
0.5
0
D
hmgcr Genotype
WT
Ki/Ki
Group
NF F R NF F R
1 2 3 4 5 6
MW (kDa)
HMGCR
100
Membranes
Relative amount of HMGCR mRNA
Group
NF
F
R
Relative amount of HMGCR protein (Normalized to mRNA)
WT
Ki/Ki
hmgcr Genotype
E
hmgcr Genotype
WT
Ki/Ki
Group
NF F R NF F R
1 2 3 4 5 6
MW (kDa)
SREBP-1
Memb.
N.E.
SREBP-2
Memb.
N.E.
150
75
150
50
Memb.
Insig-1
Insig-2
Scap
Calnexin
20
20
150
100
N.E.
LSD-1
100

Figure 13. Effect of fasting and refeeding on expression of HMGCR (TM1-8) in livers of transgenic mice and endogenous HMGCR in livers of *Hmgcr* knock-in mice. (A – C) Male WT and Tg-HMGCR (TM1-8) mice (6-8 weeks of age, 4 per group) were subjected to fasting and refeeding as described in "Materials and Methods." (A and B) Aliquots of membrane and nuclear extract fractions from homogenized livers (10-30 μg protein/lane) were analyzed by immunoblot as described in the legend to Fig. 9. (C) Equal amounts of RNA from individual mice used in (A and B) were subjected to quantitative RT-PCR as described in the legend to Fig. 9B. Values represent the amount of HMGCR (TM1-8) mRNA relative to that in chow-fed transgenic mice, which is arbitrarily defined as 1. Bars represent mean ± S.E. of data from 4 mice. Metabolic parameters of WT and Tg-HMGCR (TM1-8) mice subjected to fasting and refeeding are provided in Table 5. (D and E) Male WT and $Hmgcr^{Ki/Ki}$ littermates (6-8 weeks of age, 4 per group) were subjected to fasting and refeeding as described in (A). Aliquots of membrane (Memb., 30 μg protein/lane) and nuclear extract (N.E., 20-50 μg protein/lane) fractions from homogenized livers were subjected to immunoblot analysis as described in the legend to Fig. 7. Although shown in separate panels, Scap and calnexin serve as loading controls for the HMGCR immunoblot. Equal amounts of RNA from individual mice were subjected to quantitative RT-PCR as described in the legend to Fig. 7A. Values represent the amount of mRNA relative to that in WT nonfasted mice, which was arbitrarily set as 1. Bars represent the mean ± S.E. of data from 4 mice. The relative amount of HMGCR protein in *Hmgcr* knock-in mice was determined as described in Fig. 7. Metabolic parameters for fasted and refed WT and *Hmgcr* knock-in mice are provided in Table 5.

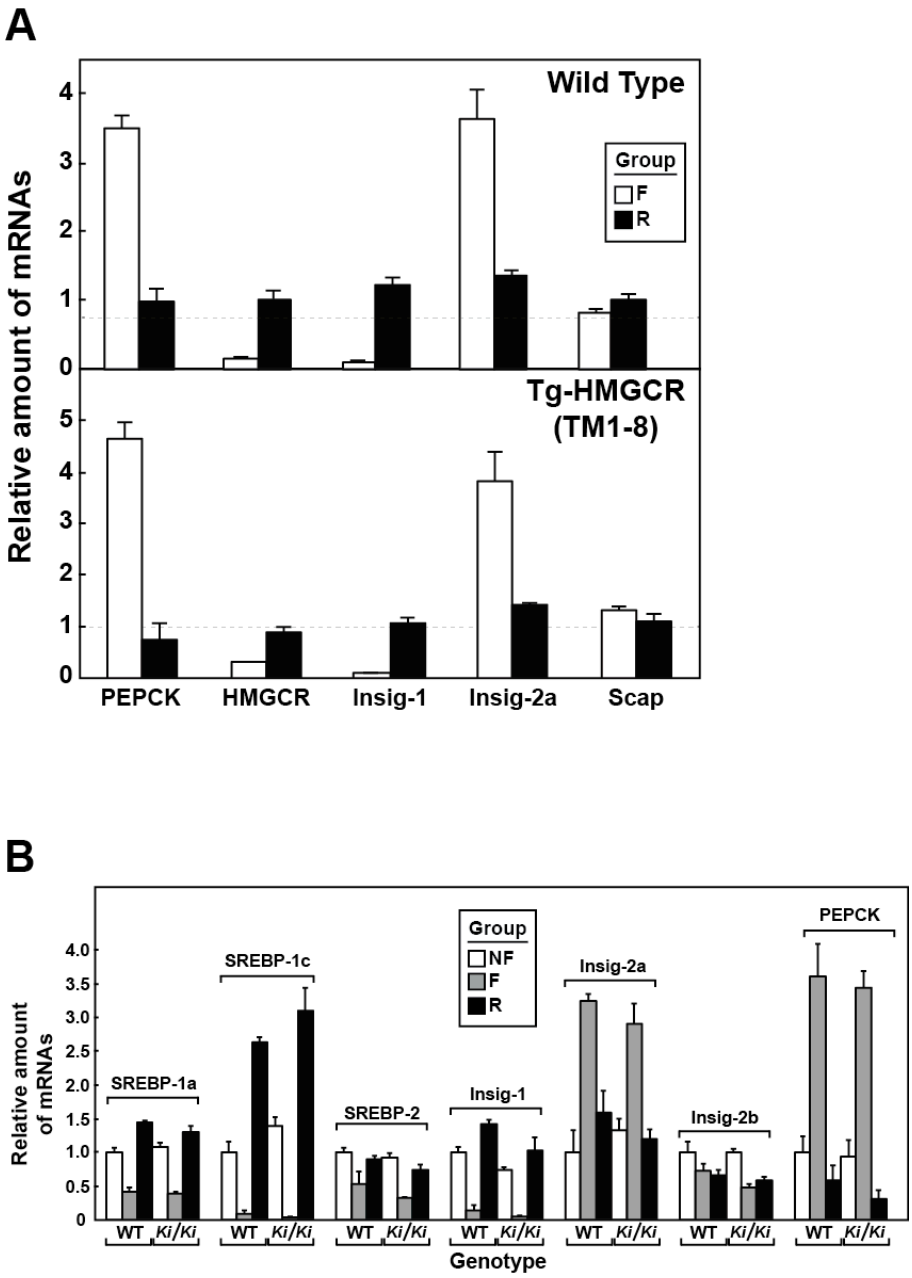

Figure 14. Effect of fasting and refeeding on expression of mRNAs encoding components of the Scap-SREBP pathway in livers of Tg-HMGCR (TM1-8) and *Hmgcr* knock-in mice. Total RNA from livers of mice used in Fig. 13A and 13D (4 mice/group) was separately isolated. Equal amounts of RNA from individual mice were subjected to quantitative RT-PCR using primers against the indicated gene; apoB mRNA was used as an invariant control. Each value represents the amount of mRNA relative to that in control, nonfasted mice, which was arbitrarily set as 1. Bars represent the mean ± S.E. of data from 4 mice. PEPCK, phosphoenolpyruvate carboxykinase.

Table 1. Comparison of lipid content between WT and *Hmgcr* knock-in mice.

A. Hepatic Neutral Lipids

Lipid Class	% Total Lipids	Fold Change*	p-Value	# Observed	# Changed
Neutral Lipid	61.5279	0.911	0.162	516	170
Triacylglycerols	61.3417	0.908	0.154	482	151
Diacylglycerols	0.1236	1.471	0.035	26	11
Cholesteryl esters	0.0625	2.704	0.004	8	8

*Fold changes are expressed as mean intensities obtained for knock-in mice divided by those obtained for WT counterparts.

B. Biliary Sterols

Sterol	WT	Knock-in	p-Value
Lanosterol	0.63 ± 0.13	1.21 ± 0.14	0.009
Lathosterol	0.16 ± 0.03	0.29 ± 0.04	0.015
Desmosterol	0.58 ± 0.05	1.05 ± 0.14	0.006
Cholesterol	116.39 ± 13.10	147.98 ±14.20	0.124
Camptosterol	7.44 ± 0.75	7.56 ± 0.87	0.922
Sitosterol	3.01 ± 0.38	2.87 ± 0.24	0.752

C. Fecal Sterols

Sterol	WT	Knock-in	p-Value
Lanosterol	114.56 ± 7.17	156.18 ± 6.76	0.001
Lathosterol	143.30 ± 24.82	216.47 ± 43.75	0.180
Desmosterol	34.01 ± 4.57	39.07 ± 3.95	0.412
Cholesterol	887.95 ± 67.74	1027.45 ± 60.17	0.143
Camptosterol	813.72 ± 21.94	855.08 ± 25.38	0.242
Sitosterol	2179.20 ± 72.10	2243.83 ± 137.54	0.694

Table 2. Comparison of WT and *Hmgcr* knock-in mice subjected to cholesterol feeding.

Parameter	WT (Chow)	WT (2% Chol.)	*Hmgcr*$^{WT/Ki}$ (Chow)	*Hmgcr*$^{WT/Ki}$ (2% Chol.)	*Hmgcr*$^{Ki/Ki}$ (Chow)	*Hmgcr*$^{Ki/Ki}$ (2% Chol.)
Body Weight (g)	25.9 ± 0.5	24.8 ± 1.0	25.2 ± 0.2	25.3 ± 0.6	25.2 ± 0.5	25.7 ± 0.8
Liver Weight (g)	1.38 ± 0.20	1.56 ± 0.10	1.32 ± 0.07	1.48 ± 0.03	1.41 ± 0.50	1.55 ± 0.06
Plasma Triglycerides (mg/dl)	127 ± 4	175 ± 13	173 ± 14	183 ± 7	142 ± 24	163 ± 11
Plasma Cholesterol (mg/dl)	104 ± 4	193 ± 3	128 ± 14	178 ± 8	116 ± 9	181 ± 6
Plasma Fatty Acids (mEq/L)	1.11 ± 0.06	1.24 ± 0.08	1.24 ± 0.08	1.31 ± 0.06	1.00 ± 0.07	1.33 ± 0.10
Liver Triglycerides (mg/g)	3.4 ± 0.6	25.2 ± 6.5	3.3 ± 0.4	22.1 ± 5.1	7.4 ± 3.1	22.2 ± 4.2
Liver Cholesterol (mg/g)	2.1 ± 0.1	9.7 ± 0.7	2.1 ± 0.1	10.5 ± 1.6	2.3 ± 0.1	11.2 ± 1.2

Male mice (8-10 weeks of age, 4 per group) were fed a chow diet in the absence or presence of 2% cholesterol (Chol.) for 5 days prior to study. WT mice were littermates of *Hmgcr*$^{WT/Ki}$ and *Hmgcr*$^{Ki/Ki}$ mice. Each value represents the mean ± S.E. of 4 values.

Table 3. Comparison of WT and *Hmgcr* knock-in mice subjected to lovastatin feeding.

Parameter	WT (Chow)	WT (0.2% Lov.)	$Hmgcr^{Ki/Ki}$ (Chow)	$Hmgcr^{Ki/Ki}$ (0.2% Lov.)
Body Weight (g)	20.2 ± 0.7	20.5 ± 0.8	20.4 ± 1.1	20.1 ± 0.3
Liver Weight (g)	1.16 ± 0.01	1.19 ± 0.04	1.33 ± 0.04	1.11 ± 0.03
Plasma Triglycerides (mg/dl)	135 ± 18	142 ± 11	140 ± 8	209 ± 34
Plasma Cholesterol (mg/dl)	99 ± 3	71 ± 5	115 ± 6	84 ± 12
Plasma Fatty acids (mEq/L)	1.04 ± 0.02	1.10 ± 0.14	1.08 ± 0.09	1.75 ± 0.61
Liver Triglycerides (mg/g)	5.6 ± 1.1	4.6 ± 0.4	7.1 ± 1.1	5.5 ± 0.7
Liver Cholesterol (mg/g)	2.0 ± 0.2	2.0 ± 0.2	2.2 ± 0.1	2.2 ± 0.2

Male mice (6-7 weeks of age, 4 per group) were fed a chow diet in the absence or presence of 0.2% lovastatin (Lov.) for 5 days prior to study. WT mice were littermates of $Hmgcr^{WT/Ki}$ and $Hmgcr^{Ki/Ki}$ mice. Each value represents the mean ± S.E. of 4 values.

Table 4. Comparison of WT and Tg-HMGCR (TM1-8) mice subjected to fasting and refeeding.

	WT			Tg-HMGCR (TM1-8)		
	Nonfasted	**Fasted**	**Refed**	**Nonfasted**	**Fasted**	**Refed**
Body Weight, Pre-Treatment (g)	25.0 ± 0.8	24.9 ± 1.2	24.9 ± 0.7	25.0 ± 0.5	24.8 ± 0.6	26.6 ± 0.4
Body Weight, Post-Treatment (g)	24.9 ± 0.6	22.7 ± 1.0	24.8 ± 0.8	26.1 ± 0.4	22.3 ± 0.8	26.9 ± 0.5
Liver Weight (g)	1.25 ± 0.13	1.11 ± 0.09	1.48 ± 0.10	1.41 ± 0.03	0.98 ± 0.06	1.75 ± 0.03
Liver Cholesterol (mg/g)	2.7 ± 0.1	2.8 ± 0.1	2.1 ± 0.0	2.3 ± 0.1	3.4 ± 0.0	2.2 ± 0.2
Liver Triglyceride (mg/g)	6.4 ± 1.1	39.1 ± 8.1	9.0 ± 1.8	6.8 ± 1.1	44.0 ± 4.9	9.1 ± 1.5
Plasma Fatty Acids (mEq/L)	0.49 ± 0.03	0.99 ± 0.16	0.41 ± 0.07	0.48 ± 0.11	0.90 ± 0.12	0.28 ± 0.02
Plasma Triglycerides (mg/dl)	236 ± 29	230 ± 20	263 ± 33	263 ± 12	219 ± 11	334 ± 15
Plasma Cholesterol (mg/dl)	113 ± 10	126 ± 6	109 ± 2	118 ± 11	127 ± 2	118 ± 3
Plasma Glucose (mg/dl)	152 ± 3	67 ± 9	133 ± 6	157 ± 5	69 ± 0	119 ± 4
Plasma Insulin (ng/ml)	2.35 ± 0.15	0.24 ± 0.04	2.74 ± 0.96	1.39 ± 0.12	0.24 ± 0.02	5.48 ± 0.48

Male mice (7-8 weeks of age) were subjected to fasting and refeeding as described in "Materials and Methods." WT mice were littermates Tg-HMGCR (TM1-8) mice. Each value represents the mean ± S.E. of 5 mice.

Table 5. Metabolic parameters of WT and *Hmgcr* knock-in mice subjected to fasting and refeeding.

	WT			*Hmgcr*$^{Ki/Ki}$		
	Nonfasted	**Fasted**	**Refed**	**Nonfasted**	**Fasted**	**Refed**
Liver Cholesterol (mg/g)	2.1 ± 0.1	3.5 ± 0.2	2.2 ± 0.1	2.5 ± 0.1	3.9 ± 0.1	2.5 ± 0.1
Liver Triglyceride (mg/g)	5.2 ± 2.1	33.1 ± 6.9	6.1 ± 0.6	3.7 ± 0.6	50.4 ± 3.2	5.1 ± 0.8
Plasma Fatty Acids (mEq/L)	0.64 ± 0.05	1.65 ± 0.30	0.40 ± 0.04	0.64 ± 0.01	1.76 ± 0.21	0.43 ± 0.08
Plasma Triglycerides (mg/dl)	182 ± 17	279 ± 27	206 ± 25	186 ± 10	211 ± 10	172 ± 19
Plasma Cholesterol (mg/dl)	127 ± 13	145 ± 11	87 ± 6	134 ± 12	144 ± 9	116 ± 9
Plasma Glucose (mg/dl)	113 ± 16	45 ± 11	83 ± 13	102 ± 7	44 ± 4	75 ± 9
Plasma Insulin (ng/ml)	0.70 ± 0.14	0.16 ± 0.03	1.82 ± 0.63	0.50 ± 0.90	0.21 ± 0.05	1.01 ± 0.26

Male mice (7-8 weeks of age) were subjected to fasting and refeeding as described in "Materials and Methods." WT mice were littermates of *Hmgcr*$^{WT/Ki}$ and *Hmgcr*$^{Ki/Ki}$ mice. Each value represents the mean ± S.E. of 4 mice.

CHAPTER THREE

Requirement of Insig-2 for Hypoxia-inducible Factor–Mediated Regulation of HMG CoA Reductase Degradation in the Liver

3.1. Introduction

A pair of ER-localized membrane proteins called Insig-1 and Insig-2 mediate two feedback regulatory mechanisms that converge on the ER membrane protein HMGCR, which catalyzes a rate-limiting step in synthesis of cholesterol and nonsterol isoprenoids including farnesyl pyrophosphate and geranylgeranyl pyrophosphate (11). One of these mechanisms involves the sterol-accelerated ERAD of HMGCR (16, 24). This ERAD is initiated by the intracellular accumulation of sterols such as the cholesterol biosynthetic intermediate 24,25-DHL (29, 65), which triggers binding of Insigs to the membrane domain of HMGCR (24). Insig-associated ubiquitin ligases subsequently facilitate ubiquitination of two cytosolically exposed lysine residues in the membrane domain of HMGCR (25, 26), marking it for membrane extraction and proteasome-mediated ERAD (33).

The second mechanism through which Insigs mediate feedback control of HMGCR involves modulating the activation of membrane-bound transcription factors called SREBPs (11). This activation requires the escort protein Scap, which mediates transport of SREBPs from the ER to Golgi for proteolytic release of transcriptionally active fragments from membranes. Upon release, these fragments migrate to the nucleus where they activate transcription of genes encoding HMGCR and other enzymes required for cholesterol

synthesis (21). Insigs inhibit the proteolytic activation of SREBPs through their sterol-induced binding to Scap. Insig binding traps Scap and its associated SREBP in the ER, thereby preventing access of SREBPs to Golgi-localized proteases (11). Thus, levels of mRNAs encoding SREBP target genes fall and cholesterol synthesis declines. Together, these Insig-mediated reactions (sterol-induced ER retention of Scap-SREBP and sterol-accelerated ERAD of HMGCR) ensure that cells maintain production of essential nonsterol isoprenoids, while avoiding over-accumulation of cholesterol or one of its sterol precursors.

The two Insig proteins share approximately 60% amino acid sequence identity and appear to be functionally redundant (14, 16, 46). Topology studies of Insig-1 indicate that the protein contains six transmembrane helices separated by short loops, with both the NH_2- and COOH-termini facing the cytosol (12). The degree of sequence similarity to Insig-1 indicates that Insig-2 is similarly oriented in ER membranes. Despite these similarities, Insig-1 and Insig-2 are differentially regulated in the mouse liver. The Insig-1 gene is a target gene of SREBP and its mRNA varies according to the amount of SREBP in the nucleus (14, 61). Two isoforms of Insig-2 mRNA, designated Insig-2a and Insig-2b, are expressed in the liver (14, 61). These isoforms are derived from a single Insig-2 gene and encode identical proteins. The nucleotide sequence of Insig-2a and Insig-2b mRNAs differ only in their non-coding first exons; Insig-2a contains exon 1a, whereas Insig-2b contains exon 1b. This difference results from transcription driven by alternative promoters, accounting for the differential regulation of Insig-2a and Insig-2b mRNAs. The Insig-2a mRNA is expressed exclusively in the liver, and its expression is repressed by

insulin. On the other hand, the Insig-2b transcript is expressed ubiquitously and its expression is not regulated by insulin.

The synthesis of one molecule of cholesterol from the precursor acetyl-CoA requires 11 molecules of dioxygen (37, 38) (Fig. 1). One molecule of dioxygen is required for the epoxidation of squalene, which is catalyzed by the enzyme squalene monooxygenase. Nine molecules of dioxygen are utilized by lanosterol 14-α demethylase and C4-methyl sterol oxidase in the successive removal of the 4α, 4β, and 14α methyl groups in lanosterol and 24,25-DHL. Finally, sterol 5-desaturase consumes one molecule of dioxygen in the reduction of lathosterol to 7-dehydrocholesterol. Previously, it was reported that oxygen deprivation (hypoxia) inhibits cholesterol synthesis and causes lanosterol and 24,25-DHL to accumulate in CHO cells (39). The accumulation of 24,25-DHL served as one signal for accelerated degradation of HMGCR, which ultimately reduces flux through early steps in cholesterol synthesis when oxygen is limiting. The second signal was provided by the hypoxic induction of Insigs through a reaction that required the oxygen-sensitive transcription factor HIF-1α (40, 41). The current study expands on these findings by demonstrating that Insig-2 is a *bona fide* HIF target gene in cultured cells and in livers of mice. Experiments utilizing genetically manipulated mice show that Insig-2-dependent degradation plays a highly significant role HIF-mediated regulation of hepatic HMGCR, highlighting the physiologic relevance of the response. Together, these findings confirm that the link between oxygen sensing and feedback mechanisms governing cholesterol synthesis extends beyond cultured cells to the whole animal.

3.2. Materials and Methods

Cell culture – SV-589 cells are a line of immortalized human fibroblasts expressing the SV40 large T-antigen (66). SV-589 and HepG2 (human hepatoma) cells were maintained in medium A (DMEM containing 1,000 mg/l glucose, 100 U/ml penicillin, and 100 μg/ml streptomycin sulfate) supplemented with 10% (v/v) fetal calf serum (FCS) at 37°C and 5% CO_2. CHO-7 cells, a subline of CHO-K1 cells selected for growth in lipoprotein-deficient serum (67), were maintained in medium B (1:1 mixture of Ham's F-12 medium and Dulbecco's modified Eagle's medium containing 100 units/ml penicillin and 100 μg/ml streptomycin sulfate) supplemented with 5% (v/v) lipoprotein-deficient serum. AML12 mouse hepatocytes (68) were maintained in medium A supplemented with 10% FCS, 5 μg/ml insulin, 5 μg/ml transferrin, 5 ng/ml selenium, and 40 ng/ml dexamethasone. All cell lines used in this study were grown in monolayer at 37 °C. CHO-7 and HepG2 cells were maintained in incubators filled with 8-9% CO_2; SV-589 and AML12 cells were maintained in incubators filled with 5% CO_2. Dimethyloxalylglycine (DMOG) was added to the culture medium in PBS or DMSO at a final concentration of 0.1% (v/v).

Animal studies – The previously described Tg-HMGCR(TM1-8) mice are a line of transgenic mice that express in the liver transmembrane domains 1-8 (amino acids 1-346) of hamster HMGCR, followed by three tandem copies of the T7 epitope tag (69). *Hmgcr*$^{Ki/Ki}$ mice harbor homozygous knock-in mutations in which lysine residues 89 and 248 are replaced with arginines; these mutations prevent Insig-mediated ubiquitination and degradation of HMGCR in liver and other tissues of the knock-in mice (69). Insig-2$^{-/-}$ mice

are homozygous for a null allele of the Insig-2 gene (17). $VHL^{f/f}$ mice carry a conditional VHL null allele and have been described previously (70). $VHL^{f/f}$ mice and age-matched WT control mice were injected with adenovirus encoding for Cre recombinase driven by the cytomegalovirus (CMV) promoter to achieve liver-specific recombination. Mice were analyzed 4 days after injection.

DMOG dissolved in saline was administered to Tg-HMGCR (TM1-8), $Hmgcr^{Ki/Ki}$, and Insig-$2^{-/-}$ mice by intraperitoneal injection at a dose of 8 mg/day for 3 (Fig. 21B – 21E) or 5 (Fig. 21A) consecutive days. Control mice received saline vehicle. At the end of these treatment periods, mice were sacrificed; the livers were removed, snap frozen, and stored in liquid N_2 until analysis. Animal procedures involving hypoxia treatment of mice and $VHL^{f/f}$ mice were performed in the Brugarolas laboratory. For the hypoxia treatments, mice were placed in a hypoxic chamber that was equilibrated to atmospheric conditions. Over a 40-min period, the oxygen level was decreased in a step-wise manner to 6% O_2 by displacement with N_2. Mice were subsequently maintained at 6% O_2 for 6 h. Control mice were kept in normal atmospheric conditions within the same room. Food was withdrawn from both groups during the treatment period to control for any effect of nutritional status on Insig-2a expression. All mice were housed in colony cages with a 12 hr light/12 hr dark cycle and fed ad libitum Teklad Mouse/Rat Diet 2016 (Harlan Teklad, Madison, WI). All animal experiments were performed with approval of the Institutional Animal Care and Research Advisory Committee at the UT Southwestern Medical Center at Dallas.

Quantitative Real Time PCR (RT-PCR) – The protocol for quantitative RT-PCR was similar to that described previously (71). Total RNA was prepared from cultured cells or mouse livers using the RNA STAT-60 kit (TEL-TEST "B", Friendswood, TX) or the RNeasy kit (Qiagen, Hilden, Germany). Equal amounts of RNA were treated with DNase I (DNA-free^{TM}, ThermoFisher Scientific). First strand cDNA was synthesized from 2 μg of DNase I-treated total RNA with random hexamer primers using TaqMan Reverse Transcription Reagents (Applied Biosystems/Roche Applied Science, Foster City, CA). Specific primers for each gene were designed using Primer Express software (Life Technologies). Triplicate RT-PCR reactions were set up in a final volume of 20 μl containing 20 ng of reverse-transcribed total RNA, 167 nM forward and reverse primers, and 10 μl of 2X SYBR Green PCR Master Mix (Life Technologies). The relative amount of all mRNAs was calculated using the comparative threshold cycle (C_T) method. Human cyclophilin B and mouse apoB mRNA were used as the invariant controls for RNA samples prepared from cultured human cells and mouse tissues, respectively. Sequences of the primers for RT-PCR used in the current study are listed in Table 6. Other primers for RT-PCR were described previously (17).

Subcellular fractionation and immunoblot analysis – Subcellular fractionation of cells and mouse livers by differential centrifugation was performed as previously described (69, 72). Aliquots of resulting membrane and nuclear extract fractions were subjected to SDS-PAGE and immunoblot analysis. Primary antibodies used for immunoblotting to detect SREBP-1 (rabbit polyclonal IgG-211C), SREBP-2 (rabbit monoclonal IgG-22D5), Insig-1

(rabbit polyclonal anti-Insig-1 antiserum), Insig-2 (rabbit polyclonal IgG-940C), HMGCR (mouse monoclonal IgG-A9 and rabbit polyclonal IgG-839C) were described previously (17, 26, 52, 73). Mouse monoclonal anti-T7 IgG was obtained from EMD Biosciences (San Diego, CA); rabbit polyclonal anti-calnexin IgG and anti-HIF-2α IgG from Novus Biologicals (Littleton, CO); rabbit polyclonal anti-LSD1 IgG from Cell Signaling (Beverly, MA); rabbit polyclonal anti-lamin B1 IgG from Abcam (Cambridge, MA); and rabbit polyclonal anti-HIF-1α IgG from Bethyl Laboratories (Montgomery, TX). Bound antibodies were visualized with peroxidase-conjugated, affinity-purified donkey anti-mouse or anti-rabbit IgG (Jackson ImmunoResearch Laboratories, West Grove, PA) using the SuperSignal CL-HRP substrate system (ThermoFisher Scientific, Waltham, MA) according to the manufacturer's instructions. Gels were calibrated with prestained molecular mass markers (Bio-Rad, Hercules, CA). Filters were exposed to film at room temperature.

RNA interference – RNA interference was carried out as previously described with minor modifications (33). Duplexes of small interfering RNA (siRNA) were designed and synthesized by GE Dharmacon (Lafayette, CO). Sequences of the siRNAs used in current study are described in Table 7. SV-589 cells were set up for experiments on day 0 as described in the figure legends. On day 1, triplicate dishes of cells were incubated with 400 pmol of siRNA duplexes mixed with Lipofectamine RNAiMAX^{TM} reagent (Invitrogen, Grand Island, NY) diluted in Opti-MEM I reduced serum medium (Life Technologies, Grand Island, NY) according to manufacturer's procedure. Following incubation for 5 hr at

37°C, the cells received a direct addition of medium A containing 10% FCS (final concentration). On day 2, the cells were treated with DMOG. Following incubation for 24 hr, the cells were harvested and analyzed as described in figure legends.

Generation of SV-589 cells lacking Insig-1 or Insig-2 using CRISPR/Cas9 – A single guide RNA (sgRNA, GCGCACAGCGCGAGGCGCCG) targeting nucleotides 40-59 (relative to the first initiating methionine) of Insig-1 was cloned into the pSpCas9(BB)-PX330 vector (Addgene, Cambridge, MA). Two sgRNAs targeting nucleotides -72-53 (GACAGTTGAGCTTTTCAGCT) and 194-213 (GCATCTTTTCTTCTGCA) of Insig-2 were cloned into the pSpCas9(BB)-2A-Puro-PX459 vector (Addgene), which harbors the puromycin-resistance gene. SV-589 (ΔInsig-1) and (ΔInsig-2) cells were generated as follows: on day 0, SV-589 cells were set up at 4 x 10^5 cells per 100-mm dish in medium A containing 10% FCS. On day 1, cells were transfected with 1 μg/dish of pSpCas9(BB)-PX330/Insig-1(40-59) together with 3 μg/dish of pcDNA3.1(+) (ThermoFisher Scientific, Waltham, MA), which harbors the neomycin-resistance gene, or 1 μg/dish of pSpCas9(BB)-S2-Puro-PX459/Insig-2 (-72-53) and 1 μg/dish of pSpCas9(BB)-S2-Puro-PX459/Insig-2 (194-213) using the FuGENE6 transfection reagent as previously described (24, 26). On day 2, cells were switched to medium A supplemented with 10% FCS and either 700 μg/ml G418 or 0.5 μg/ml puromycin to select for SV-589 (ΔInsig-1) and SV-589 (ΔInsig-2) cells, respectively. Fresh medium was added every 2-3 days until colonies formed after 2 weeks. Individual colonies were isolated using cloning cylinders, and the absence of Insig-1 and Insig-2 was determined by immunoblot analysis with rabbit

polyclonal anti-Insig-1 antiserum and rabbit polyclonal IgG-940C against human Insig-2. Clones from single colonies of SV-589 (ΔInsig-1) and (ΔInsig-2) cells were isolated by serial dilution in 96-well plates and screened by immunoblot analysis with anti-Insig-1 antiserum and IgG-940C. Sequencing of products obtained from PCR of genomic DNA revealed that SV-589 (ΔInsig-1) cells harbor a 684 bp deletion that encompasses Exon 2 encoding the initiating methionine of Insig-1 and a portion of Intron 2; SV-589 (ΔInsig-2) cells harbor a 265 bp deletion that removes the initiating methionine and 69 additional amino acids. Monolayers of SV-589 (ΔInsig-1) and (ΔInsig-2) cells were maintained in medium A containing 10% FCS and 700 μg/ml G418 (ΔInsig-1) or 0.5 μg/ml puromycin (ΔInsig-2) at 37 ºC, 5% CO_2.

Chromatin immunoprecipitation analysis – Chromatin immunoprecipitation (ChIP) analysis was carried out using EZ-ChIP kit (EMD Millipore, Billerica, MA) according to the manufacturer's instructions. For ChIP analysis of cultured cells, chromatin was crosslinked for 10 min at room temperature by adding formaldehyde to the culture medium of cells at a final concentration of 1% (w/v). After quenching the crosslinking reaction with 125 mM glycine, cells were washed with PBS, scraped, and centrifuged at 700 x g at 4 °C for 5 min. Pellets were resuspended in 1 ml of a detergent-containing buffer with protease inhibitors, subjected to sonication on ice for 10 sec intervals eight times at 30% maximum power, and subsequently precleared with protein G Agarose beads for 1 hr at 4 °C. Precleared lysates were then incubated with 4 μg of preimmune rabbit IgG (negative control) or rabbit polyclonal anti-HIF-1α for 16 hr at 4 °C, after which the mixture was

incubated with Protein G Agarose beads for 1 hr at 4 °C. For ChIP analysis of mouse liver, frozen liver tissues were thawed on ice, chopped in PBS, and incubated with formaldehyde at a final concentration of 1% (w/v). The tissues (60 mg) were subjected to sonication on ice for 10 sec intervals eight times at 30% maximum power and precleared with Protein G Agarose beads for 1 hr. Precleared lysates were incubated with 5 μg of preimmune rabbit IgG (negative control) or rabbit polyclonal anti-HIF-1α for 16 hr at 4°C, after which the mixture was incubated with Protein G Agarose beads for 1 hr at 4°C.

Precipitated protein-DNA complexes from lysates of cells and mouse tissues were washed and eluted with buffers provided by the manufacturer. The purified DNA was subjected to PCR using AccuPrime Pfx Supermix kit (ThermoFisher Scientific); ethidium bromide-stained PCR products were visualized following electrophoresis on 1.5% agarose gels. Primers used in PCR reactions are described in Table 8.

Expression plasmids – Sequences containing the 5'-flanking region of the human Insig-2 gene were amplified by PCR with the Phusion DNA polymerase kit (New England Biolabs, Ipswich, MA) using the genomic DNA isolated from SV-589 cells as a template. The primers used for these amplification reactions are described in Table 9. The resulting PCR products were gel purified, subjected to restriction digestion, and subcloned into the multiple cloning site of the promoter-less pGL4 vector (Promega, pGL4.10) upstream of a synthetic luciferase coding sequence; this plasmid was designated pInsig-2 (470) (see Fig. 19). Site-directed mutagenesis of the candidate HREs was performed using the QuikChange XL kit (Stratagene, San Diego, CA) using pInsig-2 (470) as a template and the

primers described in Table 9. The pGL4-TK-Renilla Luciferase vector, in which Renilla luciferase is constitutively expressed under the control of the thymidine kinase (TK) promoter, was obtained from Promega (pGL4.74).

Sequences containing the 5'-flanking region and the first intron of the mouse Insig-2 gene were amplified by PCR with the Phusion DNA polymerase kit. Mouse genomic DNA, isolated from the liver of a C57BL/6 mouse, was used as the template. The primers used for these amplification reactions are listed in Table 9. The PCR products were gel purified, subjected to restriction digestion, and subcloned into the multiple cloning site of pGL4 vector upstream luciferase coding sequence. Site-directed mutagenesis of the candidate HREs was performed using QuikChange XL with the pGL4-Insig-2 #2 plasmid as the template and the primers listed in Table 9.

The expression plasmids pCMV-HIF-1α and pCMV-HIF-2α encode human HIF-1α and HIF-2α, respectively, harboring alanine substitutions for two proline residues (402 and 564 in HIF-1α; 431 and 531 in HIF-2α) that abolish oxygen-dependent hydroxylation and subsequent proteasomal degradation (43, 74). These plasmids were generated by subcloning the mutant HIF-1α and HIF-2α cDNAs (provided by Drs. Elhadji M. Dioum and Joseph A. Garcia, UT Southwestern Medical Center) into the pcDNA3.1 vector (Invitrogen) under transcriptional control of the CMV promoter. The integrity of each plasmid was confirmed by DNA sequencing.

Luciferase assay – SV-589 cells were transfected with FuGENE6 transfection reagent as previously described (24, 26). Conditions of subsequent incubations are described in the

figure legends. Following treatments, cell monolayers were washed with PBS and lysed in 0.4 ml of Passive Lysis Buffer (Promega, Madison, WI) by shaking for 30 min at room temperature. The resulting lysates were then transferred to microcentrifuge tubes and briefly centrifuged to remove insoluble debris. Firefly and Renilla luciferase activities were measured in 96-well plates by mixing 20 µl of cleared lysates with the Dual-Luciferase Reporter Assay System (Promega). The amount of firefly luciferase activity of the transfected cells was normalized to Renilla luciferase and expressed relative to the value of the control as indicated in figure legends.

Isolation and Transfection of Primary Rat Hepatocytes **–** Hepatocytes were isolated by the collagenase method from nonfasted 250-g male Sprague-Dawley rats, as previously described with minor modifications (75). Rats were anesthetized with isoflurane, and the liver was perfused *in situ* via the portal vein with 200 ml of prewarmed Liver Perfusion Medium (Invitrogen) at a flow rate of 10 ml/min. The liver was subsequently perfused with 140 ml of prewarmed Liver Digest Medium (Invitrogen) containing collagenase. The liver was then removed from the animal, the hepatic capsule was stripped, and dissociated cells were dispersed by shaking. Cells were passed through a 100 µm cell strainer (BD Biosciences, San Jose, CA) into an equal volume of ice-cold medium B supplemented with 5% FCS. The cells were pelleted and washed twice in the same medium. Cells were plated in collagen I-coated 6-well plates (BD Biosciences) at a density of $1.5 \cdot 10^6$ cells per well in the same medium. After 4 h, cells were washed with PBS and switched to medium C (medium 199 containing 100 units/ml penicillin and 100 µg/ml streptomycin sulfate)

supplemented with 100 nM dexamethasone, 100 nM 3,3′,5-triiodo-L-thyronine, and 1 nM insulin.

For reporter assay experiments, cells were washed with PBS and transiently transfected on day 1 with 4 μg DNA (1.8 μg of the indicated reporter plasmid and 0.4 μg of pGL4-TK-Renilla Luciferase, without or with 1.8 μg of pCMV-HIF-1α or pCMV-HIF-2α per well using 10 μl of Lipofectamine 2000 (Invitrogen) in 2 ml of medium D (RPMI 1640). After 6 h, cells were washed with PBS and refed medium C supplemented with 100 nM dexamethasone, 100 nM 3,3′,5-triiodo-L-thyronine, and 100 nM insulin for 36 h.

Alternatively, for experiments in which mRNA levels were examined, on day 1 cells were washed twice with PBS and refed medium C containing 100 nM dexamethasone and 100 nM 3,3′,5-triiodo-L-thyronine, without or with 1 nM insulin for 6 h.

3.3. Results

HIF is a heterodimeric transcription factor composed of a labile α subunit and a stable β subunit (40, 41). Under normal oxygen conditions, the α subunit is hydroxylated on two proline residues, allowing the protein to become recognized by pVHL for subsequent ubiquitination and proteasomal degradation. Under low oxygen conditions (hypoxia), the α subunit is not hydroxylated owing to the strict requirement for molecular oxygen by prolyl hydroxylases that modify the protein. Stabilized α subunits bind to β subunits and activate transcription by binding to HREs present in more than 70 HIF target genes (44). Enhanced expression of HIF target genes, which mediate several cellular processes such as growth and apoptosis, angiogenesis, and energy metabolism, allows for

adaptation to hypoxia at the cellular, tissue, and organismal levels. Expanding on the previous discovery of HIF-mediated induction of Insig mRNAs in CHO cells (39), I examined their expression in human SV-589 cells treated with DMOG. This cell-permeable analog of 2-oxoglutarate (2-OG) inhibits 2-OG-dependent dioxygenases, including prolyl hydroxylases that modify and destabilize HIF-α subunits (76). In Fig. 15, SV-589 cells were incubated for 24 h with various concentrations of DMOG prior to harvest and subcellular fractionation. Subsequent immunoblot analysis revealed that DMOG caused nuclear accumulation of HIF-1α (Fig. 15A, lanes b-e) and enhanced expression of mRNAs for vascular endothelial growth factor (VEGF), an established HIF target gene (Fig. 15B). DMOG markedly stimulated expression of Insig-2 protein and mRNA (~10-fold); expression of Insig-1 mRNA was also enhanced by DMOG, but to a lesser extent (~2-fold) than that observed for Insig-2 mRNA (Fig. 15B). Insig-1 protein remained unchanged in presence of DMOG (Fig. 15A, lanes b-e). DMOG-induced expression of Insig-2 mRNA was observed in multiple cell lines from various tissues including CHO-7, HepG2 (human hepatoma), primary rat hepatocytes, and AML12 (mouse hepatocytes) (Fig. 16). However, induction of Insig-1 mRNA was limited to CHO-7 cells and primary rat hepatocytes (Fig. 16). The amount of HMGCR in membranes was reduced by DMOG (Fig. 15A, lanes b-e), which likely resulted from accelerated degradation as indicated by the slight reduction in the amount of HMGCR mRNA (Fig. 15B). Membrane-bound and nuclear forms of SREBPs were modestly reduced by DMOG treatment (Fig. 15A, lanes f-o), which can be attributed in part to reduced expression of mRNAs encoding SREBP-1a and SREBP-1c (Fig. 15B).

To determine the individual contribution of Insigs to the DMOG-induced degradation of HMGCR, CRISPR/Cas9 technology was used to generate Insig-deficient SV-589 cells. Fig. 17A shows that DMOG treatment of parental SV-589 cells stimulated degradation of HMGCR and accumulation of Insig-2, HIF-1α, and HIF-2α as expected (lanes 1 and 2). These responses continued in SV-589 cells deficient in Insig-1 (lanes 3 and 4). In contrast, DMOG no longer stimulated degradation of reductase in Insig-2-deficient SV-589 cells, even though the inhibitor continued to stimulate accumulation of HIF-1α and HIF-2α in the nucleus (lanes 5 and 6).

RNA interference (RNAi) was utilized to identify the HIF-α subunit required for DMOG-mediated induction of Insig-2 and subsequent degradation of HMGCR. In the experiment of Fig. 17B, SV-589 cells were transfected with siRNAs against the control gene GFP, HIF-1α, or HIF-2α; scrambled versions of the HIF-1α and HIF-2α siRNAs were utilized as negative controls. The results show that in cells transfected with the GFP siRNA, DMOG stimulated degradation of HMGCR, stabilized HIF-1α and HIF-2α, and enhanced expression of Insig-2 (Fig. 17B, lanes 1 and 2). RNAi-mediated knockdown of HIF-1α abolished DMOG-mediated induction of Insig-2 and degradation of HMGCR (lanes 3 and 4); however, both reactions continued and were somewhat enhanced in HIF-2α knockdown cells (lanes 5 and 6). DMOG stimulated Insig-2 expression and HMGCR degradation in cells transfected with scrambled HIF-1α and HIF-2α siRNAs (lanes 7-10). Consistent with this, DMOG-induced expression of Insig-2 mRNA was blunted by HIF-1α, but not by HIF-2α knockdown (Fig. 17C). DMOG continued to enhance expression of

mRNAs encoding VEGF and glucose transporter-1 (GLUT1) in HIF-1α and HIF-2α knockdown cells (Fig. 17C), indicating the two HIF-α subunits are interchangeable in the regulation of these genes.

In mice and other rodents, two transcripts designated Insig-2a and Insig-2b are produced from the Insig-2 gene (14, 46). The Insig-2a transcript is liver specific, whereas the Insig-2b transcript is ubiquitously expressed (61). Transcription of Insig-2a and Insig-2b mRNAs is driven by alternative promoters that generate distinct and noncoding first exons spliced to the same coding exons. Thus, Insig-2a and Insig-2b transcripts encode for the identical protein. The human Insig-2 gene is organized similarly to the mouse gene (Fig. 18A). Considering this, I next sought to determine whether the Insig-2a or Insig-2b transcript becomes induced upon treatment of human SV-589 cells with DMOG. Quantitative RT-PCR experiment of Fig. 18B shows that the Insig-2a transcript was barely detectable in SV-589 cells and its expression was not enhanced by DMOG treatment (primer pair A). However, DMOG-induced expression of the Insig-2b transcript was readily observed in RT-PCR reactions (primer pairs B and C). A similar magnitude of DMOG-induced expression was observed for total Insig-2 mRNA (primer pair D).

The schematic shown in Fig. 18A depicts the structure of the human Insig-2 gene. Sequence analysis reveals the presence of conserved sequences conforming to the consensus HRE (5'-CGTGX$_{(1-8)}$CA-3') within the intronic region between exons 1a and 1b of the human Insig-2 gene. In the experiment of Fig. 18C, ChIP assays were conducted to determine whether HIF physically interacts with the putative Insig-2 HRE. SV-589 cells were treated in the absence or presence of DMOG for 24 hr; following crosslinking of

protein:DNA complexes, samples were immunoprecipitated with either control IgG or anti-HIF-1α IgG. When HIF-1α was immunoprecipitated from DMOG-treated samples, the Insig-2 HRE was among the HIF-associated DNA fragments as determined by PCR analysis of precipitated material (Fig. 18C, lane 6). The Insig-2 HRE failed to be amplified from samples precipitated with control IgG (lane 4). As expected, DNA fragments corresponding to the HRE of the VEGF gene were isolated in anti- HIF-1α immunoprecipitates (lane 6).

To further explore the mechanism of HIF-mediated regulation of Insig-2, a 470-nucleotide fragment between exons 1a and 1b of the human Insig-2 gene was inserted upstream a firefly luciferase reporter gene in the promoter-less pGL4 vector (Fig. 19A). When the resultant reporter plasmid was introduced into SV-589 cells, luciferase activity was increased ~6-fold upon incubation of the cells with DMOG (Fig. 19B). DMOG-mediated induction of luciferase activity was abolished by removal of nucleotides -470 to -206 or by mutation of the HRE sequence (Fig. 19B). Fig. 19C shows that luciferase activity was stimulated 5- or 2-fold upon co-expression of non-degradable HIF-1α or HIF-2α, respectively, with the full length, WT reporter plasmid. HIF-mediated induction of luciferase activity was abolished by truncation of the Insig-2 fragment or by mutation of the HRE. Nearly identical results were obtained with Huh-7 cells (Fig. 20).

Next, Insig-2 expression was examined in livers of mice using three models in which HIF levels are modulated: prolyl hydroxylase inhibition, oxygen deprivation, and genetic manipulation. Administration of DMOG to mice by oral gavage (8 mg/day for 5 consecutive days) resulted in an 8-fold increase in the expression of hepatic Insig-2a

mRNA (Fig. 21A). Levels of Insig-1 and Insig-2b mRNAs were not increased. The mRNAs for the established HIF targets GLUT1 and VEGF were elevated in livers of DMOG-treated mice as expected.

In the oxygen deprivation model, mice were exposed to hypoxia (6% O_2) for 6h. Control mice were maintained at normoxia (21% O_2) in the same room. Food was withdrawn from both groups during the treatment period to control for any effects of insulin. Fig. 21A shows that hypoxia led to a 28-fold increase in the amount of Insig-2a mRNA in the mouse liver. Consistent with changes in the DMOG-treated mice, livers of hypoxic mice showed a slight decrease in the amount of Insig-1 and Insig-2b mRNA. Hepatic expression of the HIF target genes GLUT1 and aldolase A were elevated by hypoxia as expected.

Mice that harbor a floxed VHL allele ($VHL^{f/f}$) were examined as a genetic model of hypoxia (70). $VHL^{f/f}$ and control WT mice were injected with adenovirus encoding for Cre recombinase driven by the cytomegalovirus promoter. Because pVHL is required for oxygen-dependent degradation of HIF-α subunits, recombination of the VHL allele results in constitutive HIF activation. Four days after injection, expression of HIF target genes VEGF and GLUT1 were found to be increased in the livers of VHL knock-out mice, indicating successful recombination in the liver (Fig. 21A). Hepatic Insig-2a mRNA was increased 12-fold in VHL knock-out mice compared to that in their WT counterparts. The levels of Insig-1 and Insig-2b mRNA were not different between VHL knock-out and WT mice.

Sequence analysis of the mouse *Insig-2* gene, including ~8 kb upstream the transcriptional start site of exon 1b, revealed the presence of 3 putative HRE sequences (Fig. 22A). Thus, a series of reporter plasmids were generated in the pGL4 vector that contain different portions of the mouse Insig-2 5'-flanking region and the first intron fused to firefly luciferase. These plasmids were then co-expressed in primary rat hepatocytes, which mimic the liver in expression of Insig-2a and Insig-2b (61), together with non-degradable HIF-1α to identify a functional HRE. Luciferase activity was not stimulated when non-degradable HIF-1α was co-expressed with empty pGL4 vector or the reporter plasmid containing the 3.64 kb region directly upstream of exon 1a of the *Insig-2* gene (Fig. 22B). In contrast, HIF-1α expression led to a marked induction of luciferase activity in hepatocytes transfected with the reporter plasmid containing nucleotides that span the intronic region between exons 1a and 1b (Fig. 22B). Analyses of several truncation mutants traced this HIF-mediated induction to a pair of HRE sequences approximately 200 nucleotides upstream exon 1b of the mouse *Insig-2* gene.

Two sequences that conform to the consensus HRE are present in the 440-nucleotide region upstream exon 1b of the *Insig-2* gene. The more distal sequence was designated candidate HRE-1 and the more proximal sequence was designated candidate HRE-2. The experiment of Fig. 22C evaluated HIF-dependent regulation of the truncated pGL4 reporter plasmid harboring mutations in HRE-1 or HRE-2. HIF-mediated induction of luciferase activity was observed with the reporter plasmid containing the wild type upstream sequence as expected. Similar results were observed with the plasmid harboring mutations in the candidate HRE-2 sequence. However, HIF-mediated induction of

luciferase activity was abolished by mutation of the HRE-1 sequence. A direct role for HIF-1α in regulation of hepatic Insig-2 is indicated by the ChIP experiment of Fig. 21B, which shows that in livers of mice, DMOG treatment stimulated binding of HIF-1α to HREs present in the first intron of the Insig-2 gene and the VEGF promoter.

Studies were next carried out to determine whether DMOG-induced expression of Insig-2 modulates degradation of HMGCR. For this purpose, I utilized a recently developed line of transgenic mice designated Tg-HMGCR (TM1-8) (69) expressing in the liver, the membrane domain of HMGCR that is both necessary and sufficient for Insig-mediated, sterol-accelerated degradation (24). Fig. 21C shows that administration of DMOG caused an increase of Insig-2 protein and a reduction of endogenous reductase protein in membranes from WT (lane 2) and Tg-HMGCR (TM1-8) mice (lane 4). This was accompanied by enhanced expression of the Insig-2a mRNA and reduced expression of HMGCR mRNA (Fig. 23A). DMOG also caused a reduction of HMGCR (TM1-8) protein in livers of transgenic mice (Fig. 21C, lane 4); however, the compound failed to inhibit expression of HMGCR (TM1-8) mRNA (Fig. 23A). DMOG stabilized HIF-1α in the nucleus (Fig. 21C, lane 4) and enhanced expression of HIF-target genes VEGF and GLUT1 (Fig. 23A) in WT and transgenic mouse livers as expected. Degradation of HMGCR (TM1-8) was also accelerated in the livers of Tg-HMGCR (TM1-8) mice when exposed to 10% O_2 for 6 hr (data not shown), indicating that not only pharmacological stabilization but also physiological stabilization of HIF-1α is able to stimulate the degradation of HMGCR in the liver of mice.

In addition to Tg-HMGCR (TM1-8) mice, a line of knock-in mice designated *Hmgcr*$^{Ki/Ki}$ was developed to determine the contribution of accelerated degradation to the overall regulation of HMGCR in the liver (69). *Hmgcr*$^{Ki/Ki}$ mice harbor mutations in the endogenous HMGCR gene that abolish sterol-induced ubiquitination and degradation of HMGCR protein (16). Administration of DMOG stabilized HIF-1α and enhanced expression of Insig-2 protein and mRNA in livers of both WT and *Hmgcr*$^{Ki/Ki}$ mice (Fig. 21D, lanes 2 and 4; Fig. 23B). DMOG reduced HMGCR protein in livers of WT mice (Fig. 21D, lane 2); however, the protein remained constant in *Hmgcr*$^{Ki/Ki}$ livers (lane 4), even though expression of HMGCR mRNA in the liver of both was inhibited by DMOG treatment (Fig. 23B). Importantly, DMOG also failed to enhance degradation of HMGCR in livers of Insig-2 knock-out mice (designated *Insig-2*$^{-/-}$), even though the compound stabilized HIF-1α (Fig. 21E, lane 4).

3.4. Discussion

Nguyen et al. previously described a mechanism for oxygen-sensitive feedback regulation of HMGCR in CHO cells (39). This novel regulatory mechanism involves the hypoxia-induced accumulation of the cholesterol synthesis intermediate 24,25-DHL and HIF-mediated induction of Insigs. These responses converge to accelerate the degradation of HMGCR, which limits cholesterol synthesis under conditions of oxygen deprivation. The current data provide further insight into molecular mechanisms that link oxygen sensing and the pathway for HMGCR ERAD. This link is illustrated when human SV-589 cells are treated with the prolyl hydroxylase inhibitor DMOG, which mimics hypoxia by

stabilizing the oxygen-sensitive transcription factor HIF-1α. The treatment stimulated degradation of HMGCR (Fig. 15); the reaction required the presence of Insig-2 and HIF-1α as revealed by RNAi and CRISPR/Cas9 knockdown/knock-out studies (Fig. 17A and 17B). These results led to the identification of a functional HRE within the intronic region between exon 1a and exon 1b of the human *INSIG-2* gene (Fig. 18A, 18B, and 19). Finally, ChIP experiments reveal a physical association between the highly conserved human *INSIG-2* HRE and HIF-1α (Fig. 18C). Considered together, these observations are consistent with the scenario depicted in Fig. 23D, which shows that HIF-1α becomes stabilized upon prolyl hydroxylase inhibition and subsequently binds to HRE sequences within the promoter of the *INSIG-2* gene so as to activate transcription. This activation leads to enhanced expression of Insig-2 mRNA and accumulation of Insig-2 protein. Accumulated Insig-2 protein then binds to HMGCR, triggering accelerated ubiquitination and degradation of the enzyme.

The physiologic relevance of HIF-mediated regulation of Insig-2 was indicated by hepatic induction of the transcript in three mouse models of actual or approximated hypoxia: oxygen deprivation, pharmacologic prolyl hydroxylase inhibition, and VHL knock-out (Fig. 21A). In addition, DNA:protein complexes containing HIF-1α and the conserved mouse Insig-2 HRE were observed in livers of DMOG-treated mice (Fig. 21B). Experiments in three lines of genetically-manipulated mice demonstrate that accelerated degradation plays a significant role in DMOG-mediated regulation of HMGCR in the mouse liver. DMOG stimulated the degradation of the membrane domain of HMGCR that was expressed under liver-specific, sterol-independent transcriptional control (Fig. 21C).

In contrast, HMGCR harboring mutations that prevent sterol-induced ubiquitination resisted DMOG-induced degradation in the liver (Fig. 21D). Finally, HMGCR failed to become degraded in livers of Insig-2-deficient mice subjected to DMOG treatment (Fig. 21E). DMOG is a non-specific prolyl hydroxylase inhibitor; however, resistance of HMGCR to DMOG-induced degradation in *Hmgcr*$^{Ki/Ki}$ and *Insig-2*$^{-/-}$ mice indicates the reaction occurs through a HIF-mediated mechanism similar to that characterized in cultured cells.

In mice, alternative promoters are utilized to produce Insig-2a and Insig-2b mRNAs from a single Insig-2 gene (61). The mouse Insig-2 HRE identified in this study is located ~ 4500 nucleotides downstream exon 1a and 285 nucleotides upstream exon 1b (see Fig. 22). Despite the close proximity of the HRE to exon 1b, HIF modulates expression of Insig-2a, but not Insig-2b in mouse livers (Fig. 21A) and primary rat hepatocytes (Fig. 22). This discrepancy can be explained by the fact that transcription factors can modulate gene transcription from distal sites. In fact, the classic HIF target gene *EPO* contains a functional HRE in its 3'-untranslated region (77, 78). The human *INSIG-2* gene is organized similarly to that of the mouse *Insig-2* gene (79). It is noteworthy that the Insig-2b mRNA is regulated by HIF-1α in human SV-589 cells, a fibroblast cell line that does not express Insig-2a (Fig. 18B). Similarly, HIF-mediated regulation of Insig-2 mRNA was observed in CHO-7 cells (Fig. 16), a non-hepatic cell line that does not express Insig-2a. Thus, it appears that HIF can mediate regulation of Insig-2b transcription in absence of Insig-2a. The molecular basis for this observation merits further investigation.

Insigs play a crucial role in feedback regulation of cholesterol synthesis by modulating ERAD of HMGCR and proteolytic activation of SREBPs (11). Considering previous studies in cultured cells and livers of animals (39, 59), it is anticipated that HIF-1α-mediated modulation of Insig-2 expression will sensitize these feedback mechanisms and render cells more responsive to sterols. Indeed, sterols stimulated ERAD of HMGCR and blocked processing of SREBPs at lower concentrations in DMOG-treated cells compared to their untreated counterparts (39). Thus, in the setting of hypoxia, the accumulation of 24,25-DHL coupled with HIF-1α mediated induction of Insig-2 first triggers degradation of HMGCR, which limits flux through early steps in the cholesterol synthetic pathway (Fig. 1). Upon prolonged hypoxia, processing of SREBPs becomes inhibited owing to accumulation of Insig-2, which sensitizes the reaction to sterols. This is consistent with a previous report in which downregulation of SREBP target genes including HMGCR, Insig-1, and HMG CoA synthase was observed in livers of hypoxic mice (80). Together, these regulatory mechanisms guard against wasting of oxygen and inappropriate cell growth in the face of hypoxic stress. An interesting avenue for future studies will be to examine the role of the cholesterol biosynthetic pathway in other processes modulated by HIF, including angiogenesis and erythropoiesis. Most renal carcinomas exhibit a clear-cell phenotype and are designated clear-cell renal cell carcinomas (ccRCCs) (81). The clear-cell phenotype, which results from the abnormal accumulation of neutral lipid such as triglycerides and cholesterol esters (82, 83), is associated with genetic mutation or silencing of VHL and enhanced stability of HIF-1α and/or HIF-2α (84). Considering data that link dysregulation of cholesterol metabolism

and malignant transformation (85), another exciting line of investigation will be to determine the significance of HIF-mediated regulation of Insig-2 expression/HMGCR degradation in development of ccRCC.

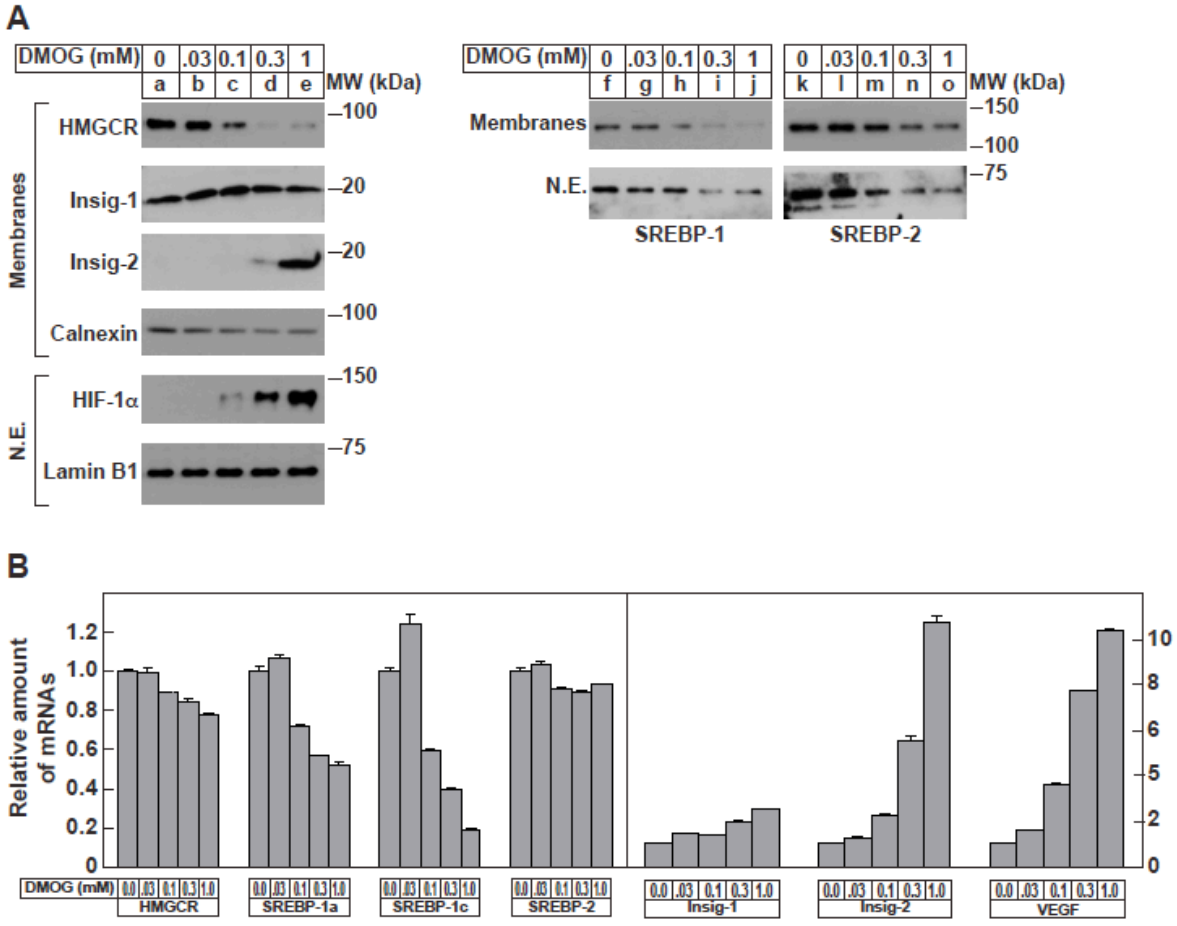

Figure 15. DMOG enhances expression of Insig-2 and suppresses HMGCR in SV-589 cells. SV-589 cells were set up on day 0 at 6.0 X 10^5 cells per 100 mm dish in medium A containing 10% FCS. On day 1, cells were switched to the identical medium with the indicated concentration of DMOG. Following incubation for 24 h at 37°C, cells were harvested for subcellular fractionation (A) or isolation of total RNA (B) as described in "Materials and Methods." (A) Resulting membrane and nuclear extract (N.E.) fractions were subjected to SDS-PAGE (10-30 μg total protein/lane), followed by immunoblot analysis with antibodies against HMGCR, Insig-1, Insig-2, calnexin, HIF-1α, Lamin B1, SREBP-1, and SREBP-2. (B) Total RNA from each condition was subjected to quantitative RT-PCR using primers against the indicated gene; cyclophilin B mRNA was used as an invariant control. Each value represents the amount of mRNA relative to that in vehicle-treated cells, which is arbitrarily defined as 1. *Bars* represent ± S.E. of triplicate samples. *VEGF*, vascular endothelial growth factor.

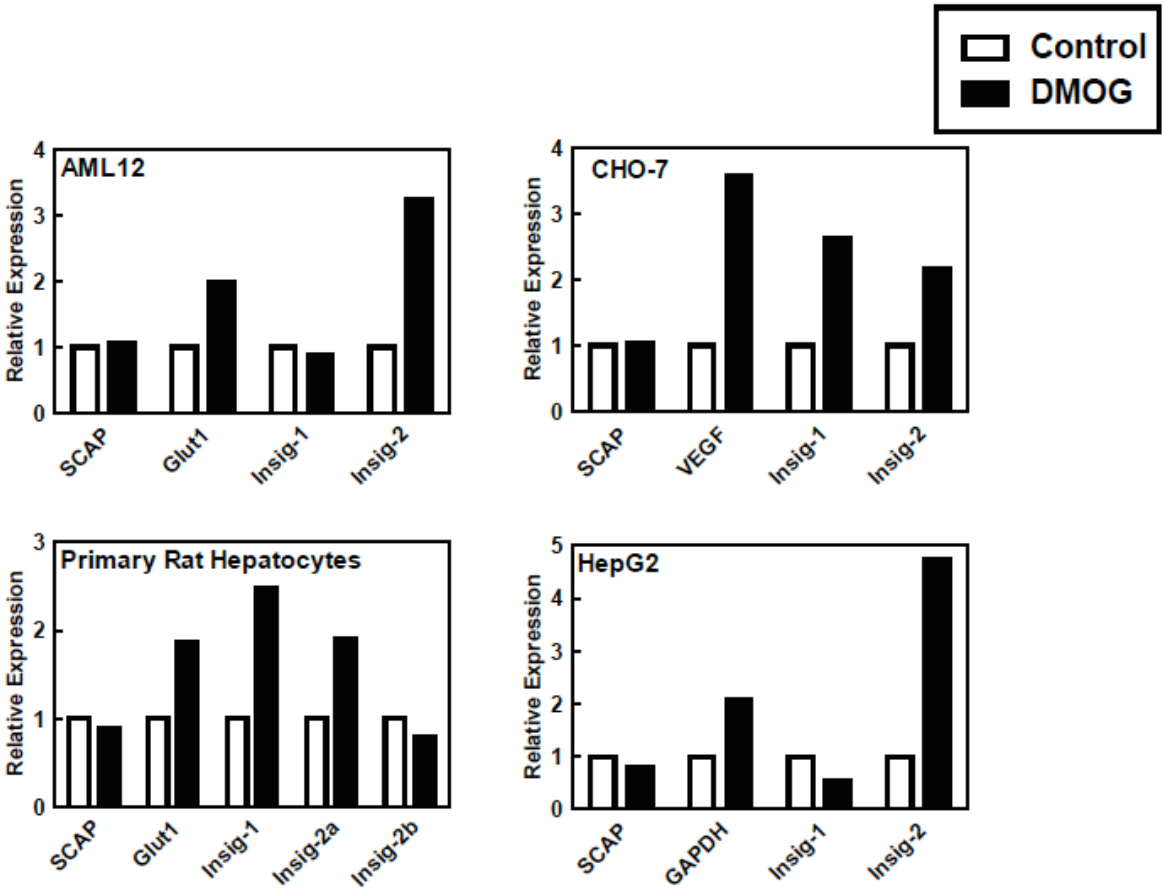

Figure 16. 2-Oxoglutarate-dependent dioxygenase inhibition enhances expression of Insig-2 mRNA in various cell lines. Cells were set up on day 0 at a density of $5 \cdot 10^5$ cells per 100-mm dish (CHO-7, HepG2, and AML12 cells) or $1.5 \cdot 10^6$ cells per well in 6-well plates (primary rat hepatocytes) in the respective culture medium described in "Materials and Methods." On day 1, cells were treated in the identical medium without or with 1 mM DMOG. On day 2, cells were harvested and total RNA was subjected to quantitative RT-PCR analysis using specific primer pairs for the indicated genes and an invariant control gene as described in "Materials and Methods." Each value represents expression of the indicated gene relative to that in control cells.

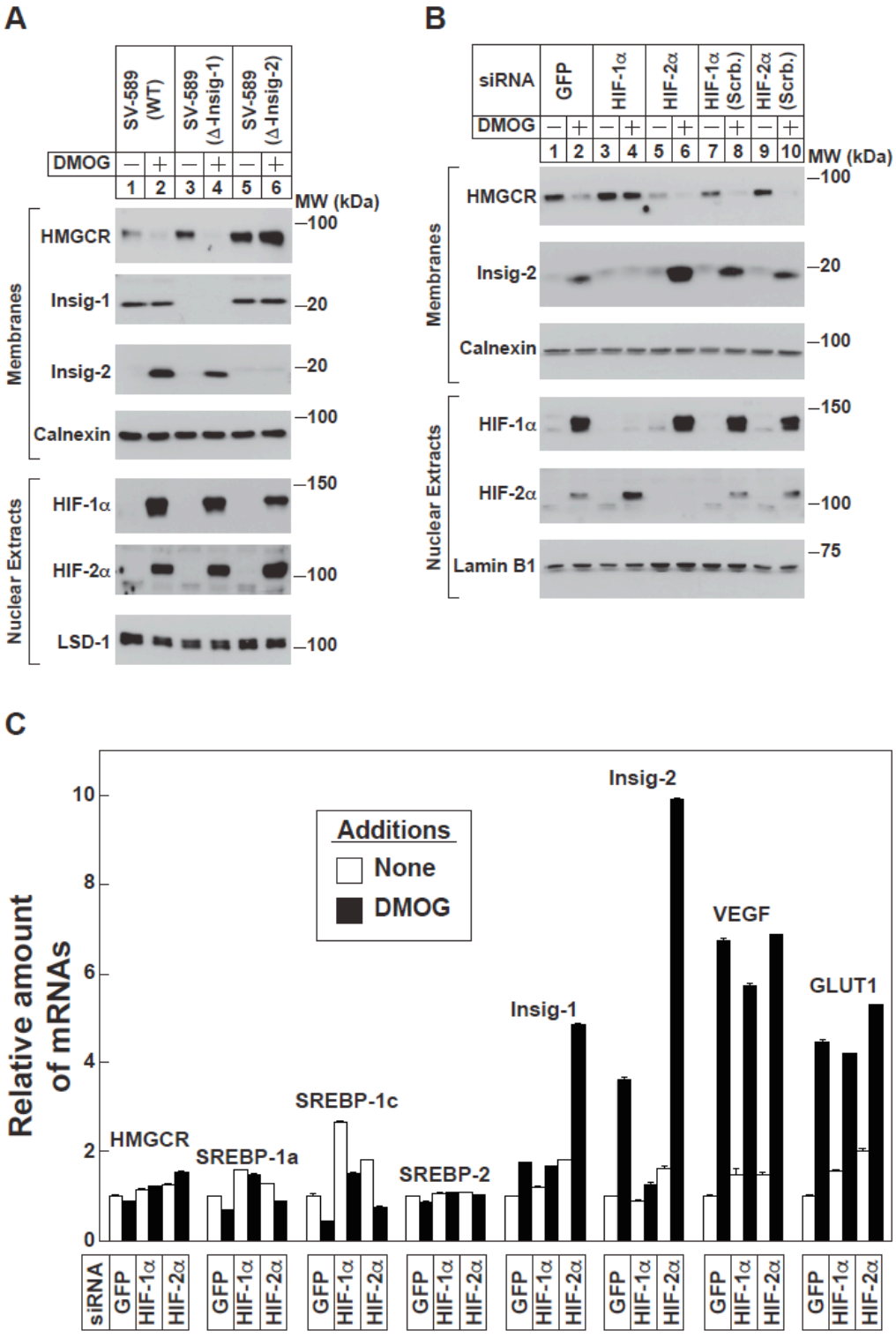
A
SV-589 (WT)
SV-589 (Δ-Insig-1)
SV-589 (Δ-Insig-2)
DMOG
1 2 3 4 5 6
MW (kDa)
Membranes
HMGCR
Insig-1
Insig-2
Calnexin
Nuclear Extracts
HIF-1α
HIF-2α
LSD-1
100
20
150
B
siRNA
GFP
HIF-1α
HIF-2α
HIF-1α (Scrb.)
HIF-2α (Scrb.)
1 2 3 4 5 6 7 8 9 10
Lamin B1
75
C
Relative amount of mRNAs
Additions
None
DMOG
HMGCR
SREBP-1a
SREBP-1c
SREBP-2
Insig-1
Insig-2
VEGF
GLUT1

Figure 17. DMOG suppresses HMGCR in SV-589 cells through mechanism requiring HIF-1α and Insig-2. (A) SV-589 (WT), SV-589 (Δ-Insig-1), and SV-589 (Δ-Insig-2) cells were set up on day 0 at 6.0 X 10^5 cells per 100 mm dish in medium A containing 10% FCS. On day 1, cells were switched to the identical medium in the absence or presence of 0.3 mM DMOG. Following incubation for 24 h at 37°C, cells were harvested for subcellular fractionation. Resulting membrane and nuclear extract fractions were subjected to SDS-PAGE (10-30 μg total protein/lane), followed by immunoblot analysis with antibodies against HMGCR, Insig-1, Insig-2, calnexin, HIF-1α, HIF-2α, and LSD-1. (B-C) SV-589 cells were set up on day 0 at 2.5 X 10^5 cells per 100 mm dish in medium A containing 10% FCS. On day 1, cells were transfected with siRNAs targeting mRNAs encoding GFP, HIF-1α, and HIF-2α as indicated and described in "Materials and Methods;" scrambled (Scrb.) HIF-1α and HIF-2α siRNAs were used as additional negative controls. On day 2, cells were treated in the absence or presence of 0.3 mM DMOG for 24 hr at 37°C, after which they were harvested for subcellular fractionation (B) and total RNA isolation (C) as described in "Materials and Methods." (B) Aliquots of membrane and nuclear extract fractions (10-30 μg total protein/lane) were subjected to SDS-PAGE, followed by immunoblot analysis with antibodies against HMGCR, Insig-2, calnexin, HIF-1α, HIF-2α, and Lamin B1. (C) Total RNA from each condition was subjected to quantitative RT-PCR as described in the legend to Fig. 15B. *Bars* denote ± S.E. of triplicate samples. *LSD-1*, lysine-specific demethylase 1; *GLUT1*, glucose transporter 1.

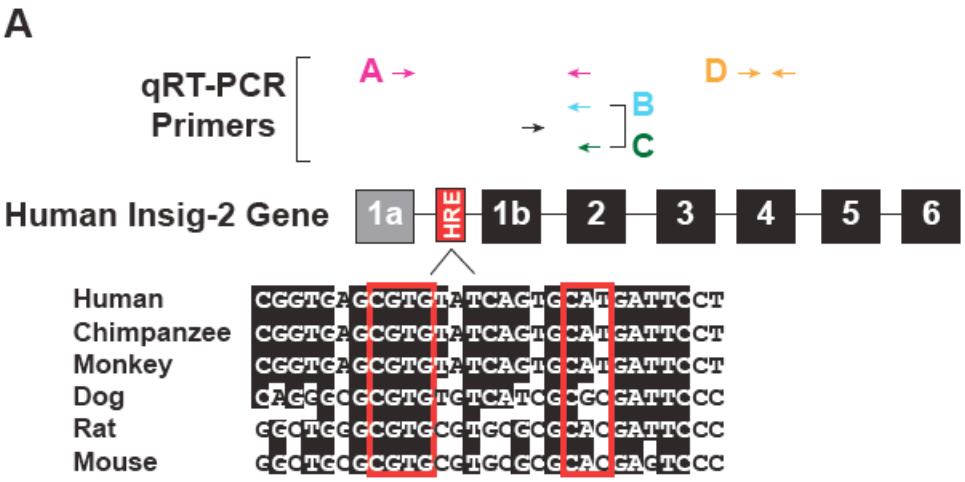
A
qRT-PCR Primers
A
B
C
D
Human Insig-2 Gene
1a
HRE
1b
2
3
4
5
6
Human
Chimpanzee
Monkey
Dog
Rat
Mouse

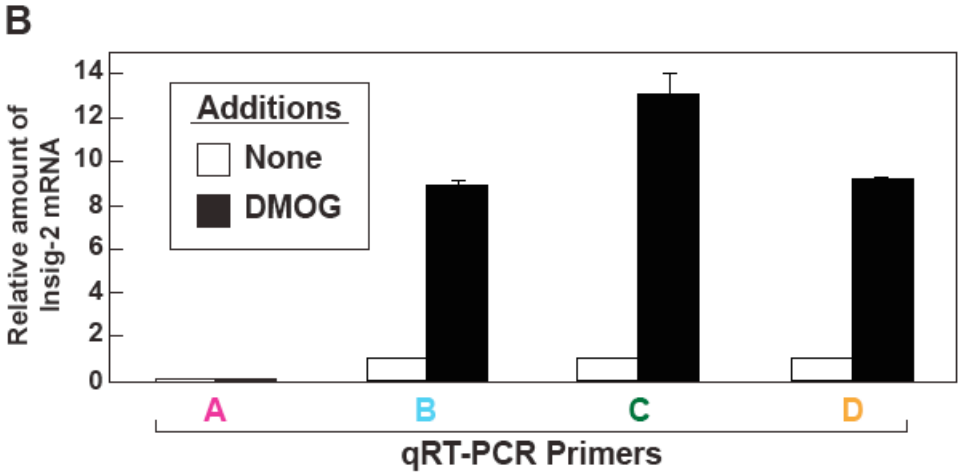
B
Relative amount of Insig-2 mRNA
14
12
10
8
6
4
2
0
Additions
None
DMOG
A
B
C
D
qRT-PCR Primers

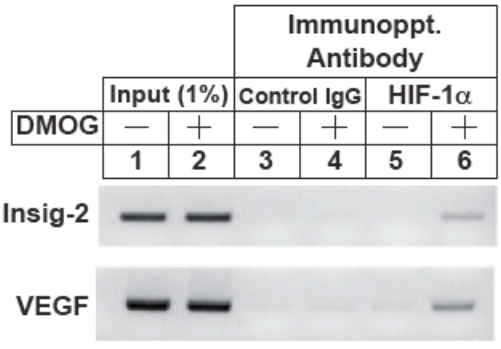
C
Immunoppt. Antibody
Input (1%)
Control IgG
HIF-1α
DMOG
—
+
—
+
—
+
1
2
3
4
5
6
Insig-2
VEGF

Figure 18. DMOG enhances binding of HIF-1α to HRE within intron-1 of the human Insig-2 gene. (A) Schematic diagram of human Insig-2 gene, showing the location of exons and HRE (top), and conservation of the Insig-2 HRE sequence across species (bottom). Exons are indicated by boxes labeled with corresponding exon numbers. The position of HRE conserved in mammalian species is indicated by a red box. Arrows denote the location of the primers used in the quantitative RT-PCR experiment shown in (B). (B) Total RNA isolated from SV-589 cells treated with or without 1 mM DMOG for 24 h at 37 ºC was subjected to quantitative RT-PCR as described in the legend to Fig. 15B using primer pairs A-D; cyclophilin B mRNA was used as an invariant control. Each value represents the amount of mRNA relative to that in untreated cells, which is arbitrarily defined as 1. *Bars* represent the ± S.E. of triplicate samples. (C) SV-589 cells were set up on day 0 at 1.0 X 10^6 cells per 150 mm dish in medium A containing 10% FCS. On day 1, cells were switched to the identical medium in the absence or presence of 1 mM DMOG. Following incubation for 24 h at 37°C, cells were fixed with formalin. After the sheared chromatin was incubated with 4 μg anti-HIF-1α IgG or control IgG, DNA was purified from each immunoprecipitate and subjected to PCR with primers that flank the HREs in the human Insig-2 or VEGF genes as described in "Materials and Methods." The resulting PCR products were visualized on an agarose gel by ethidium bromide staining.

A

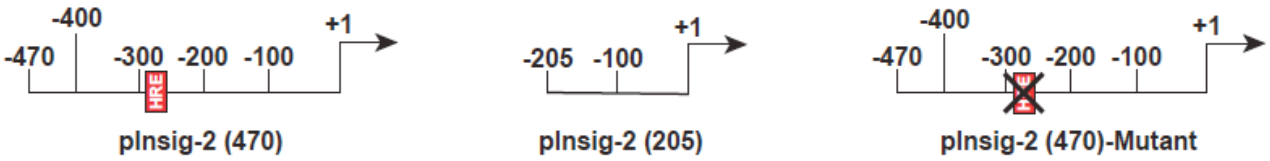

Sequences from -281 to -268

Wild Type 5′-CGTGtatcagtgCA-3′

Mutant A 5′-ATTGtatcagtgAT-3′

Mutant B 5′-CGCTtatcagtgAT-3′

Mutant C 5′-ATCTtatcagtgAT-3′

B

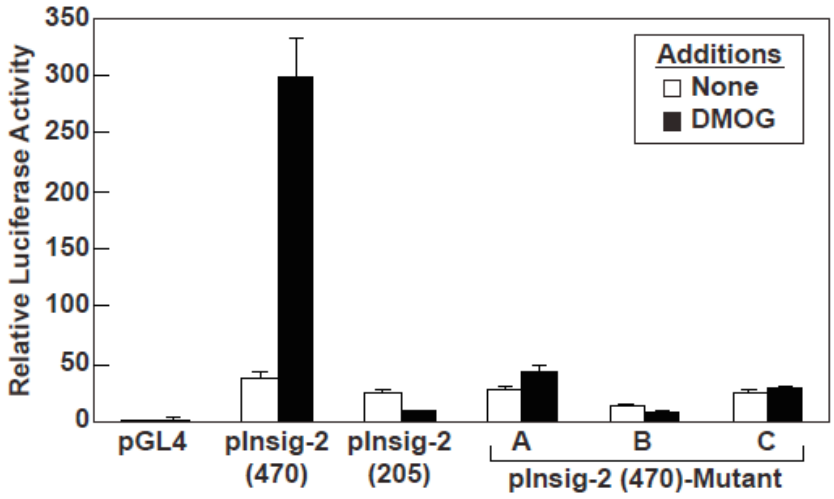

C

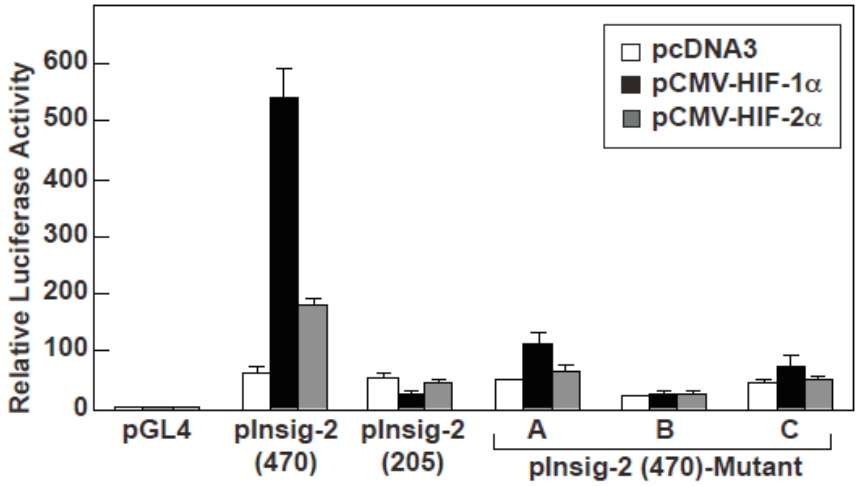

Figure 19. DMOG treatment and HIF overexpression in SV-589 cells activate the human Insig-2 promoter through an HRE-dependent mechanism. (A) Schematic diagram of pInsig-2 (470) encoding a fragment of intron 1 of the human Insig-2 gene containing the putative HRE (nucleotides -470 to +1, relative to the start site of transcription of the Insig-2 mRNA) linked to pGL4 firefly luciferase reporter; pInsig-2 (205) contains the luciferase reporter linked to intronic sequences -205 to +1 of the Insig-2 gene, whereas pInsig-2 (470)-Mutant contains the luciferase reporter linked to the 470 nucleotide intronic fragment harboring various mutations within the putative HRE. The sequence of the WT and mutant HRE in the human Insig-2 promoter is shown with mutated nucleotides highlighted in red (bottom). (B and C) SV-589 cells were set up on day 0 at 4.5 X 10^4 cells per each well of 6-well plate in medium A containing 10% FCS. (B) On day 1, cells were transfected with Renilla luciferase and the indicated Insig-2 HRE-luciferase reporter plasmids as described in "Materials and Methods." Following incubation for 5 hr at 37°C, cells were switched to medium A containing 10% FCS in the absence or presence of 1 mM DMOG. After 24 hr at 37°C, cells were harvested and luciferase activity was measured. Each value represents the amount of firefly luciferase activity normalized to Renilla luciferase activity relative to that in untreated cells transfected with pGL4, which is arbitrarily defined as 1. *Bars* denote ± S.E. of three independent experiments. (C) SV-589 cells were set up on day 0 and transfected on day 1 with Renilla luciferase and the Insig-2 HRE-luciferase reporter plasmids in the absence or presence of plasmids encoding non-degradable HIF-1α (pCMV-HIF-1α) or HIF-2α (pCMV-HIF-2α) as described in (B). On day 2, cells were harvested and luciferase activity was measured. Each value represents the firefly luciferase activity normalized to Renilla luciferase activity relative to that in cells transfected with empty vector, which is arbitrarily defined as 1. *Bars* denote mean ± S.E. of three independent experiments.

A

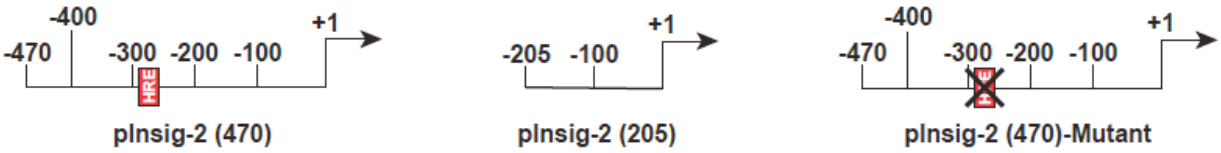

Sequences from -281 to -268

Wild Type 5′-CGTGtatcagtgCA-3′

Mutant A 5′-ATTGtatcagtgAT-3′

Mutant B 5′-CGCTtatcagtgAT-3′

Mutant C 5′-ATCTtatcagtgAT-3′

B

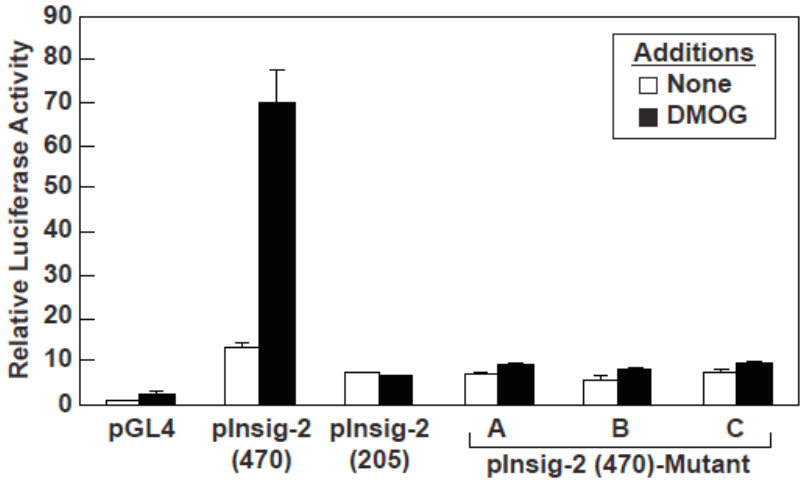

C

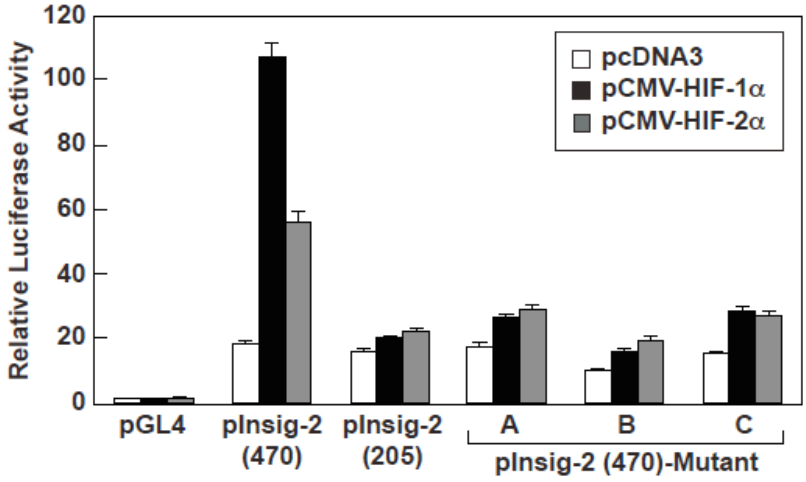

Figure 20. DMOG treatment and HIF overexpression in Huh-7 cells activate the human Insig-2 promoter through an HRE-dependent mechanism. (A) Schematic diagram of pInsig-2 (470) encoding a fragment of intron 1 of the human Insig-2 gene containing the putative HRE (nucleotides -470 to +1, relative to the start site of transcription of the Insig-2 mRNA) linked to pGL4 firefly luciferase reporter; pInsig-2 (205) contains the luciferase reporter linked to intronic sequences -205 to +1 (relative to start site of transcription of the Insig-2 mRNA) of the Insig-2 gene, whereas pInsig-2 (470)-Mutant contains the luciferase reporter linked to the 470 nucleotide intronic fragment harboring various mutations within the putative HRE. The sequence of the WT and mutant HRE in the human Insig-2 promoter is shown with mutated nucleotides highlighted in red (bottom). (B and C) Huh-7 cells were set up on day 0 at 1.0×10^5 cells per each well of 6 well plate in medium A containing 10% FCS. (B) On day 1, cells were transfected with Renilla luciferase and the indicated Insig-2 HRE-luciferase reporter plasmids as described in "Materials and Methods." Following incubation for 5 hr at 37°C, cells were switched to medium A containing 10% FCS in the absence or presence of 1 mM DMOG. After 24 hr at 37°C, cells were harvested and luciferase activity was measured. Each value represents the amount of firefly luciferase activity normalized to Renilla luciferase activity relative to that in untreated cells transfected with pGL4, which is arbitrarily defined as 1. *Bars* denote ± S.E. of three independent experiments. (C) Huh-7 cells were set up on day 0 and transfected on day 1 with Renilla luciferase and the Insig-2 HRE-luciferase reporter plasmids in the absence or presence of plasmids encoding non-degradable HIF-1α (pCMV-HIF-1α) or HIF-2α (pCMV-HIF-2α) as described in (B). On day 2, cells were harvested and luciferase activity was measured. Each value represents the firefly luciferase activity normalized to Renilla luciferase activity relative to that in cells transfected with empty vector, which is arbitrarily defined as 1. *Bars* denote mean ± S.E. of three independent experiments.

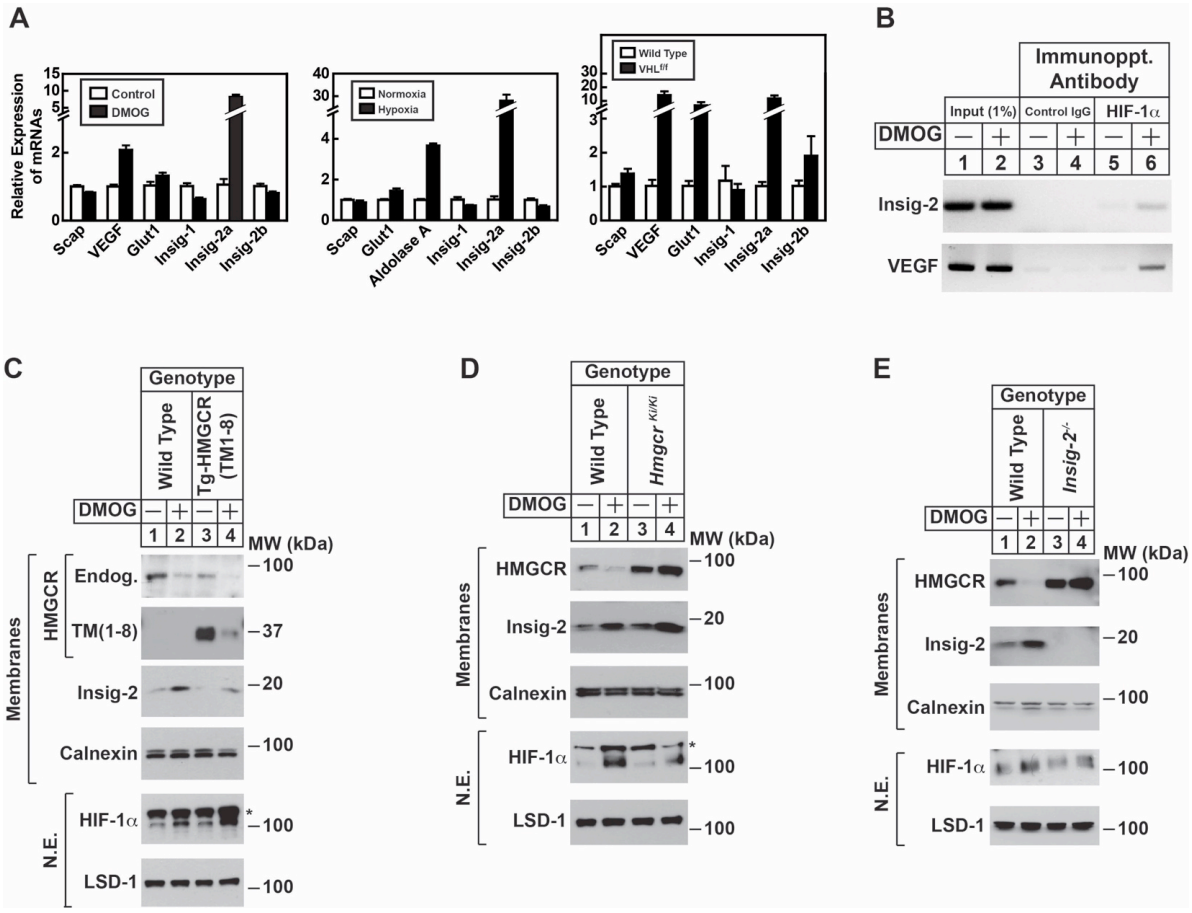

Figure 21. DMOG-induced expression of the Insig-2a transcript stimulates degradation of HMGCR in livers of mice. (A) WT C57BL/6J male mice (8-11 weeks of age) were either administered with 8 mg/day of DMOG in saline by oral gavage for 5 consecutive days or exposed to normoxia (21% O_2) or hypoxia (6% O_2) for 6 h as described in "Materials and Methods." *VHL*$^{f/f}$ mice and WT littermates were injected with adenovirus encoding for Cre recombinase driven by the CMV promoter. Mice were analyzed 4 days after injection. At the end of the treatment periods, the mice were sacrificed; RNA was isolated from the liver and quantitative RT-PCR analysis was performed as described in the legend of Fig. 15. Each value represents the expression of the indicated gene relative to that in the control group. Data are presented as means ± S.E. (n=3 for each group subjected to DMOG and hypoxia treatment; n=6 for each group injected with adenovirus encoding Cre recombinase). (B) ChIP assays were performed with livers from male C57BL/6J mice administered intraperitoneally with DMOG (8 mg) or saline once daily for three days. Four hours after the final injection, liver tissues were fixed with formalin and subjected to ChIP assays using primers that flank HRE in the mouse Insig-2 or VEGF genes as described in "Materials and Methods." (C-E) Male mice (8-11 weeks of

age, 4-6 mice/group) of the indicated genotypes were injected intraperitoneally with DMOG (8 mg) or saline once daily for three days. Mice were sacrificed 6 hr following the third injection and livers were harvested for subcellular fractionation as described in "Materials and Methods." Aliquots of membrane and nuclear extract (N.E.) fractions (20-50 μg total protein/lane) for each group were pooled and subjected to immunoblot analysis using anti-T7 IgG (against HMGCR (TM1-8)) and antibodies against endogenous (Endog.) HMGCR, Insig-2, calnexin, HIF-1α, and LSD-1. Asterisk (*) in the HIF-1α blot denotes a cross-reactive nonspecific band.

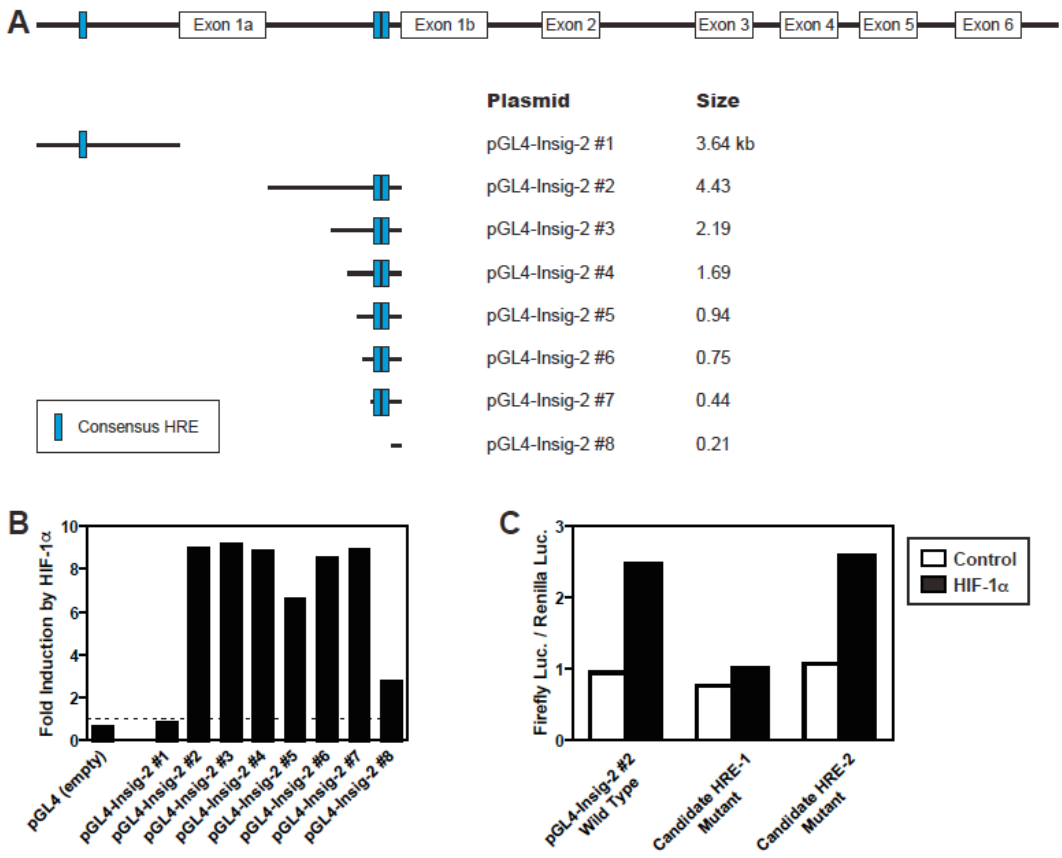

Figure 22. Identification of a functional HRE in the mouse Insig-2 gene. (A) Schematic representation of the mouse Insig-2 gene and reporter plasmids used for promoter analysis. Sequences conforming to the consensus HRE (5'-CGTGX$_{(1-8)}$ CA-3') are indicated by blue boxes. (B) On day 0, primary rat hepatocytes were isolated and plated in 6-well plates at a density of $5 \cdot 10^5$ cells per well in medium B supplemented with 5% FCS. After 4 h, cells were switched to medium C supplemented with 1 nM insulin, 100 nM dexamethasone, and 100 nM 3,3′,5-triiodo-L-thyronine. On day 1, cells were transfected with 4 µg DNA (1.8 µg of the indicated reporter plasmid and 0.4 µg of pGL4-TK-Renilla Luciferase, without or with 1.8 µg of pCMV-HIF-1α) per well in medium D. After 6 h, cells were refed medium C containing 100 nM insulin, 100 nM dexamethasone, and 100 nM 3,3′,5-triiodo-L-thyronine for 36 h. At the end of the incubation period, cells were harvested and lysed in a detergent-containing buffer. Firefly and Renilla luciferase activities were measured as described in "Materials and Methods." Firefly luciferase activities were normalized to Renilla luciferase activities, and data are presented as the fold induction by HIF-1α. (C) Mutation of candidate HRE-1 abolishes HIF-mediated induction of the Insig-2 reporter plasmid. Primary rat hepatocytes were isolated, transfected, and treated as described in

"Material and Methods." Data are presented as the normalized ratio of firefly luciferase activities divided by Renilla luciferase activities.

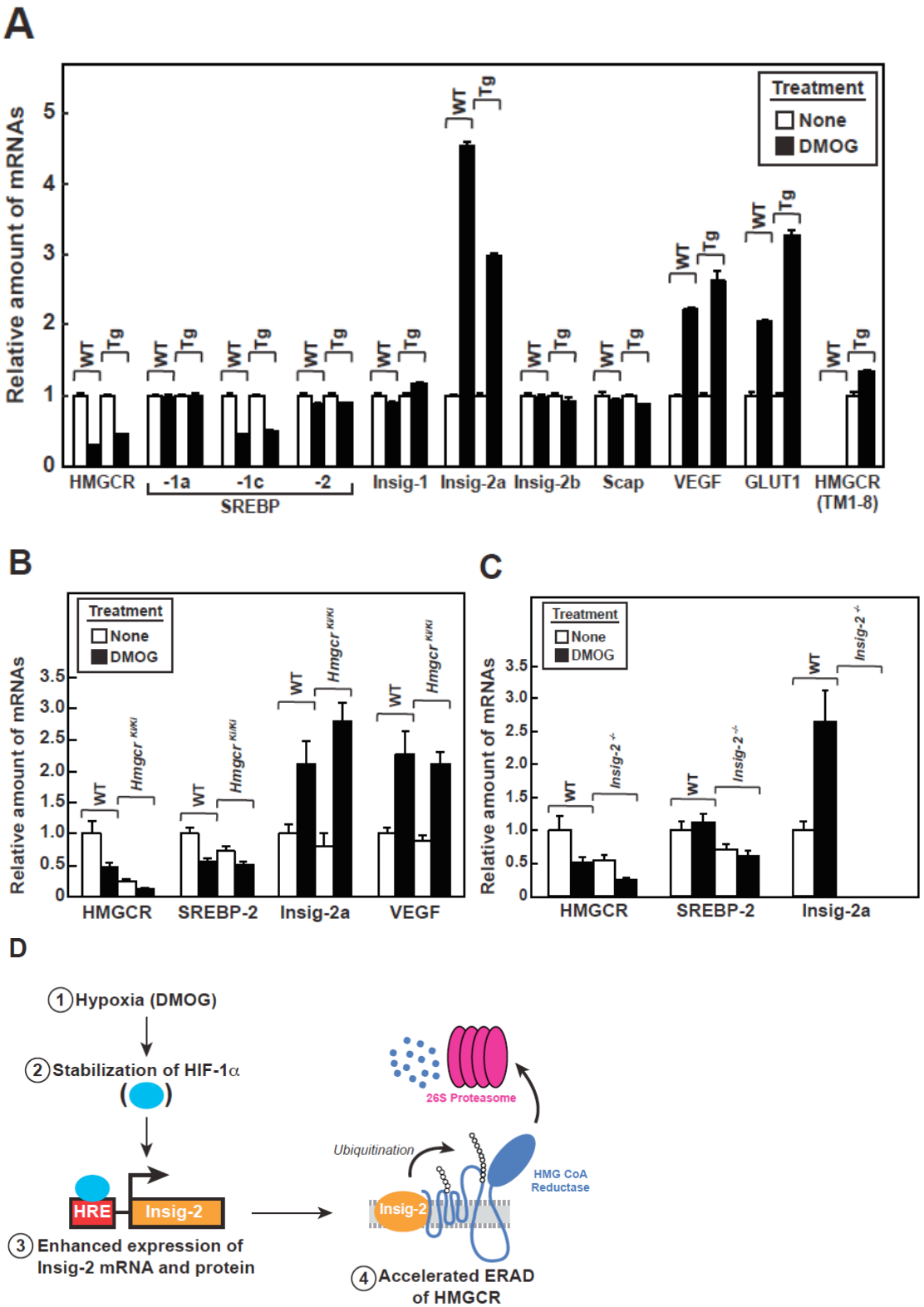
A
Relative amount of mRNAs
Treatment
None
DMOG
WT
Tg
HMGCR
-1a
-1c
-2
SREBP
Insig-1
Insig-2a
Insig-2b
Scap
VEGF
GLUT1
HMGCR (TM1-8)
B
Hmgcr KI/KI
HMGCR
SREBP-2
Insig-2a
VEGF
C
Insig-2 -/-
D
1 Hypoxia (DMOG)
2 Stabilization of HIF-1α
HRE
Insig-2
3 Enhanced expression of Insig-2 mRNA and protein
26S Proteasome
Ubiquitination
HMG CoA Reductase
4 Accelerated ERAD of HMGCR

Figure 23. DMOG modulates expression of mRNAs encoding components of the Scap-SREBP pathway in livers of mice. Male mice (8-11 weeks of age, 4-6 mice/group) of the indicated genotypes were administered intraperitoneally with saline in the absence or presence of DMOG (8 mg) once daily for three days. Mice were sacrificed 6 hr after the third injection and livers were harvested for total RNA isolation. (A) Total RNA from each tissue was reverse-transcribed. Aliquots of resulting first-strand cDNA were pooled for each group and subjected to quantitative PCR using primers for the indicated mRNAs; apoB mRNA was used as an invariant control. Each value represents the amount of mRNA relative to that in WT administered with saline, which is arbitrarily defined as 1. *Bars,* mean ± S.E. of triplicate samples. (B-C) Equal amounts of RNA from the individual mice were subjected to quantitative RT-PCR using primers against the indicated gene; apoB mRNA was used as an invariant control. Each value represents the amount of mRNA relative to that in WT administered with saline, which is arbitrarily defined as 1. *Bars* denote ± S.E. of 4-6 individual mice. (D) Proposed model for HIF-mediated regulation of HMGCR degradation.

Table 6. Primers used for RT-PCR analysis.

Gene	Species	Primers (Forward and Reverse)
β-Actin (control)	Hamster	5'-GGCTCCCAGCACCATGAA-3' 5'-GCCACCGATCCACACAGAGT-3'
Insig-1	Hamster	5'-GGCTTGTGGTGGACATTCG-3' 5'-GGCGATGGTGATCCCAAGT-3'
Insig-2	Hamster	5'-GGGTGGTGCTCTTCTTCATTG-3' 5'-CAGGTGGAAAAAGTGTCACGTTT-3'
Scap	Hamster	5'-GTACCTGCAGATGATGTCCATTG-3' 5'-CTGCCATCCCGGAAAGTG-3'
VEGF	Hamster	5'-AGCGGAGAAAGCATTTGTTTG-3' 5'-CCAAGATCCGCAGACGTGTAAATGTTCC-3'
36B4 (control)	Rat	5'-TTCCCACTGGCTGAAAAGGT-3' 5'-CGCAGCCGCAAATGC-3'
GLUT1	Rat	5'-CAGTGTATCCTGTTGCCCTTCTG-3' 5'-CCCGGTTCTCCTCGTTACG-3'
Insig-1	Rat	5'-TGCAGATCCAGCGGAATGT-3' 5'-CCAGGCGGAGGAGAAGATG-3'
Insig-2a	Rat	5'-GACGGATGTGTTGAAGGATTTCT-3' 5'-TGGACTGAAGCAGACCAATGTC-3'
Insig-2b	Rat	5'-CCGGCAGAGCTCAGGATTT-3' 5'-AACTGTGGACTGAAGCAGACCAA-3'
Scap	Rat	5'-TGCTCACCGTGGAGATGTCA-3' 5'-TCGGTCCCAGATGTTGATGA-3'
Cyclophilin B (control)	Human	5'-GGAGATGGCACAGGAGGAAA-3' 5'-CCGTAGTGCTTCAGTTTGAAGTTCT-3'
HMGCR	Human	5'-CAAGGAGCATGCAAAGATAATCC-3' 5'-GCCATTACGGTCCCACACA-3'
SREBP-1a	Human	5'-CGAAGACATGCTTCAGCTTATCA-3' 5'-CCAGCATAGGGTGGGTCAAA-3'
SREBP-1c	Human	5'-TCGCGGAGCCATGGATT-3' 5'-GGAAGTCACTGTCTTGGTTGTTGA-3'
SREBP-2	Human	5'-CGGTAATGATCACGCCAACAT-3' 5'-TGGTATATCAAAGGCTGCTGGAT-3'

Insig-1	Human	5’-CCCAGATTTCCTCTATATTCGTTCTT-3’ 5’-CACCCATAGCTAACTGTCGTCCTA-3’
Insig-2 set A	Human	5’-TGAATTTATTGATGGCAAGAGATCTG-3’ 5’-GGTACCACATCTTGTCCTAAAGTAGGA-3’
Insig-2 set B	Human	5’-GTGGGAGTGGAGGAGGAAGAG-3’ 5’-GGTACCACATCTTGTCCTAAAGTAGGA-3’
Insig-2 set C	Human	5’-GTGGGAGTGGAGGAGGAAGAG-3’ 5’-TTGTCCTAAAGTAGGACCTACCAGAAAT-3’
Insig-2 set D	Human	5’-TGTCTCTCACACTGGCTGCACTA-3’ 5’-CTCCAAGGCCAAAACCACTTC-3’
Scap	Human	5’-GGGTCAGCCATGTGTTTGC-3’ 5’-TGCTGCGGTCCCAGATG-3’
VEGF	Human	5’-CGCAGCTACTGCCATCCAAT-3’ 5’-TGGCTTGAAGATGTACTCGATCTC-3’
GLUT1	Human	5’-CCTGTGTATGCCACCATTGG-3’ 5’-GCTCGCTCCACCACAAACA-3’
36B4 (control for cells)	Mouse	5’-CACTGGTCTAGGACCCGAGAAG-3’ 5’-GGTGCCTCTGGAGATTTTCG-3’
ApoB (control)	Mouse	5’-CGTGGGCTCCAGCATTCTA-3’ 5’-TCACCAGTCATTTCTGCCTTTG-3’
HMGCR	Mouse	5’-CTTGTGGAATGCCTTGTGATTG-3’ 5’-AGCCGAAGCAGCACATGAT-3’
HMGCR (TM1-8)	Mouse	5’-GCCCTAAGTTCAAACTCTCAGGATGAAG-3’ 5’-GGGCCCTCTAGATCACATATTAATTAAACCC-3’
SREBP-1a	Mouse	5’-GGCCGAGATGTGCGAACT-3’ 5’-TTGTTGATGAGCTGGAGCATGT-3’
SREBP-1c	Mouse	5’-GGAGCCATGGATTGCACATT-3’ 5’-GGCCCGGGAAGTCACTGT-3’
SREBP-2	Mouse	5’-GCGTTCTGGAGACCATGGA-3’ 5’-ACAAAGTTGCTCTGAAAACAAATCA-3’
Insig-1	Mouse	5’-TCACAGTGACTGAGCTTCAGCA-3’ 5’-TCATCTTCATCACACCCAGGAC-3’
Insig-2a	Mouse	5’-CCCTCAATGAATGTACTGAAGGATT-3’ 5’-TGTGAAGTGAAGCAGACCAATGT-3’

Insig-2b	Mouse	5’-CCGGGCAGAGCTCAGGAT-3’ 5’-GAAGCAGACCAATGTTTCAATGG-3’
Scap	Mouse	5’-ATTTGCTCACCGTGGAGATGTT-3’ 5’-GAAGTCATCCAGGCCACTACTAATG-3’
Aldolase A	Mouse	5’-TCCCTTCCCCCAAGTTATCAA-3’ 5’-GGCACCACACCCTTATCTACCT-3’
VEGF	Mouse	5’-CACGACAGAAGGAGAGCAGAA-3’ 5’-CGCTGGTAGACGTCCATGA-3’
GLUT1	Mouse	5’-GGTGTGCAGCAGCCTGTGTA-3’ 5’-CAACAAACAGCGACACCACAGT-3’

Table 7. Sequences of the siRNAs used for RNA interference.

Gene	siRNA
HIF-1α	5'-CAGAAAUGGCCUUGUGAAAUU-3'
HIF-2α	5'-ACACAGAGGCCAAGGACCAUU-3'
HIF-1α scrambled	5'-CAGAGGUGGCCUUGUGGAAUU-3'
HIF-2α scrambled	5'-ACACAGGGGCCGGGGACCAUU-3'
GFP	5'-CAGCCACAACGUCUAUAUCUU-3'

Table 8. Primers used for ChIP assays.

Region	Primers (Forward and Reverse)
Human Insig-2 HRE	5'-GTAGCATGGAGACGAGAGACAAAT-3' 5'-GTTGTCGGATCTGCTGTTGTTTG-3'
Human VEGF HRE	5'-CCTACAGACGTTCCTTAGTGCTG-3' 5'-ACCAAGTTTGTGGAGCTGAGA-3'
Mouse Insig-2 HRE	5'-GCTGCCTTTAATCCGTATTCAGAAA-3' 5'-CAGAGGTTCTGGATGGGCATCTG-3'
Mouse Insig-2 HRE	5'-CTAGAGTTATGCTTCCGAGGTCAA-3' 5'-TGAGGATAGGGACAACTAGAGTGA-3'

Table 9. Primers used for generation of plasmids.

Plasmid	Primers (Forward and Reverse)
Cloning	
pGL4-Insig-2 #1	5’-CAGGACCCAAACAACAGCACATTC-3’ 5’-GAGGCAATGGCAGGGGTCAGA-3’
pGL4-Insig-2 #2	5’-GGTGTCGAATTCAGAGGGGTTAGG-3’ 5’-CGTCCCCGGCCAAATAAGC-3’
pGL4-Insig-2 #3	5’-GCAGGGCAACAGCAGAACTATCAA-3’ 5’-CGTCCCCGGCCAAATAAGC-3’
pGL4-Insig-2 #4	5’-CCATTGGGGCTGCTCACATCC-3’ 5’-CGTCCCCGGCCAAATAAGC-3’
pGL4-Insig-2 #5	5’-CTCCCCACTTCCCTGACACATCTC-3’ 5’-CGTCCCCGGCCAAATAAGC-3’
pGL4-Insig-2 #6	5’-GGAAGGTCTTAGCTGGGCGTGGTG-3’ 5’-CGTCCCCGGCCAAATAAGC-3’
pGL4-Insig-2 #7	5’-TGCAGGCGACAACCGTGGAG-3’ 5’-CGTCCCCGGCCAAATAAGC-3’
pGL4-Insig-2 #8	5’-GAAGTCCTTTTGCCCCGTCTCC-3’ 5’-CGTCCCCGGCCAAATAAGC-3’
pInsig-2 (470)	5’-GGAGCTCCATGGAGACGAGAGACAAATAACTATG-3’ 5’-TCCCAGGCTGCAAAAACACAAGTAG-3’
pInsig-2 (205)	5’-CAAACAACAGCAGATCCGACAAC-3’ 5’-TCCCAGGCTGCAAAAACACAAGTAG-3’
pCMV-HIF-1α	5’-ATGGAGGGCGCCGGC-3’ 5’-CTAAATAATTCCTACTGCTTGAAAAAGTGAACCATCATGTTCCA-3’
Mutagenesis	
pInsig-2 (470)	5’-CGCCCCTCGGTGAGTGTGATTGTATCAGTGAGTGATTCCTTTACTCCGCC-3’
Mutant A	5’-GGCGGAGTAAAGGAATCACTCACTGATACAATCACACTCACCGAGGGGCG-3’
pInsig-2 (470)	5’-CGCCCCTCGGTGAGTGTGCGCTTATCAGTGAGTGATTCCTTTACTCCGCC-3'
Mutant B	5’-GGCGGAGTAAAGGAATCACTCACTGATAAGCGCACACTCACCGAGGGGCG-3’
pInsig-2 (470)	5’-CGCCCCTCGGTGAGTGTGATCTTATCAGTGAGTGATTCCTTTACTCCGCC-3’
Mutant C	5’-GGCGGAGTAAAGGAATCACTCACTGATAAGATCACACTCACCGAGGGGCG-3’

Candidate HRE-1	5’-GCTGCGTACTTACTCGCGGTAGAGTCC-3’
Mutant	5’-GGACTCTACCGCGAGTAAGTACGCAGC-3’
Candidate HRE-2	5’-GACAACTACTGAGCCTGTGTACCGGC-3’
Mutant	5’-GCCGGTACACAGGCTCAGTAGTTGTC-3’

CHAPTER FOUR
Conclusions and Perspectives

4.1. Significance of HMGCR ERAD in Cholesterol Homeostasis

A class of drugs called statins, competitive inhibitors of HMGCR, are the most commonly prescribed medications for cholesterol-lowering and reducing the risk of cardiovascular diseases (86-88). Statins exert cholesterol-lowering action by inhibiting cholesterol synthesis, which leads to activation of SREBP-2, up-regulation of LDL receptor, and increased uptake of circulating LDL cholesterol. Paradoxically, cholesterol synthesis is only slightly reduced or unchanged in animals and humans administered with statins (62, 89-91). This resistance results from the reduction in sterols and nonsterol isoprenoids that normally inhibit HMGCR through transcriptional and post-transcriptional regulations. As a result, humans and other animals subjected to statins develop marked accumulation of hepatic HMGCR protein (63, 64). Inhibition of sterol-accelerated ERAD is one plausible reason for the statin-induced compensatory increase in HMGCR protein. This increase in HMGCR would partially overcome inhibitory effects of statins and thereby limit lowering of LDL, which may explain why only a subset of patients benefit from the medication. Therefore, it is probable that the ability of statins to inhibit the enzyme will be enhanced by blocking the compensatory increase in HMGCR by accelerating its ERAD, which will eventually lead to further lowering of LDL cholesterol and the incidence of cardiovascular events. For this reason, the molecular mechanisms that govern the degradation of HMGCR (e.g. ERAD) have been actively investigated. However, the

physiological relevance of the system that regulates the rapid degradation of HMGCR has been unclear *in vivo*.

The data presented in the current study provides compelling evidence that ERAD of HMGCR is a critical player in homeostatic regulation of cholesterol synthesis *in vivo*. There have been attempts to assess the stability of HMGCR using indirect techniques (such as measurement of HMGCR activity after cycloheximide treatment) (49); however, it was not known whether HMGCR is properly degraded in a regulated manner by cholesterol or cholesterol biosynthetic intermediates *in vivo* through the identical mechanisms that have been revealed in cultured cells. This was partly due to the inability to directly measure these parameters *in vivo*. Thus, the current study utilized a novel animal model: the liver-specific transgenic mouse that harbors the transgene encoding for the membrane domain of HMGCR, which is necessary and sufficient for sterol-induced degradation of HMGCR. Fig. 9 and 11 demonstrate that this mouse model is a valuable tool for monitoring the degradation of HMGCR in the liver by the end-products of mevalonate metabolism. A diet containing 2% cholesterol robustly reduced the levels of both endogenous HMGCR and the membrane domain of HMGCR in the liver of mice. Sterol-dependent modulation of the stability of HMGCR protein *in vivo* was further confirmed in another experiment where the animals were fed a diet containing lovastatin (Fig. 11); lovastatin-induced depletion of sterols elevated HMGCR expression at least in part due to increased half-life of the membrane domain of HMGCR.

Preceded by the finding that HMGCR is degraded in a regulated manner by sterol in animals, the current study also investigated the extent to which the degradative regulation

of HMGCR contributes to the overall regulation of HMGCR and homeostatic control of cholesterol biosynthesis in multiple settings. This was achieved by exploiting another genetically-manipulated mouse model: a whole-body knock-in mouse model that expresses a mutant HMGCR which is resistant to Insig-mediated ubiquitination and ERAD. In the steady state, HMGCR was markedly accumulated in the liver of *Hmgcr*$^{Ki/Ki}$ mice (Fig. 7A) and hepatic cholesterol level was elevated (Fig. 6A) which led to transcriptional inhibition of HMGCR through prevention of SREBP-2 processing (Fig. 7B). A battery of cholesterol synthetic genes such as HMG CoA synthase (Fig. 8C, 10B) and squalene synthase (Fig. 10B) that are under the transcriptional control of SREBP-2 were also suppressed. However, another axis of the negative feedback control, the ERAD of HMGCR, was not effectively stimulated in *Hmgcr*$^{Ki/Ki}$ mice as revealed by the suppressed ubiquitination (Fig. 8B). The expression of HMGCR in the liver also remained elevated in *Hmgcr*$^{Ki/Ki}$ mice, indicating the significant role of the degradative regulation in the overall control of HMGCR in the steady state. Notably, the sterol synthesis rate in *Hmgcr*$^{Ki/Ki}$ mice was not greater than that of WT littermates, despite the accumulation of cholesterol and cholesteryl ester in the liver. The failure for sterol synthesis rate to reflect the accumulated HMGCR can be explained by the fact that the technique employed here does not specifically detect the synthesis of cholesterol, but that of all the sterol species. Thus, there is still a possibility that the synthetic rate of cholesterol is greater in *Hmgcr*$^{Ki/Ki}$ mice as compared to WT littermates. Indeed, a recent study reported that administration of statins to mice, which leads to a remarkable accumulation of HMGCR similarly to *Hmgcr*$^{Ki/Ki}$ mice in the steady state, increases hepatic cholesterol biosynthesis (92). It is also probable that

suppression of SREBP-2 target genes overcomes the excessive flux of mevalonate into the mevalonate pathway; accumulation of hepatic cholesterol in *Hmgcr*$^{Ki/Ki}$ mice could result from other sources than *de novo* synthesis such as uptake from the bloodstream. Further studies are required to address this question.

An important finding in the current study with clinical implications is that statin-induced compensatory accumulation of HMGCR is primarily mediated through slowed degradation of the enzyme. The extent to which HMGCR is increased by lovastatin administration was markedly blunted in the *Hmgcr*$^{Ki/Ki}$ mice where HMGCR is resistant to sterol-dependent ubiquitination (Fig. 11D). This indicates that inhibition of ubiquitination and proteasomal degradation of HMGCR is the major factor contributing to the statin-induced accumulation of HMGCR. This phenomenon contrasts with negligible contribution of the degradative control to cholesterol-induced reduction in HMGCR: feeding WT mice a high-cholesterol diet robustly decreased hepatic HMGCR, which was not reversed in *Hmgcr*$^{Ki/Ki}$ mice (Fig. 9D). One potential explanation for the differential contribution of the degradative regulation to HMGCR expression by a high-cholesterol diet and lovastatin administration is the critical role of nonsterol isoprenoids in degradation of HMGCR. The change in HMGCR expression caused by cholesterol replenishment is largely triggered by an excess of cholesterol in the diet, which the transcriptional regulation depends on. Thus, in *Hmgcr*$^{Ki/Ki}$ mice where the degradative regulation is impaired, cholesterol replenishment could still markedly reduce HMGCR through transcriptional inhibition. In contrast, lovastatin administration reduces both the levels of sterols and nonsterol isoprenoids. As the maximal degradation of HMGCR requires the presence of

both sterols and nonsterol isoprenoids, lovastatin administration can fully trigger the degradative axis of the feedback regulation in contrast to cholesterol-feeding. Therefore, the lovastatin-induced accumulation of HMGCR is markedly blunted in *Hmgcr*$^{Ki/Ki}$ mice where the degradative regulation is impaired, indicating that the compensatory accumulation of HMGCR by statins is significantly mediated through the retarded turnover of the protein. This finding supports the notion that a novel therapy that targets the degradation of HMGCR will improve the efficacy of statins by preventing HMGCR accumulation.

4.2. Recommendations for the Future Studies Using *Hmgcr*$^{Ki/Ki}$ Mice

There have been a few reports on animal models that feature elevated expression of HMGCR; however, the mechanisms for the elevated expression were not specific to HMGCR stabilization. For example, liver-specific deletion of gp78, an E3 ubiquitin ligase involved in Insig-mediated ubiquitination of HMGCR, accumulates HMGCR in the liver of mice. However, deletion of gp78 simultaneously stabilizes Insig and suppresses SREBP, thereby altering the transcription of genes involved in fatty acid synthesis and cholesterol synthesis (27). Therefore, gp78 knock-out mouse model is not proper for studying the physiological role of HMGCR ERAD in animals. In this regard, it is expected that *Hmgcr*$^{Ki/Ki}$ mouse model will specifically address the physiological impact of HMGCR ERAD and discover the novel functions of cholesterol biosynthetic intermediates beyond homeostatic regulation of cholesterol synthesis. Especially, the mouse model will help unveil the function of HMGCR-derived nonsterol isoprenoids that participate in vital

cellular processes such as protein prenylation. Prenylation is a protein post-translational modification defined by the covalent bonding of farnesyl pyrophosphate or geranylgeranyl pyrophosphate to cysteine residues (93). A group of proteins that are modified through prenylation is small guanine triphosphate (GTP)-binding proteins such as Ras, Rac, and Rho. Preliminary experiments revealed that the levels of farnesylated proteins (N-Ras and K-Ras) and geranylgeranylated protein (RhoA) in the membrane fraction of *Hmgcr*$^{Ki/Ki}$ mice were increased as compared to that of WT littermates, while the unprenlyated forms were reduced or unchanged (data not shown). This indicates that stabilization of HMGCR increases the levels of geranylgeranyl pyrophosphate and farnesyl pyrophosphate and stimulates the prenylation of proteins, thereby increasing their affinity to plasma membrane.

Ras activates signaling pathways related to cell proliferation and thus is involved in the development of various types of cancer (94, 95). Especially, mutations in *KRAS* that favor GTP binding and render it constitutively active are common in pancreatic adenocarcinoma (96-98), non-small cell lung cancer (99), and colon adenoma (100). *NRAS* mutations are frequently found in patients of hematological malignancies (101, 102). As substitution of GTP for guanine diphosphate occurs preferentially in the membrane-localized Ras, it would be an interesting question whether *Hmgcr*$^{Ki/Ki}$ mice are more susceptible to tumor induction and whether the enhanced tumorigenesis is associated with slowed ERAD of HMGCR and subsequent increase in HMGCR-derived nonsterol isoprenoids. This hypothesis is also in line with the attempts to develop geranylgeranyl transferase inhibitors and statins as anti-cancer agents (103-105).

Another prenylated protein of interest is liver kinase B1 (LKB1). *LKB1* is a tumor suppressor gene whose mutation causes a rare hereditary disease Peutz-Jeghers cancer syndrome (106). LKB1 also regulates energy homeostasis by directly activating adenosine monophosphate-activated protein kinase (AMPK). The activity of LKB1 is regulated in part through post-translational modification including the farnesylation at a highly conserved CAAX motif within its COOH-terminal residues (107-109). In mice, Cys433 in CAAX motif is farnesylated (110, 111). LKB1 farnesylation promotes association with the plasma membrane, which is required for efficient phosphorylation and activation of AMPK in mice (110). Preliminary studies demonstrated that the level of farnesylated LKB1 protein in the membrane fraction was increased in the liver of $Hmgcr^{Ki/Ki}$ mice (data not shown). This indicates that HMGCR-derived farnesyl pyrophosphate promotes the farnesylation and membrane translocation of LKB1, leading to a robust increase in phosphorylation of AMPK in $Hmgcr^{Ki/Ki}$ mice (data not shown). As a sensor of energy level in cells, AMPK is widely considered to be a potential therapeutic target for metabolic syndrome. Anti-diabetic drugs such as metformin and thiazolidinediones and a hormone adiponectin are known to activate AMPK and possess an ability to improve insulin resistance (112). In this regard, it would be an interesting project to determine whether $Hmgcr^{Ki/Ki}$ mice are able to resist metabolic dysregulation caused by inducers of insulin resistance such as long-term feeding of a high-fat diet. Completion of this project will link ERAD of HMGCR to energy homeostasis.

The preliminary studies mentioned above are not accompanied by the quantification of nonsterol isoprenoids, which is necessary for better understanding of their involvement

in cancer development and energy metabolism. The combination of the animal model and techniques for quantification of nonsterols such as LC-MS/MS (113, 114) will create a synergy for studying the physiological relevance of ERAD of HMGCR in animals.

4.3. Physiological Relevance of HIF-1-Mediated Degradation of HMGCR

Pharmacological and physiological stabilization of HIF-1α up-regulates Insig-2 and accelerates the degradation of HMGCR, which was revealed by the attenuated expression of the membrane domain of HMGCR in Tg-HMGCR (TM1-8) mice (Fig. 21). As the rationale behind the usage of the membrane domain as an indicator of HMGCR turnover is its necessity and sufficiency for sterol-induced ubiquitination and degradation, the primary signal that triggers the reduction in the membrane domain is considered to be cellular sterols. Therefore, the significant reduction in the levels of the membrane domain by HIF-1α stabilization is thought to be mediated by either 1) elevated sterol levels or 2) the sensitization of the ubiquitination machinery to the cellular sterols. The current study does not include the data that directly supports the first scenario; however, it is conceivable that accumulation of 24,25-DHL observed in CHO cells cultured under hypoxic conditions (39) can similarly occur in mouse liver tissues and trigger the degradation of HMGCR in mice. Further studies are warranted to quantify the levels of various sterols in animal tissues using analytic techniques such as LC-MS/MS. The second scenario is strongly underpinned by the evidence provided in the current study: HIF-1α stabilization up-regulates Insig-2, and thereby sensitizes Insig-2-dependent ubiquitination to existing sterols and promotes proteasomal degradation of HMGCR.

To the best of my knowledge, this is the first work showing that Insig-2 is a *bona fide* transcriptional target of HIF-1. Intron 1 of human and mouse Insig-2 genes contains a consensus HRE sequence (Fig. 18), which was confirmed as a functional HRE by luciferase promoter assays (Fig. 19, 20, and 22). Despite the conservation of the HRE in mouse and human, the consensus HRE differentially controls the transcription of Insig-2 in human and mouse. Fig. 18B shows that the consensus HRE activates the transcription of Insig-2b, but not Insig-2a, in human skin fibroblasts (SV-589). However, in mouse liver, Insig-2a is transactivated by HRE upon DMOG administration (Fig. 21). Fernandez-Alvarez et al. reported that Insig-2a transcript does not express in human liver, human hepatoma cell line (HepG2), or human embryonic kidney cell line (HEK293T) in the steady state (79). Thus, it is conceivable that human selectively expresses Insig-2b transcript in various tissues. Further studies are needed to rule out the possibility that, unlike in the steady state, hypoxic stress can activate the transcription of Insig-2a in human.

A remarkable conservation of HRE in the intron 1 of mammalian Insig-2 gene (Fig. 18A) raises a question on the physiological meaning of HIF-1 regulation of Insig-2: why have mammals evolved to develop a system that up-regulates Insig-2 under the conditions where HIF-1 signaling is activated? Since Insig-2 was first reported (14), it has been mostly studied in the context of cholesterol metabolism as an inhibitor of Scap-SREBP pathway and a regulator of the degradation of HMGCR. Considering Insig-2-mediated inhibition of cholesterol synthesis, it is likely that HIF-1 induction of Insig-2 expression prevents wasting of oxygen in cholesterol biosynthesis and diverts oxygen to more crucial processes in cells to survive under hypoxic conditions. Another interesting question is

whether Insig-2 links inflammation-activated HIF-1 signaling to cholesterol metabolism. It has been reported that pathologic conditions in the liver (e.g. fatty liver and liver inflammation) cause hypoxia due to hepatocyte swelling and subsequent blood vessel constriction. Independently of hypoxia, the pro-inflammatory transcription factor NF-kB is a critical transcriptional activator of HIF-1α (115). As high cholesterol contents in the liver exacerbates inflammation (116-120), it is possible that inflammatory signaling stimulates HMGCR degradation and suppresses cholesterol synthesis to prevent uncontrolled inflammation. Anti-inflammatory role of HMGCR degradation could be also explained by the reduction of nonsterol isoprenoids, which is speculated to be the mechanism for the anti-inflammatory effect of statins (121, 122). Notably, there are reports supporting the pro-inflammatory role of HMGCR degradation as well: stressed cells induce inflammation to remove damaged cells supposedly through a mechanism that requires the inhibition of cholesterol synthesis (123-125). The two opposing hypotheses will open up many questions regarding the role of HMGCR in inflamed cells with hypoxic stress. Further studies are encouraged to elucidate the role for HIF-1α-mediated Insig-2 up-regulation and HMGCR degradation in the modulation of innate immunity in the liver.

In the current study, the mice administered with DMOG or exposed to hypoxia did not show a significant decrease in cholesterol levels in the plasma or liver (data not shown), despite the augmented degradation of HMGCR and suppression of SREBP-2-dependent cholesterol biosynthetic genes. The failure to see dramatic changes in metabolic parameters is likely due to the time frame chosen for the current study. The conditions employed such as 3-day administration of DMOG and 6-hr hypoxia challenge are

appropriate for studying the molecular basis of the homeostatic regulation of cellular processes against acute hypoxic stress, whereas long-term hypoxic challenge such as 3-week exposure to mild hypoxia (126) and multiple weeks of administration of prolyl hydroxylase inhibitor (127, 128) could be a better model for studying the role for hypoxia/HIF in cholesterol metabolism. Another possible explanation for this is hypoxia-induced suppression of cholesterol secretion via bile duct. ABCG5 and ABCG8 which are responsible for the biliary secretion of hepatic cholesterol were down-regulated in DMOG-administered liver (data not shown), which is consistent with a previous report that the expression of ABCG5 and ABCG8 was suppressed in HepG2 cells cultured under hypoxic conditions (129). Physiological studies such as measurement of biliary cholesterol and fecal cholesterol are required to test this hypothesis.

4.4. The Mechanism Underlying HIF-1α-Selective Up-Regulation of Insig-2

The current study demonstrates that Insig-2 is selectively activated by HIF-1α although consensus HRE sequence can interact with both HIF-1α and HIF-2α. The selectivity of HIF-1α versus HIF-2α target genes may depend on several factors and vary with duration of hypoxia and/or the abundance of stabilized HIF-α proteins (130). Two independent groups reported that DNA-binding domain in the NH_2-terminal of HIF-1α and HIF-2α does not distinguish between HIF-1α-selective and HIF-2α-selective target genes; COOH-terminal transcriptional activation domain is responsible for the selectivity (131, 132). It has been also reported that target gene selectivity depends on the interaction between HIF-α and other proteins such as co-activators and transcription factors that bind

to cis-regulatory regions near the HREs (133, 134). Considering this, it would be interesting to test whether the functional HRE sequence in Insig-2 has a cis-regulatory region that interacts with the protein which enhances the transcription of Insig-2 cooperatively with HIF-1α, but not with HIF-2α, presumably through interaction with the HIF-1α COOH-terminal domain. This information will better clarify the mechanism for selective regulation of Insig-2 and will lead to an identification of a novel protein that regulates the transcription of Insig-2.

4.5. Clinical Implications of Prolyl Hydroxylase Inhibition and ERAD of HMGCR

Researchers have increasingly studied the role for HIFs in metabolism of lipid, cholesterol, and glucose. However, there is a discrepancy in the function of HIFs between different studies. For example, inhibition of prolyl hydroxylase-2 using gene trap technology mildly stabilizes HIF-2α, protects against fatty liver, and does not increase hepatic cholesterol synthesis (127), whereas knock-out of prolyl hydroxylase-2 and extensive stabilization of HIF-2α increases cholesterol contents in the serum and liver (135, 136). Other studies reported that inhibition of HIF-α by chemical inhibitors, antisense oligonucleotides, and genetic disruption protects against metabolic dysregulation such as hepatic steatosis and insulin resistance (137-139). These findings collectively suggest a context-dependent function of HIFs in energy metabolism. Therefore, here I specifically discuss the potential of pharmacological inhibition of prolyl hydroxylase, which was utilized in the current study to determine the molecular mechanism by which HIF regulates cholesterol biosynthetic pathway.

Pharmacological inhibition of prolyl hydroxylase has been investigated as a strategy for treatment of metabolic disorder. FG-4497 is a small-molecule competitive inhibitor of all three forms of prolyl hydroxylases (prolyl hydroxlase-1, -2, and -3) (127). Administration of FG-4497 for 6 weeks to aged mice improves metabolic phenotypes such as body weight, adipocyte area, adipocyte macrophage infiltration, plasma cholesterol levels, and insulin resistance (127). A similar benefit is obtained in diet-induced obese mice administered with FG-4497. FG-4497 also ameliorates atherosclerosis in LDL receptor-deficient mice fed a high-fat diet (128). Another prolyl hydroxylase inhibitor under clinical trial, roxadustat (FG-4592), reduces plasma cholesterol levels in human (140). Considering the effect of DMOG on HMGCR degradation, it would be exciting to determine whether FG-4497 and roxadustat reduce cholesterol levels and improve atherosclerosis through a mechanism requiring Insig-2-mediated HMGCR degradation. Successful completion of this project will identify the ERAD of HMGCR as a cholesterol-lowering and anti-atherosclerotic mechanism that is amenable to clinical investigation.

BIBLIOGRAPHY

1. Ikonen E. Mechanisms for cellular cholesterol transport: defects and human disease. Physiol Rev. 2006;86(4):1237-61.
2. Russell DW. Nuclear orphan receptors control cholesterol catabolism. Cell. 1999;97(5):539-42.
3. Steinberg D. Thematic review series: the pathogenesis of atherosclerosis. An interpretive history of the cholesterol controversy: part I. J Lipid Res. 2004;45(9):1583-93.
4. Brown MS, Goldstein JL. Cholesterol feedback: from Schoenheimer's bottle to Scap's MELADL. J Lipid Res. 2009;50 Suppl:S15-27.
5. Horton JD, Goldstein JL, Brown MS. SREBPs: activators of the complete program of cholesterol and fatty acid synthesis in the liver. J Clin Invest. 2002;109(9):1125-31.
6. DeBose-Boyd RA. Feedback regulation of cholesterol synthesis: sterol-accelerated ubiquitination and degradation of HMG CoA reductase. Cell Res. 2008;18(6):609-21.
7. Jo Y, Debose-Boyd RA. Control of cholesterol synthesis through regulated ER-associated degradation of HMG CoA reductase. Crit Rev Biochem Mol Biol. 2010;45(3):185-98.
8. Nakanishi M, Goldstein JL, Brown MS. Multivalent control of 3-hydroxy-3-methylglutaryl coenzyme A reductase. Mevalonate-derived product inhibits translation of mRNA and accelerates degradation of enzyme. J Biol Chem. 1988;263(18):8929-37.
9. Brown MS, Goldstein JL. Multivalent feedback regulation of HMG CoA reductase, a control mechanism coordinating isoprenoid synthesis and cell growth. J Lipid Res. 1980;21(5):505-17.
10. Goldstein JL, Brown MS. Regulation of the mevalonate pathway. Nature. 1990;343(6257):425-30.
11. Goldstein JL, DeBose-Boyd RA, Brown MS. Protein sensors for membrane sterols 1. Cell. 2006;124(1):35-46.
12. Feramisco JD, Goldstein JL, Brown MS. Membrane topology of human insig-1, a protein regulator of lipid synthesis. J Biol Chem. 2004;279(9):8487-96.
13. Radhakrishnan A, Ikeda Y, Kwon HJ, Brown MS, Goldstein JL. Sterol-regulated transport of SREBPs from endoplasmic reticulum to Golgi: oxysterols block transport by binding to Insig. Proc Natl Acad Sci USA. 2007;104(16):6511-8.
14. Yabe D, Brown MS, Goldstein JL. Insig-2, a second endoplasmic reticulum protein that binds SCAP and blocks export of sterol regulatory element-binding proteins. Proc Natl Acad Sci USA. 2002;99(20):12753-8.
15. Adams CM, Reitz J, De Brabander JK, Feramisco JD, Li L, Brown MS, et al. Cholesterol and 25-hydroxycholesterol inhibit activation of SREBPs by different mechanisms, both involving SCAP and Insigs. J Biol Chem. 2004;279(50):52772-80.

16. Sever N, Song BL, Yabe D, Goldstein JL, Brown MS, DeBose-Boyd RA. Insig-dependent ubiquitination and degradation of mammalian 3-hydroxy-3-methylglutaryl-CoA reductase stimulated by sterols and geranylgeraniol. J Biol Chem. 2003;278(52):52479-90.
17. Engelking LJ, Liang G, Hammer RE, Takaishi K, Kuriyama H, Evers BM, et al. Schoenheimer effect explained - feedback regulation of cholesterol synthesis in mice mediated by Insig proteins 1. J Clin Invest. 2005;115(9):2489-98.
18. Brown MS, Goldstein JL. A proteolytic pathway that controls the cholesterol content of membranes, cells, and blood. Proc Natl Acad Sci USA. 1999;96(20):11041-8.
19. Sakai J, Nohturfft A, Cheng D, Ho YK, Brown MS, Goldstein JL. Identification of complexes between the COOH-terminal domains of sterol regulatory element-binding proteins (SREBPs) and SREBP cleavage-activating protein. J Biol Chem. 1997;272(32):20213-21.
20. Horton JD, Goldstein JL, Brown MS. SREBPs: activators of the complete program of cholesterol and fatty acid synthesis in the liver. J Clin Invest. 2002;109(9):1125-31.
21. Horton JD, Shah NA, Warrington JA, Anderson NN, Park SW, Brown MS, et al. Combined analysis of oligonucleotide microarray data from transgenic and knockout mice identifies direct SREBP target genes. Proc Natl Acad Sci USA. 2003;100(212):12027-32.
22. Roitelman J, Olender EH, Bar-Nun S, Dunn WA, Jr., Simoni RD. Immunological evidence for eight spans in the membrane domain of 3-hydroxy-3-methylglutaryl coenzyme A reductase: implications for enzyme degradation in the endoplasmic reticulum. J Biol Chem. 1992;117(5):959-73.
23. Liscum L, Finer-Moore J, Stroud RM, Luskey KL, Brown MS, Goldstein JL. Domain structure of 3-hydroxy-3-methylglutaryl coenzyme A reductase, a glycoprotein of the endoplasmic reticulum. J Biol Chem. 1985;260(1):522-30.
24. Sever N, Yang T, Brown MS, Goldstein JL, DeBose-Boyd RA. Accelerated degradation of HMG CoA reductase mediated by binding of insig-1 to its sterol-sensing domain. Mol Cell. 2003;11(1):25-33.
25. Song BL, Sever N, DeBose-Boyd RA. Gp78, a membrane-anchored ubiquitin ligase, associates with Insig-1 and couples sterol-regulated ubiquitination to degradation of HMG CoA reductase. Mol Cell. 2005;19(6):829-40.
26. Jo Y, Lee PC, Sguigna PV, DeBose-Boyd RA. Sterol-induced degradation of HMG CoA reductase depends on interplay of two Insigs and two ubiquitin ligases, gp78 and Trc8. Proc Natl Acad Sci USA. 2011;108(51):20503-8.
27. Liu TF, Tang JJ, Li PS, Shen Y, Li JG, Miao HH, et al. Ablation of gp78 in liver improves hyperlipidemia and insulin resistance by inhibiting SREBP to decrease lipid biosynthesis. Cell Metab. 2012;16(2):213-25.
28. Radhakrishnan A, Sun LP, Kwon HJ, Brown MS, Goldstein JL. Direct binding of cholesterol to the purified membrane region of SCAP: mechanism for a sterol-sensing domain. Mol Cell. 2004;15(2):259-68.

29. Song BL, Javitt NB, DeBose-Boyd RA. Insig-mediated degradation of HMG CoA reductase stimulated by lanosterol, an intermediate in the synthesis of cholesterol. Cell Metab. 2005;1(3):179-89.
30. Lange Y, Ory DS, Ye J, Lanier MH, Hsu FF, Steck TL. Effectors of rapid homeostatic responses of endoplasmic reticulum cholesterol and 3-hydroxy-3-methylglutaryl-CoA reductase. J Biol Chem. 2008;283(3):1445-55.
31. Schumacher MM, Elsabrouty R, Seemann J, Jo Y, DeBose-Boyd RA. The prenyltransferase UBIAD1 is the target of geranylgeraniol in degradation of HMG CoA reductase. Elife. 2015;4:e05560.
32. Schumacher MM, Jun DJ, Jo Y, Seemann J, DeBose-Boyd RA. Geranylgeranyl-regulated transport of the prenyltransferase UBIAD1 between membranes of the ER and Golgi. J Lipid Res. 2016;57(7):1286-99.
33. Morris LL, Hartman IZ, Jun DJ, Seemann J, DeBose-Boyd RA. Sequential Actions of the AAA-ATPase Valosin-containing Protein (VCP)/p97 and the Proteasome 19 S Regulatory Particle in Sterol-accelerated, Endoplasmic Reticulum (ER)-associated Degradation of 3-Hydroxy-3-methylglutaryl-coenzyme A Reductase. J Biol Chem. 2014;289(27):19053-66.
34. Hartman IZ, Liu P, Zehmer JK, Luby-Phelps K, Jo Y, Anderson RG, et al. Sterol-induced dislocation of 3-hydroxy-3-methylglutaryl coenzyme A reductase from endoplasmic reticulum membranes into the cytosol through a subcellular compartment resembling lipid droplets. J Biol Chem. 2010;285(25):19288-98.
35. Gil G, Faust JR, Chin DJ, Goldstein JL, Brown MS. Membrane-bound domain of HMG CoA reductase is required for sterol-enhanced degradation of the enzyme. Cell. 1985;41(1):249-58.
36. Skalnik DG, Narita H, Kent C, Simoni RD. The membrane domain of 3-hydroxy-3-methylglutaryl-coenzyme A reductase confers endoplasmic reticulum localization and sterol-regulated degradation onto beta-galactosidase. J Biol Chem. 1988;263(14):6836-41.
37. Summons RE, Bradley AS, Jahnke LL, Waldbauer JR. Steroids, triterpenoids and molecular oxygen 2. Phil Trans R Soc B. 2006;361(1470):951-68.
38. Bloch K. Biological synthesis of cholesterol 17. Harvey Lect. 1952;48:68-88.
39. Nguyen AD, McDonald JG, Bruick RK, DeBose-Boyd RA. Hypoxia stimulates degradation of 3-hydroxy-3-methylglutaryl-coenzyme A reductase through accumulation of lanosterol and hypoxia-inducible factor-mediated induction of insigs. J Biol Chem. 2007;282(37):27436-46.
40. Semenza GL. Hypoxia-inducible factors in physiology and medicine. Cell. 2012;148(3):399-408.
41. Kaelin WG, Jr., Ratcliffe PJ. Oxygen sensing by metazoans: the central role of the HIF hydroxylase pathway. Mol Cell. 2008;30(4):393-402.
42. Schofield CJ, Ratcliffe PJ. Oxygen sensing by HIF hydroxylases. Nature reviews Mol Cell Biol. 2004;5(5):343-54.
43. Semenza GL. Hydroxylation of HIF-1: Oxygen Sensing at the Molecular Level. Physiology. 2004;19(4):176-82.

44. Wenger RH, Stiehl DP, Camenisch G. Integration of oxygen signaling at the consensus HRE. Sci STKE. 2005;2005(306):re12.
45. Sharpe LJ, Brown AJ. Controlling cholesterol synthesis beyond 3-hydroxy-3-methylglutaryl-CoA reductase (HMGCR). J Biol Chem. 2013;288(26):18707-15.
46. Yang T, Espenshade PJ, Wright ME, Yabe D, Gong Y, Aebersold R, et al. Crucial step in cholesterol homeostasis: sterols promote binding of SCAP to INSIG-1, a membrane protein that facilitates retention of SREBPs in ER. Cell. 2002;110(4):489-500.
47. Goldstein JL, Brown MS. A century of cholesterol and coronaries: from plaques to genes to statins. Cell. 2015;161(1):161-72.
48. Keller RK, Zhao Z, Chambers C, Ness GC. Farnesol is not the nonsterol regulator mediating degradation of HMG-CoA reductase in rat liver. Arch Biochem Biophys. 1996;328(2):324-30.
49. Edwards PA, Gould RG. Turnover rate of hepatic 3-hydroxy-3-methylglutaryl coenzyme A reductase as determined by use of cycloheximide. J Biol Chem. 1972;247(5):1520-4.
50. Ness GC, Holland RC. Degradation of HMG-CoA reductase in rat liver is cholesterol and ubiquitin independent. FEBS Lett. 2005;579(14):3126-30.
51. Simonet WS, Bucay N, Lauer SJ, Taylor JM. A far-downstream hepatocyte-specific control region directs expression of the linked human apolipoprotein E and C-I genes in transgenic mice. J Biol Chem. 1993;268(11):8221-9.
52. McFarlane MR, Liang G, Engelking LJ. Insig proteins mediate feedback inhibition of cholesterol synthesis in the intestine. J Biol Chem. 2014;289(4):2148-56.
53. Jo Y, Sguigna PV, Debose-Boyd RA. Membrane-associated Ubiquitin Ligase Complex Containing gp78 Mediates Sterol-accelerated Degradation of 3-Hydroxy-3-methylglutaryl-coenzyme A Reductase. J Biol Chem. 2011;286(17):15022-31.
54. McDonald JG, Smith DD, Stiles AR, Russell DW. A comprehensive method for extraction and quantitative analysis of sterols and secosteroids from human plasma. J Lipid Res. 2012;53(7):1399-409.
55. Mitsche MA, McDonald JG, Hobbs HH, Cohen JC. Flux analysis of cholesterol biosynthesis in vivo reveals multiple tissue and cell-type specific pathways. Elife. 2015;4:e07999.
56. Shimano H, Horton JD, Hammer RE, Shimomura I, Brown MS, Goldstein JL. Overproduction of cholesterol and fatty acids causes massive liver enlargement in transgenic mice expressing truncated SREBP-1a. J Clin Invest. 1996;98(7):1575-84.
57. Doolman R, Leichner GS, Avner R, Roitelman J. Ubiquitin is conjugated by membrane ubiquitin ligase to three sites, including the N terminus, in transmembrane region of mammalian 3-hydroxy-3-methylglutaryl coenzyme A reductase: implications for sterol-regulated enzyme degradation. J Biol Chem. 2004;279(37):38184-93.
58. Repa JJ, Liang G, Ou J, Bashmakov Y, Lobaccaro JM, Shimomura I, et al. Regulation of mouse sterol regulatory element-binding protein-1c gene (SREBP-1c) by oxysterol receptors, LXRalpha and LXRbeta. Genes Dev. 2000;14(22):2819-30.

59. Engelking LJ, Kuriyama H, Hammer RE, Horton JD, Brown MS, Goldstein JL, et al. Overexpression of Insig-1 in the livers of transgenic mice inhibits SREBP processing and reduces insulin-stimulated lipogenesis. J Clin Invest. 2004;113(8):1168-75.
60. DeBose-Boyd RA, Ou J, Goldstein JL, Brown MS. Expression of sterol regulatory element-binding protein 1c (SREBP-1c) mRNA in rat hepatoma cells requires endogenous LXR ligands. Proc Natl Acad Sci USA. 2001;98(4):1477-82.
61. Yabe D, Komuro R, Liang G, Goldstein JL, Brown MS. Liver-specific mRNA for Insig-2 down-regulated by insulin: implications for fatty acid synthesis. Proc Natl Acad Sci USA. 2003;100(6):3155-60.
62. Engelking LJ, Evers BM, Richardson JA, Goldstein JL, Brown MS, Liang G. Severe facial clefting in Insig-deficient mouse embryos caused by sterol accumulation and reversed by lovastatin 1. J Clin Invest. 2006;116(9):2356-65.
63. Kita T, Brown MS, Goldstein JL. Feedback regulation of 3-hydroxy-3-methylglutaryl coenzyme A reductase in livers of mice treated with mevinolin, a competitive inhibitor of the reductase. J Clin Invest. 1980;66(5):1094-100.
64. Reihner E, Rudling M, Stahlberg D, Berglund L, Ewerth S, Bjorkhem I, et al. Influence of pravastatin, a specific inhibitor of HMG-CoA reductase, on hepatic metabolism of cholesterol. N Engl J Med. 1990;323(4):224-8.
65. Nguyen AD, Lee SH, DeBose-Boyd RA. Insig-mediated, sterol-accelerated degradation of the membrane domain of hamster 3-hydroxy-3-methylglutaryl-coenzyme A reductase in insect cells. J Biol Chem. 2009;284(39):26778-88.
66. Russell DW, Schneider WJ, Yamamoto T, Luskey KL, Brown MS, Goldstein JL. Domain map of the LDL receptor: sequence homology with the epidermal growth factor precursor. Cell. 1984;37(2):577-85.
67. Metherall JE, Goldstein JL, Luskey KL, Brown MS. Loss of transcriptional repression of three sterol-regulated genes in mutant hamster cells. J Biol Chem. 1989;264(26):15634-41.
68. Wu J, Merlino G, Fausto N. Establishment and characterization of differentiated, nontransformed hepatocyte cell lines derived from mice transgenic for transforming growth factor alpha. Proc Natl Acad Sci USA. 1994;91(2):674-8.
69. Hwang S, Hartman IZ, Calhoun LN, Garland K, Young GA, Mitsche MA, et al. Contribution of Accelerated Degradation to Feedback Regulation of 3-Hydroxy-3-methylglutaryl Coenzyme A Reductase and Cholesterol Metabolism in the Liver. J Biol Chem. 2016;291(26):13479-94.
70. Haase VH, Glickman JN, Socolovsky M, Jaenisch R. Vascular tumors in livers with targeted inactivation of the von Hippel–Lindau tumor suppressor. Proc Natl Acad Sci USA. 2001;98(4):1583-8.
71. Liang G, Yang J, Horton JD, Hammer RE, Goldstein JL, Brown MS. Diminished hepatic response to fasting/refeeding and liver X receptor agonists in mice with selective deficiency of sterol regulatory element-binding protein-1c. J Biol Chem. 2002;277(11):9520-8.
72. Jo Y, Hartman IZ, DeBose-Boyd RA. Ancient ubiquitous protein-1 mediates sterol-induced ubiquitination of 3-hydroxy-3-methylglutaryl CoA reductase in lipid

droplet-associated endoplasmic reticulum membranes. Mol Biol Cell. 2013;24(3):169-83.
73. Liscum L, Luskey KL, Chin DJ, Ho YK, Goldstein JL, Brown MS. Regulation of 3-hydroxy-3-methylglutaryl coenzyme A reductase and its mRNA in rat liver as studied with a monoclonal antibody and a cDNA probe. J Biol Chem. 1983;258(13):8450-5.
74. Schofield CJ, Ratcliffe PJ. Oxygen sensing by HIF hydroxylases 23. Nat Rev Mol Cell Biol. 2004;5(5):343-54.
75. Horton JD, Shimano H, Hamilton RL, Brown MS, Goldstein JL. Disruption of LDL receptor gene in transgenic SREBP-1a mice unmasks hyperlipidemia resulting from production of lipid-rich VLDL. J Clin Invest. 1999;103(7):1067-76.
76. Jaakkola P, Mole DR, Tian YM, Wilson MI, Gielbert J, Gaskell SJ, et al. Targeting of HIF-alpha to the von Hippel-Lindau ubiquitylation complex by O2-regulated prolyl hydroxylation 68. Science. 2001;292(5516):468-72.
77. Firth JD, Ebert BL, Pugh CW, Ratcliffe PJ. Oxygen-regulated control elements in the phosphoglycerate kinase 1 and lactate dehydrogenase A genes: similarities with the erythropoietin 3' enhancer 115. Proc Natl Acad Sci USA. 1994;91(14):6496-500.
78. Wang GL, Semenza GL. Characterization of hypoxia-inducible factor 1 and regulation of DNA binding activity by hypoxia 155. J Biol Chem. 1993;268(29):21513-8.
79. Fernandez-Alvarez A, Soledad Alvarez M, Cucarella C, Casado M. Characterization of the human insulin-induced gene 2 (INSIG2) promoter: the role of Ets-binding motifs. J Biol Chem. 2010;285(16):11765-74.
80. Dolt KS, Karar J, Mishra MK, Salim J, Kumar R, Grover SK, et al. Transcriptional downregulation of sterol metabolism genes in murine liver exposed to acute hypobaric hypoxia. Biochem Biophys Res Commun. 2007;354(1):148-53.
81. Drabkin HA, Gemmill RM. Cholesterol and the development of clear-cell renal carcinoma. Curr Opin Pharmacol. 2012;12(6):742-50.
82. Gebhard RL, Clayman RV, Prigge WF, Figenshau R, Staley NA, Reesey C, et al. Abnormal cholesterol metabolism in renal clear cell carcinoma. J Lipid Res. 1987;28(10):1177-84.
83. Tugnoli V, Trinchero A, Tosi MR. Evaluation of the lipid composition of human healthy and neoplastic renal tissues. Ital J Biochem. 2004;53(4):169-82.
84. Yang H, Minamishima YA, Yan Q, Schlisio S, Ebert BL, Zhang X, et al. pVHL acts as an adaptor to promote the inhibitory phosphorylation of the NF-kappaB agonist Card9 by CK2. Mol Cell. 2007;28(1):15-27.
85. Gruenbacher G, Thurnher M. Mevalonate metabolism in cancer. Cancer Lett. 2015;356(2 Pt A):192-6.
86. McKenney JM. Pharmacologic characteristics of statins. Clin Cardiol. 2003;26(4 Suppl 3):III32-8.
87. Schachter M. Chemical, pharmacokinetic and pharmacodynamic properties of statins: an update. Fundam Clin Pharmacol. 2005;19(1):117-25.

88. Vaughan CJ, Gotto AM, Jr. Update on statins: 2003. Circulation. 2004;110(7):886-92.
89. Goldberg IJ, Holleran S, Ramakrishnan R, Adams M, Palmer RH, Dell RB, et al. Lack of effect of lovastatin therapy on the parameters of whole-body cholesterol metabolism. J Clin Invest. 1990;86(3):801-8.
90. Grundy SM, Bilheimer DW. Inhibition of 3-hydroxy-3-methylglutaryl-CoA reductase by mevinolin in familial hypercholesterolemia heterozygotes: effects on cholesterol balance. Proc Natl Acad Sci USA. 1984;81(8):2538-42.
91. Gylling H, Miettinen TA. Effects of inhibiting cholesterol absorption and synthesis on cholesterol and lipoprotein metabolism in hypercholesterolemic non-insulin-dependent diabetic men. J Lipid Res. 1996;37(8):1776-85.
92. Schonewille M, de Boer JF, Mele L, Wolters H, Bloks VW, Wolters JC, et al. Statins increase hepatic cholesterol synthesis and stimulate fecal cholesterol elimination in mice. J Lipid Res. 2016;57(8):1455-64.
93. Schonbeck U, Libby P. Inflammation, immunity, and HMG-CoA reductase inhibitors: statins as antiinflammatory agents? Circulation. 2004;109(21 Suppl 1):II18-26.
94. Pylayeva-Gupta Y, Grabocka E, Bar-Sagi D. RAS oncogenes: weaving a tumorigenic web. Nat Rev Cancer. 2011;11(11):761-74.
95. Downward J. Targeting RAS signalling pathways in cancer therapy. Nature reviews Cancer. 2003;3(1):11-22.
96. Biankin AV, Waddell N, Kassahn KS, Gingras MC, Muthuswamy LB, Johns AL, et al. Pancreatic cancer genomes reveal aberrations in axon guidance pathway genes. Nature. 2012;491(7424):399-405.
97. Jones S, Zhang X, Parsons DW, Lin JC, Leary RJ, Angenendt P, et al. Core signaling pathways in human pancreatic cancers revealed by global genomic analyses. Science. 2008;321(5897):1801-6.
98. Jaffee EM, Hruban RH, Canto M, Kern SE. Focus on pancreas cancer. Cancer Cell. 2002;2(1):25-8.
99. Castellano E, Santos E. Functional specificity of ras isoforms: so similar but so different. Genes Cancer. 2011;2(3):216-31.
100. Grady WM, Markowitz SD. Genetic and epigenetic alterations in colon cancer. Annu Rev of Genomics Hum Genet. 2002;3:101-28.
101. Almoguera C, Shibata D, Forrester K, Martin J, Arnheim N, Perucho M. Most human carcinomas of the exocrine pancreas contain mutant c-K-ras genes. Cell. 1988;53(4):549-54.
102. Rodenhuis S, Slebos RJ. Clinical significance of ras oncogene activation in human lung cancer. Cancer Res. 1992;52(9 Suppl):2665s-9s.
103. Graaf MR, Richel DJ, van Noorden CJ, Guchelaar HJ. Effects of statins and farnesyltransferase inhibitors on the development and progression of cancer. Cancer Treat Rev. 2004;30(7):609-41.
104. Philips MR, Cox AD. Geranylgeranyltransferase I as a target for anti-cancer drugs. J Clin Invest. 2007;117(5):1223-5.

105. Cox AD, Der CJ, Philips MR. Targeting RAS Membrane Association: Back to the Future for Anti-RAS Drug Discovery? *Clin Cancer Res*. 2015;21(8):1819-27.
106. Hemminki A, Markie D, Tomlinson I, Avizienyte E, Roth S, Loukola A, et al. A serine/threonine kinase gene defective in Peutz-Jeghers syndrome. Nature. 1998;391(6663):184-7.
107. Collins SP, Reoma JL, Gamm DM, Uhler MD. LKB1, a novel serine/threonine protein kinase and potential tumour suppressor, is phosphorylated by cAMP-dependent protein kinase (PKA) and prenylated in vivo. Biochem J. 2000;345 Pt 3:673-80.
108. Shaw RJ, Kosmatka M, Bardeesy N, Hurley RL, Witters LA, DePinho RA, et al. The tumor suppressor LKB1 kinase directly activates AMP-activated kinase and regulates apoptosis in response to energy stress. Proc Natl Acad Sci USA. 2004;101(10):3329-35.
109. Shaw RJ, Lamia KA, Vasquez D, Koo SH, Bardeesy N, Depinho RA, et al. The kinase LKB1 mediates glucose homeostasis in liver and therapeutic effects of metformin. Science. 2005;310(5754):1642-6.
110. Houde VP, Ritorto MS, Gourlay R, Varghese J, Davies P, Shpiro N, et al. Investigation of LKB1 Ser431 phosphorylation and Cys433 farnesylation using mouse knockin analysis reveals an unexpected role of prenylation in regulating AMPK activity. Biochem J. 2014;458(1):41-56.
111. Sapkota GP, Kieloch A, Lizcano JM, Lain S, Arthur JS, Williams MR, et al. Phosphorylation of the protein kinase mutated in Peutz-Jeghers cancer syndrome, LKB1/STK11, at Ser431 by p90(RSK) and cAMP-dependent protein kinase, but not its farnesylation at Cys(433), is essential for LKB1 to suppress cell growth. J Biol Chem. 2001;276(22):19469-82.
112. Ruderman NB, Carling D, Prentki M, Cacicedo JM. AMPK, insulin resistance, and the metabolic syndrome. J Clin Invest. 2013;123(7):2764-72.
113. Henneman L, van Cruchten AG, Denis SW, Amolins MW, Placzek AT, Gibbs RA, et al. Detection of nonsterol isoprenoids by HPLC-MS/MS. Anal Biochem. 2008;383(1):18-24.
114. Nagel R, Gershenzon J, Schmidt A. Nonradioactive assay for detecting isoprenyl diphosphate synthase activity in crude plant extracts using liquid chromatography coupled with tandem mass spectrometry. Anal Biochem. 2012;422(1):33-8.
115. Rius J, Guma M, Schachtrup C, Akassoglou K, Zinkernagel AS, Nizet V, et al. NF-kappaB links innate immunity to the hypoxic response through transcriptional regulation of HIF-1alpha. Nature. 2008;453(7196):807-11.
116. Wouters K, van Gorp PJ, Bieghs V, Gijbels MJ, Duimel H, Lutjohann D, et al. Dietary cholesterol, rather than liver steatosis, leads to hepatic inflammation in hyperlipidemic mouse models of nonalcoholic steatohepatitis. Hepatology. 2008;48(2):474-86.
117. Subramanian S, Goodspeed L, Wang S, Kim J, Zeng L, Ioannou GN, et al. Dietary cholesterol exacerbates hepatic steatosis and inflammation in obese LDL receptor-deficient mice. J Lipid Res. 2011;52(9):1626-35.

118. Van Rooyen DM, Larter CZ, Haigh WG, Yeh MM, Ioannou G, Kuver R, et al. Hepatic free cholesterol accumulates in obese, diabetic mice and causes nonalcoholic steatohepatitis. Gastroenterology. 2011;141(4):1393-403, 403.e1-5.
119. Matsuzawa N, Takamura T, Kurita S, Misu H, Ota T, Ando H, et al. Lipid-induced oxidative stress causes steatohepatitis in mice fed an atherogenic diet. Hepatology. 2007;46(5):1392-403.
120. Min HK, Kapoor A, Fuchs M, Mirshahi F, Zhou H, Maher J, et al. Increased hepatic synthesis and dysregulation of cholesterol metabolism is associated with the severity of nonalcoholic fatty liver disease. Cell Metab. 2012;15(5):665-74.
121. Lefer DJ. Statins as potent antiinflammatory drugs. Circulation. 2002;106(16):2041-2.
122. Antonopoulos AS, Margaritis M, Lee R, Channon K, Antoniades C. Statins as anti-inflammatory agents in atherogenesis: molecular mechanisms and lessons from the recent clinical trials. Curr Pharm Des. 2012;18(11):1519-30.
123. Lu H, Talbot S, Robertson KA, Watterson S, Forster T, Roy D, et al. Rapid proteasomal elimination of 3-hydroxy-3-methylglutaryl-CoA reductase by interferon-gamma in primary macrophages requires endogenous 25-hydroxycholesterol synthesis. Steroids. 2015;99(Pt B):219-29.
124. Cyster JG, Dang EV, Reboldi A, Yi T. 25-Hydroxycholesterols in innate and adaptive immunity. Nat Rev Immunol. 2014;14(11):731-43.
125. York AG, Williams KJ, Argus JP, Zhou QD, Brar G, Vergnes L, et al. Limiting Cholesterol Biosynthetic Flux Spontaneously Engages Type I IFN Signaling. Cell. 2015;163(7):1716-29.
126. Ramakrishnan SK, Taylor M, Qu A, Ahn SH, Suresh MV, Raghavendran K, et al. Loss of von Hippel-Lindau protein (VHL) increases systemic cholesterol levels through targeting hypoxia-inducible factor 2alpha and regulation of bile acid homeostasis. Mol Cell Biol. 2014;34(7):1208-20.
127. Rahtu-Korpela L, Karsikas S, Horkko S, Blanco Sequeiros R, Lammentausta E, Makela KA, et al. HIF prolyl 4-hydroxylase-2 inhibition improves glucose and lipid metabolism and protects against obesity and metabolic dysfunction. Diabetes. 2014;63(10):3324-33.
128. Rahtu-Korpela L, Maatta J, Dimova EY, Horkko S, Gylling H, Walkinshaw G, et al. Hypoxia-Inducible Factor Prolyl 4-Hydroxylase-2 Inhibition Protects Against Development of Atherosclerosis. Arterioscler Thromb Vasc Biol. 2016;36(4):608-17.
129. Cao R, Zhao X, Li S, Zhou H, Chen W, Ren L, et al. Hypoxia induces dysregulation of lipid metabolism in HepG2 cells via activation of HIF-2alpha. Cell Physiol Biochem. 2014;34(5):1427-41.
130. Dengler VL, Galbraith MD, Espinosa JM. Transcriptional regulation by hypoxia inducible factors. Crit Rev Biochem Mol Biol. 2014;49(1):1-15.
131. Lau KW, Tian YM, Raval RR, Ratcliffe PJ, Pugh CW. Target gene selectivity of hypoxia-inducible factor-alpha in renal cancer cells is conveyed by post-DNA-binding mechanisms. Br J Cancer. 2007;96(8):1284-92.

132. Hu CJ, Sataur A, Wang L, Chen H, Simon MC. The N-terminal transactivation domain confers target gene specificity of hypoxia-inducible factors HIF-1alpha and HIF-2alpha. Mol Biol Cell. 2007;18(11):4528-42.
133. Mole DR, Blancher C, Copley RR, Pollard PJ, Gleadle JM, Ragoussis J, et al. Genome-wide association of hypoxia-inducible factor (HIF)-1alpha and HIF-2alpha DNA binding with expression profiling of hypoxia-inducible transcripts. J Biol Chem. 2009;284(25):16767-75.
134. Villar D, Ortiz-Barahona A, Gomez-Maldonado L, Pescador N, Sanchez-Cabo F, Hackl H, et al. Cooperativity of stress-responsive transcription factors in core hypoxia-inducible factor binding regions. PLoS One. 2012;7(9):e45708.
135. Taniguchi CM, Finger EC, Krieg AJ, Wu C, Diep AN, LaGory EL, et al. Cross-talk between hypoxia and insulin signaling through Phd3 regulates hepatic glucose and lipid metabolism and ameliorates diabetes. Nat Med. 2013;19(10):1325-30.
136. Rankin EB, Rha J, Selak MA, Unger TL, Keith B, Liu Q, et al. Hypoxia-inducible factor 2 regulates hepatic lipid metabolism. Mol Cell Biol. 2009;29(16):4527-38.
137. Sun K, Halberg N, Khan M, Magalang UJ, Scherer PE. Selective inhibition of hypoxia-inducible factor 1alpha ameliorates adipose tissue dysfunction. Mol Cell Biol. 2013;33(5):904-17.
138. Jiang C, Qu A, Matsubara T, Chanturiya T, Jou W, Gavrilova O, et al. Disruption of hypoxia-inducible factor 1 in adipocytes improves insulin sensitivity and decreases adiposity in high-fat diet-fed mice. Diabetes. 2011;60(10):2484-95.
139. Shin MK, Drager LF, Yao Q, Bevans-Fonti S, Yoo DY, Jun JC, et al. Metabolic consequences of high-fat diet are attenuated by suppression of HIF-1alpha. PLoS One. 2012;7(10):e46562.
140. Provenzano R BA, Dua S, Nguyen P, Wright S, Zeig S, Leong R, Chou J, Shi W, Saikali K, Yu K, Neff T. FG-4592, a Novel Oral Hypoxia-Inducible Factor Prolyl Hydroxylase Inhibitor (HIF-PHI), Maintains Hemoglobin Levels and Lowers Cholesterol in Hemodialysis Patients: Phase 2 Comparison with Epoetin Alfa. J Am Soc Nephrol. 2012;23:428A.